Measurements of differential cross-sections in top-quark pair events with a high transverse momentum top quark and limits on beyond the Standard Model contributions to top-quark pair production with the ATLAS detector at $\sqrt{s} = 13\,\text{TeV}$

The ATLAS collaboration

ABSTRACT: Cross-section measurements of top-quark pair production where the hadronically decaying top quark has transverse momentum greater than 355 GeV and the other top quark decays into $\ell\nu b$ are presented using $139\,\text{fb}^{-1}$ of data collected by the ATLAS experiment during proton-proton collisions at the LHC. The fiducial cross-section at $\sqrt{s} = 13\,\text{TeV}$ is measured to be $\sigma = 1.267 \pm 0.005 \pm 0.053$ pb, where the uncertainties reflect the limited number of data events and the systematic uncertainties, giving a total uncertainty of 4.2%. The cross-section is measured differentially as a function of variables characterising the $t\bar{t}$ system and additional radiation in the events. The results are compared with various Monte Carlo generators, including comparisons where the generators are reweighted to match a parton-level calculation at next-to-next-to-leading order. The reweighting improves the agreement between data and theory. The measured distribution of the top-quark transverse momentum is used to search for new physics in the context of the effective field theory framework. No significant deviation from the Standard Model is observed and limits are set on the Wilson coefficients of the dimension-six operators O_{tG} and $O_{tq}^{(8)}$, where the limits on the latter are the most stringent to date.

KEYWORDS: Top Physics, Beyond Standard Model, Hadron-Hadron Scattering

Contents

1 Introduction

The high mass of the top quark means that it is often intimately involved in models of physics beyond the Standard Model (SM). In effective models of new physics [1–4], non-resonant deviations from the SM often appear at high transverse momentum (p_{T}) of the top quark and high invariant mass of the top-quark–top-antiquark ($t\bar{t}$) system [5–8]. The high rate of $t\bar{t}$ production at the Large Hadron Collider (LHC) provides a unique opportunity

to test for deviations from the SM predictions. This motivates precise differential $t\bar{t}$ cross-section measurements of high-p_{T} (boosted) top quarks.

In this paper, $t\bar{t}$ events containing a boosted top quark that has decayed hadronically are selected from data collected by the ATLAS detector in proton-proton collisions at $\sqrt{s} =$ 13 TeV from 2015 to 2018. The selected events correspond to the semileptonic $t\bar{t}$ decay channel ($t\bar{t} \to WbWb \to \ell\nu bqq'b$) and the decay products are used to fully reconstruct the kinematics of the $t\bar{t}$ system. The measured event properties are corrected for detector effects to obtain differential cross-sections as a function of various observables. These differential cross-section measurements characterise both the $t\bar{t}$ system and the additional radiation in the events. The analysis introduces a novel use of the reconstructed top-quark mass to reduce the impact of uncertainties from the jet energy scale compared to the previous ATLAS publication [9] and significantly improves the precision of the measurements. ATLAS has also measured the cross-section of $t\bar{t}$ events with boosted top quarks in the all-hadronic channel [10] and CMS has performed a measurement in the semileptonic channel [11]. These three measurements used smaller datasets, corresponding to an integrated luminosity of 36 fb^{-1}, than the one used in this article, which corresponds to 139 fb^{-1}. The measurements follow on from analyses performed at $\sqrt{s} = 8$ TeV [12, 13].

The measured cross-sections are compared with available SM predictions. Precise predictions for SM $t\bar{t}$ production are available at next-to-next-to-leading order (NNLO) in quantum chromodynamics (QCD) [14–16]. The predictions are fully differential but are only available for stable top quarks or in the dilepton channel ($t\bar{t} \to WbWb \to \ell\nu b\ell\nu b$) [17]. Predictions at NLO in QCD are available for the semileptonic decay channel including the full decay of the top quarks and parton shower and hadronisation effects in various Monte Carlo (MC) generators. The measured cross-sections are compared with the NLO MC predictions and the impact of the higher-order corrections is tested by reweighting the MC predictions at parton level to match predictions at NNLO in QCD.

The measurements presented in this article are also used to test for the presence of new physics beyond the SM. The absence of direct evidence for the production of new particles beyond the SM at the LHC suggests that any new physics is separated in mass from the SM fields. In this situation the new physics can be parameterised in a model-independent way through the framework of effective field theory (EFT), in which the Lagrangian of the SM is modified by adding an infinite series of higher-dimensional effective operators [1–4] that are suppressed by the new-physics scale. Assuming that the energy scale is sufficiently large, the impact of new physics can be approximated by dimension-six operators. The ability of the presented measurements to constrain new physics is illustrated by using the measured top-quark p_{T} distribution to set limits on the effective operators O_{tG} and $O_{tq}^{(8)}$, where the Warsaw basis [18] is used to define the operators.

This paper is structured as follows. Section 2 presents the data and simulated event samples. Section 3 discusses the object and event selection and the reconstruction of the $t\bar{t}$ system. The methodology of the cross-section measurement, including the new method to use the reconstructed top-quark mass to reduce the impact of the jet energy scale uncertainties, is described in section 4. The systematic uncertainties are discussed in section 5 and the results of the measurement are compared with the theoretical predictions

in section [6]. Section [7] presents the interpretation of the measured top-quark p_T distribution in the EFT framework. Finally, conclusions are presented in section [8].

2 Data and simulated event samples

The ATLAS detector [19–21] surrounds one of the collision points at the LHC.[1] The detector consists of an inner tracking system surrounded by a superconducting solenoid producing a 2 T axial magnetic field, electromagnetic and hadronic calorimeters and an external muon spectrometer incorporating three toroidal magnet assemblies. An extensive software suite [22] is used in the reconstruction and analysis of real and simulated data, in detector operations, and in the trigger and data acquisition systems of the experiment.

The analysis was performed on data collected from pp collisions at $\sqrt{s} = 13$ TeV during 2015–2018. The dataset must fulfil standard data quality requirements [23] and corresponds to an integrated luminosity of 139 fb^{-1}. The uncertainty in the integrated luminosity is 1.7% [24], obtained using the LUCID-2 detector [25] for the primary luminosity measurements. Events are required to pass a single-electron or single-muon trigger [26, 27].

MC simulated event samples are used to determine background contributions, derive corrections for detector effects, simulate potential new-physics contributions, and to compare with data. Samples were processed using either the full ATLAS detector simulation [28] based on GEANT4 [29], or with a faster simulation making use of parameterised showers in the calorimeters [30]. The effects of multiple collisions during a single bunch crossing (pile-up) were simulated by overlaying additional inelastic pp collisions generated with PYTHIA 8 [31] and the A3 [32] set of tuned parameters (tune) onto the primary simulated events. These events were then processed with the same reconstruction software as the data. The top-quark mass (m_t) is set to 172.5 GeV in all samples aside from those used to study the impact of the uncertainty in m_t.

The nominal simulated $t\bar{t}$ sample was generated using POWHEG BOX v2 [33–36] (hereafter referred to as POWHEG), which provides matrix elements at NLO in the strong coupling constant, with the NNPDF3.0NLO [37] parton distribution functions (PDFs). The h_{damp} parameter, which controls the matching of the matrix element to the parton shower and effectively regulates the high-p_T radiation against which the $t\bar{t}$ system recoils, was set to $1.5m_t$ [38]. The functional form of the renormalisation (μ_r) and factorisation (μ_f) scales was set to $\sqrt{m_t^2 + p_T^2}$, where p_T is the transverse momentum of the top quark. PYTHIA 8.230 was used to model the parton shower, hadronisation and underlying event, using the A14 tune [39] and the NNPDF2.3LO [40] set of PDFs. In the figures, this sample is referred to as PWG+PY8.

---

[1]ATLAS uses a right-handed coordinate system with its origin at the nominal interaction point (IP) in the centre of the detector and the z-axis along the beam pipe. The x-axis points from the IP to the centre of the LHC ring, and the y-axis points upwards. Cylindrical coordinates (r, ϕ) are used in the transverse plane, ϕ being the azimuthal angle around the z-axis. The pseudorapidity is defined in terms of the polar angle θ as $\eta = -\ln\tan(\theta/2)$. The rapidity is defined as $y = (1/2)[(E + p_z)/(E - p_z)]$. Angular distance is measured in units of $\Delta R \equiv \sqrt{(\Delta\eta)^2 + (\Delta\phi)^2}$.

Additional $t\bar{t}$ samples are used to assess the uncertainty in the modelling of $t\bar{t}$ events and to compare with the data measurements. The dependence of the analysis on the h_{damp} parameter is tested using a sample where the parameter is varied as described in ref. [41]. The impact of using a different parton shower and hadronisation model is evaluated using a sample produced with POWHEG interfaced to HERWIG 7.04 [42, 43]. The settings in POWHEG are the same as for the nominal sample, and the H7UE tune [43] and the MMHT2014LO PDF set [44] are used for HERWIG. To assess the uncertainty due to the choice of generator, events were generated with MADGRAPH5_AMC@NLO 2.6.0 [45] and the NNPDF3.0NLO PDF set. The choice of μ_{r} and μ_{f} is the same as for the POWHEG set-up. The events were interfaced with PYTHIA 8.230. The uncertainty due to the top-quark mass is evaluated by using samples generated in the same way as the nominal $t\bar{t}$ sample, but with the top-quark mass changed to $172, 173, 169$ and 176 GeV. These samples were simulated using the fast simulation of the calorimeter, while all the previously described $t\bar{t}$ samples used the full simulation of the calorimeter. A version of the nominal sample was also produced using the fast simulation to ensure samples with consistent simulation settings were compared when evaluating the impact of the top-quark mass.

All $t\bar{t}$ samples are normalised to the cross-section prediction at NNLO in QCD including the resummation of next-to-next-to-leading logarithmic (NNLL) soft-gluon terms calculated using TOP++ 2.0 [46–52]. For proton-proton collisions at a centre-of-mass energy of $\sqrt{s} = 13$ TeV, this cross-section corresponds to $\sigma(t\bar{t})_{\mathrm{NNLO+NNLL}} = 832 \pm 51$ pb using a top-quark mass of $m_t = 172.5$ GeV. The uncertainties in the cross-section due to the PDF and α_{s} are calculated using the PDF4LHC prescription [53] with the MSTW2008NNLO 68% CL [54, 55], CT10NNLO [56, 57] and NNPDF2.3 5f FFN [40] PDF sets, and are added in quadrature to the effect of the scale uncertainty. Predictions for $t\bar{t}$ production at NNLO matched to the parton shower to produce particle-level predictions are not yet available for the semileptonic final state. In order to evaluate the impact of NNLO QCD corrections, the MC events are reweighted at parton level to match higher-order predictions. The reweighting is performed on the three variables $p_{\mathrm{T}}(t)$, $m(t\bar{t})$ and $p_{\mathrm{T}}(t\bar{t})$, using the kinematics of the top quarks in the MC samples after initial- and final-state radiation. The predictions for $p_{\mathrm{T}}(t)$ and $m(t\bar{t})$ are calculated at NNLO in QCD with NLO electroweak (EW) corrections [15] with the NNPDF3.0QED PDF set using the dynamic renormalisation and factorisation scales $m_{\mathrm{T}}(t)/2$ for $p_{\mathrm{T}}(t)$ and $H_{\mathrm{T}}/4$ for $m(t\bar{t})$ as proposed in ref. [15]. The prediction for $p_{\mathrm{T}}(t\bar{t})$ is calculated at NNLO in QCD [16, 58] with the NNPDF3.0 PDF set and with μ_{r} and μ_{f} set to $H_{\mathrm{T}}/4$. All the predictions use $m_t = 173.3$ GeV.[2] The reweighting was performed iteratively [59], such that at the end of the procedure the reweighted MC sample agrees well with the higher-order prediction for each of the three variables. These samples are referred to as being reweighted to the NNLO prediction in the remainder of the document. The reweighted predictions themselves are not equivalent to complete NNLO plus parton shower calculations and are used to estimate the effect of the NNLO contributions on the measured observables.

---

[2]It was verified that the changes in the distributions from the reweighting procedure are much larger than those expected from changing m_t by 0.8 GeV.

To examine the predictions provided by generators that use higher-order calculations for the additional jets in $t\bar{t}$ events, a sample was generated using SHERPA 2.2.10 [60]. The sample uses NLO-accurate matrix elements for up to one additional parton, and LO-accurate matrix elements for up to four additional partons, calculated with the COMIX [61] and OPENLOOPS [62–64] libraries. They are matched with the SHERPA parton shower [65] using the MEPS@NLO prescription [66–69] and the set of tuned parameters developed by the SHERPA authors to match the NNPDF3.0NNLO set of PDFs [37]. The central scale has the functional form $\mu^2 = m_t^2 + \frac{1}{2}(p_{\mathrm{T},t}^2 + p_{\mathrm{T},\bar{t}}^2)$. The CKKW matching scale [68] of the additional emissions was set to $30\,\mathrm{GeV}$. As this sample contains parts of the inclusive NNLO corrections to $t\bar{t}$ there are two possibilities for normalising the sample: first to use the prediction provided by the generator (referred to as NLO norm. in the following) and second to normalise the sample to the NNLO+NNLL prediction in the same way as for $t\bar{t}$ samples from the other MC generators. The prediction of the inclusive $t\bar{t}$ cross-section from the NNLO+NNLL calculation is 21% higher than the prediction from the SHERPA generator.

The possible contributions from high-energy-scale new physics are modelled using an EFT approach. In this approach the SM Lagrangian is expanded with higher-dimensional operators according to:

$$\mathcal{L}_{\mathrm{EFT}} = \mathcal{L}_{\mathrm{SM}} + \sum_{i,D} \frac{C_i^D}{\Lambda^{D-4}} O_i^D,$$

where each operator O_i^D of dimension D has a corresponding Wilson coefficient C_i, and Λ is the energy scale associated with the new physics. Assuming that the energy scale is high, the sum can be truncated at dimension six, which is the first term that gives non-zero contributions when assuming lepton and baryon number conservation. At dimension six, assuming baryon number conservation and minimal flavour violation [70], there are 59 independent operators. The SM is recovered by setting all the Wilson coefficients to zero. This analysis is restricted to two operators in the Warsaw basis [18] that are expected to have a significant impact on $t\bar{t}$ production: O_{tG} and $O_{tq}^{(8)}$. MC samples were generated with the SMEFT@NLO 1.0.0 UFO model [71] at LO to provide events with $\left(C_{tG}, C_{tq}^{(8)}\right) = (\pm 1\ \mathrm{or}\ 0,\ \pm 1\ \mathrm{or}\ 0)$ and $\Lambda = 1\,\mathrm{TeV}$. The renormalisation and factorisation scales were set to $\mu_{\mathrm{r}} = \mu_{\mathrm{f}} = m_t$ and the $\{m_W, m_Z, G_\mu\}$ EW input scheme was used as outlined in ref. [72]. Two sets of samples were produced: one set includes contributions proportional to Λ^{-2}, corresponding to the interference between the SM and dimension-six operators, and the second set additionally includes terms proportional to Λ^{-4}, corresponding to the square of dimension-six operators. An additional sample including the Λ^{-2} and Λ^{-4} contributions was generated with $\left(C_{tG}, C_{tq}^{(8)}\right) = (0.2, 0.2)$ and $\Lambda = 1\,\mathrm{TeV}$ in order to test for possible biases in the EFT fit. The parton shower and hadronisation were performed using PYTHIA 8.244.

Backgrounds from other processes that include the decay of at least one W or Z boson into leptons were simulated using MC generators. Top-quark production in association with a W boson (tW) and the production of single top quarks in the s-channel were modelled by the POWHEG [73, 74] generator at NLO in QCD using the five-flavour scheme and the NNPDF3.0NLO set of PDFs interfaced to PYTHIA 8.230. The diagram removal scheme [75]

was used to remove interference and overlap between tW and $t\bar{t}$ production. The production of single top quarks in the t-channel was simulated using POWHEG+PYTHIA in the four-flavour scheme [76] with the corresponding NNPDF3.0NLO set of PDFs. The production of $V+$jets ($V = W$ or Z) was simulated with SHERPA 2.2.1 using NLO matrix elements for up to two partons, and LO matrix elements for up to four partons, calculated with the COMIX and OPENLOOPS libraries. They were matched with the SHERPA parton shower using the MEPS@NLO prescription. The NNPDF3.0NNLO set of PDFs was used and the samples were normalised to an NNLO prediction [77]. Events with diboson final states (VV) were also simulated with the SHERPA generator using matrix elements at NLO accuracy in QCD for up to one additional parton and at LO accuracy for up to three additional parton emissions. The showering and hadronisation were performed in the same way as for the $V+$jets samples. Production of $t\bar{t}V$ events forms a small background in the analysis and was modelled using the MADGRAPH5_AMC@NLO 2.3.3 [45] generator at NLO with the NNPDF3.0NLO parton distribution functions. Finally, $t\bar{t}H$ events were modelled using the POWHEG generator at NLO with the NNPDF3.0NLO PDF set. The events were interfaced to PYTHIA 8.230 in a similar way to the nominal $t\bar{t}$ sample.

3 Event selection and reconstruction

All events must contain a primary vertex with at least two associated tracks with $p_{\mathrm{T}} >$ 0.5 GeV. The vertex with the highest $\sum p_{\mathrm{T}}^2$ of the associated tracks is taken as the primary vertex. Electrons are reconstructed from energy deposits in the electromagnetic (EM) calorimeter matched to a track in the inner detector. They must have transverse energy $E_{\mathrm{T}} > 27$ GeV and pass the 'Tight' likelihood-based requirement [78]. They must have pseudorapidity $|\eta| < 2.47$ and be outside the transition region between the barrel and endcap EM calorimeters ($1.37 < |\eta| < 1.52$). Electrons are required to be isolated by applying the 'Tight' requirements on the sum of nearby energy in the calorimeter and the sum of the momenta of nearby tracks [78]. The track associated with the electron must satisfy a requirement of $|d_0|/\sigma_{d_0} < 5$ on the transverse impact parameter significance calculated relative to the beam line, and a requirement of $|z_0 \sin(\theta)| < 0.5$ mm on the longitudinal impact parameter calculated relative to the event primary vertex, where θ is the polar angle of the track. Muons are reconstructed by combining a track found in the inner detector with a matching track found in the muon spectrometer. Selected muons must have $p_{\mathrm{T}} > 27$ GeV and $|\eta| < 2.5$, and pass the 'Medium' identification requirements and 'Tight' isolation requirements [79]. The muons must have impact parameters satisfying $|d_0|/\sigma_{d_0} < 3$ and $|z_0 \sin(\theta)| < 0.5$ mm.

Jets are reconstructed using the anti-k_t clustering algorithm [80, 81] with radius parameter $R = 0.4$ starting from particle-flow objects that exploit both calorimeter and track measurements [82]. Jets are calibrated using measurements in both simulation and data [83] and are required to have $p_{\mathrm{T}} > 26$ GeV and $|\eta| < 2.5$ so that they are within the acceptance of the inner detector. Jets with $p_{\mathrm{T}} < 60$ GeV must also pass a pile-up rejection threshold placed on the output of the multivariate jet-vertex tagger (JVT) [84]. Jets that are close to an electron, $\Delta R(e, j) < 0.2$, are removed to avoid double counting the energy of the elec-

tron. Jets that have less than three tracks and are either close to a muon ($\Delta R(\mu, j) < 0.2$) or have a track that is part of the muon are also removed. This avoids counting the energy deposits of muons as jets. An additional requirement of $\Delta R(\ell, j) > 0.4$ then ensures that electrons and muons are well separated from jets; leptons failing this requirement are rejected. Jets that contain b-hadrons (b-jets) are identified by the use of the DL1r multivariate algorithm [85, 86]. The selected working point results in an efficiency of 77% per b-jet, as measured in simulated $t\bar{t}$ events. These jets are hereafter referred to as b-tagged jets.

Highly boosted top quarks ($p_T \gtrsim 2m_t$) that decay hadronically can produce decay products that are not resolved as three separate jets. These boosted top quarks are therefore identified using large-radius jets so as to capture all the decay products in a single jet. These large-R jets are reconstructed by applying the anti-k_t clustering algorithm with radius parameter $R = 1.0$ to the selected $R = 0.4$ (small-R) jets [87]. Any small-R jets that have less than 5% of the p_T of the corresponding large-R jet are removed from that large-R jet. This trimming procedure [87, 88] is designed to remove jets that are more likely to originate from pile-up. The large-R jets must have $p_T > 355$ GeV and $|\eta| < 2.0$. In order to select jets consistent with a hadronically decaying top quark, the large-R jets must contain at least one b-tagged jet and have an invariant mass in the range $120 < m < 220$ GeV. If more than one large-R jet passes these requirements, the one with the highest p_T is assumed to be the one originating from the hadronically decaying top quark. This selected large-R jet is referred to as the top-tagged jet. The missing transverse momentum (E_T^{miss}) is reconstructed from the negative vector sum of calibrated leptons, small-R jets and the soft term (calculated using other tracks associated with the primary vertex) [89].

Events are required to have exactly one selected lepton, at least one top-tagged jet and at least two b-tagged jets. At least one of the b-tagged jets must not be a constituent of the top-tagged jet. The selected lepton must match a corresponding electron or muon trigger object. Consistency with the expected boosted topology is ensured by requiring the lepton to be close to a b-tagged jet, $\Delta R(\ell, b) < 2.0$, and the same b-tagged jet must not be a constituent of the top-tagged jet. A requirement of $\Delta R(e, t) > 1.0$ prevents the selection of large-R jets seeded by a high-p_T electron. To reduce the multijet background, events must have $E_T^{\text{miss}} > 20$ GeV and $E_T^{\text{miss}} + m_T^W > 60$ GeV, where $m_T^W = \sqrt{2p_T^\ell E_T^{\text{miss}} \left(1 - \cos \Delta\phi\left(p_T^\ell, E_T^{\text{miss}}\right)\right)}$ is the transverse mass of the W boson. The invariant mass of the lepton and the nearest b-tagged jet, $m_{\ell b}$, must be less than 180 GeV. This selection requirement retains signal events where the lepton and b-jet originate from an on-shell top-quark decay, while rejecting events from tW single top-quark production [90].

The kinematics of the top quarks are obtained from the selected objects. The selected top-tagged jet is used as the estimate of the hadronically decaying top quark. The leptonically decaying top quark is reconstructed from the four-vector sum of the lepton, the closest b-tagged jet and the neutrino. The x and y components of the missing transverse momentum provide estimates of the corresponding components of the neutrino four-vector. The z-component is calculated using the constraint that the lepton-neutrino system has invariant mass equal to the W boson mass [91]. If there are two real solutions to the corresponding quadratic equation, the solution that gives the smallest value for the mass of the

leptonically decaying top quark is used. In the case of complex solutions, only the real part is used. Any jets other than the constituents of the top-tagged jet and the *b*-tagged jet used in reconstructing the leptonically decaying top quark are referred to as additional jets.

4   Cross-section measurements

The strategy used to measure differential cross-sections is to correct (unfold) the data for detector effects and can be summarised in the following equations:

$$\frac{d\sigma}{dX} = \frac{N_i^u}{\mathcal{L}\Delta X_i}$$

$$N_i^u = \frac{1}{f_{\text{eff}}^i} \sum_j M_{ij}^{-1} f_{\text{acc}}^j \left(N_{\text{d}}^j(\text{JSF}) - N_{\text{b}}^j \right),$$

(4.1)

where X represents the variable being measured. The data are first corrected by applying a jet energy scale factor (JSF) that ensures that the mean of the reconstructed top-quark mass agrees with the simulation, as discussed in section 4.2. The number of events in each bin after that correction, $N_{\text{d}}^j(\text{JSF})$, then have the background contributions (N_{b}^j) subtracted. The yields are then corrected with the factor f_{acc}^j to account for $t\bar{t}$ events that do not pass the fiducial requirements. An iterative Bayesian unfolding [92] (denoted by M_{ij}^{-1}) implemented in RooUnfold [93] is used to correct for the limited resolution of the detector. The factor f_{eff}^i corrects for events that pass the fiducial requirements but do not pass the detector-level event selection. Finally, the events are corrected for the integrated luminosity $(\mathcal{L})$ and the bin width (ΔX_i). The same methodology is used for double-differential distributions. The inclusive cross-section is determined by using all the selected events in a single bin as input to eq. (4.1). All the correction factors are determined using the nominal $t\bar{t}$ simulation. In addition to the absolute differential cross-section measurements, normalised differential cross-section measurements are produced by dividing by the measured inclusive cross-section. The normalised measurements provide a way to evaluate how well a distribution's shape agrees between data and theory without considering the overall normalisation. This is relevant, for example, in new-physics searches where the normalisation of $t\bar{t}$ production can be fitted from the data, while the shape relies on the simulation [94]. As the normalised measurements contain less information than the absolute measurements, they are presented in appendix A. The different components of the measurement methodology are discussed in the following subsections and the section is concluded by comparing the observed data with the expectation from the $t\bar{t}$ simulation and the background estimates.

4.1   Background estimate

The event selection is designed to reject the vast majority of background events such that the modelling of the background processes has a minor impact on the measurements. The main backgrounds to the signal process are expected to be from tW single top-quark production and $W+$jets production. These backgrounds, along with smaller backgrounds from $t\bar{t}V$, $t\bar{t}H$, $Z+$jets and diboson production, are estimated from the simulated samples described in section 2. Events can also pass the selection if the lepton originates from the

decay of a light- or heavy-flavour hadron, or due to the misreconstruction of a jet as a lepton. These events are referred to as the multijet background in the remainder of the paper. The contribution from this background is estimated using the matrix method [95], which uses a selection of events in data where the lepton requirements are less stringent than the nominal requirements.

4.2   Correction of the jet energy

Uncertainties in the jet energy scale are significant in many $t\bar{t}$ cross-section measurements [9, 96–99]. In order to reduce the impact of such uncertainties in this analysis, the reconstructed invariant mass of the selected hadronically decaying top quark ($m^{t,h}$) is used in conjunction with the precisely known value of the top-quark mass [100, 101]. The overall jet energy scale difference between data and simulation for small-R jets is parameterised with a jet energy scale factor, JSF. Assuming that the top-quark mass is known, the $m^{t,h}$ distribution can be used to measure the JSF in the data. In this way, any overall jet energy scale difference between data and simulation is absorbed into the JSF and does not impact the extracted cross-sections, thereby reducing the impact of the jet energy scale uncertainties on the measured cross-sections. The jet energy scale uncertainties, which are included in the measurement as described in section 5, are not completely suppressed by the method because they have kinematic dependencies that cannot be absorbed by the JSF. The uncertainty in the top-quark mass effectively limits the precision to which the overall jet energy scale difference between data and simulation can be absorbed by the method, but the high precision of the top-quark mass measurements means the corresponding systematic uncertainty is not significant in the measurements (see section 5.4). Figure 1a shows the $m^{t,h}$ distribution for three different JSF values. The distributions are obtained by applying the JSF to the energy of every jet in the nominal $t\bar{t}$ sample and the simulation samples used for the background estimates. The JSF is applied on top of the standard ATLAS jet calibration discussed in section 3. Figure 1b shows that the mean of the $m^{t,h}$ distribution[3] ($\overline{m^{t,h}}$) depends linearly on the JSF, as expected from the fact the top-tagged jet four-vector is a sum of the four-vectors of the constituent small-R jets. The $\overline{m^{t,h}}$ value in data is used to determine the JSF in data from this linear relationship. The distribution of $m^{t,h}$ in data is shown in figure 1c with JSF $= 1$. In order to visualise possible differences in the shape of the distribution, the expectation is normalised to the data yield. Good agreement is seen between the data and the expectation, and the JSF is measured to be 0.99965 ± 0.00087, where the uncertainty is due to the number of observed data events. The energy of each reconstructed jet in the data is then corrected with $1/\text{JSF}$ and the event selection is reapplied, yielding the corrected distributions that are used as input for the cross-section calculation. The statistical uncertainty of the JSF is included in the measurement as discussed in section 5.3.

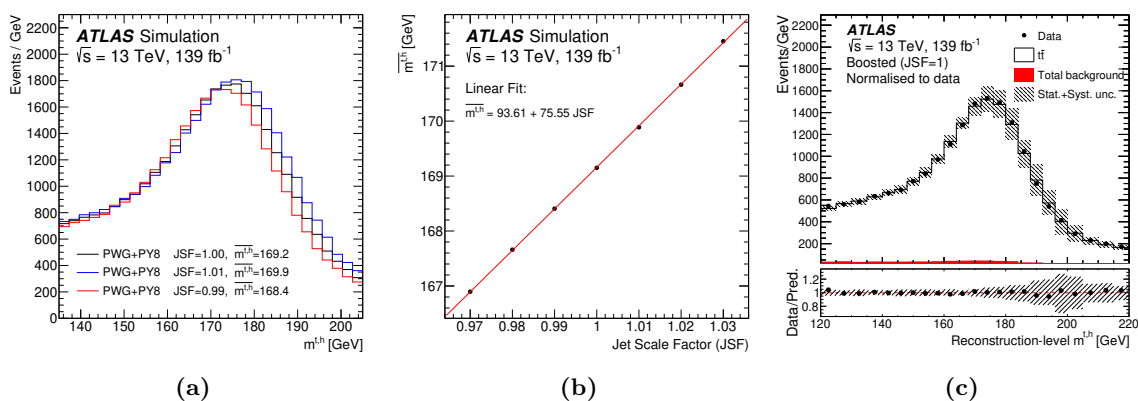[3]The mean is calculated from events that have $135 < m^{t,h} < 205$ GeV.

Figure 1. (a) The distribution of the invariant mass of the top-tagged jet ($m^{t,h}$) for the expected signal plus background for three example values of the JSF. PWG+PY8 corresponds to the POWHEG+PYTHIA sample. (b) The mean of the same distribution ($\overline{m^{t,h}}$) as a function of JSF and a linear fit to the simulated samples. Uncertainties in the mean due to limited MC sample size are included for each point, but are too small to be visible. (c) The $m^{t,h}$ distribution observed in the data compared with the expected signal and background processes for JSF = 1, where the expectation is normalised to the number of events observed in data.

4.3 Fiducial requirements

The cross-sections are measured at particle level with a set of requirements designed to keep the measured phase-space close to that selected by the event selection. Particle-level objects are defined using only stable particles, defined to have a lifetime > 30 ps, taken from the MC generator record. Electrons, muons and neutrinos not originating, either directly or through a τ-lepton decay, from a hadron are referred to as prompt in the following. The four-momenta of prompt photons within $\Delta R < 0.1$ are added to the leptons ('dressing') and the corresponding photons are removed from the list of stable particles. The dressed leptons, considered in the particle-level selection, are then required to have $p_{\rm T} > 27$ GeV and $|\eta| < 2.5$.

Particle-level small-R jets are obtained by clustering all stable particles with $|\eta| < 4.5$ with the anti-k_t algorithm ($R = 0.4$), excluding dressed leptons and prompt neutrinos. These jets are required to have $p_{\rm T} > 26$ GeV and $|\eta| < 2.5$. A small-R jet is considered a b-jet if it is ghost-matched [102] to a b-hadron with $p_{\rm T} > 5$ GeV. Dressed muons and electrons separated by $\Delta R < 0.4$ from a jet are excluded. The large-R jets at particle level are built by clustering the selected small-R jets with the anti-k_t algorithm ($R = 1.0$), using the same approach as for the data. To remain consistent with the detector-level selection, the large-R jets are required to have $p_{\rm T} > 355$ GeV, $|\eta| < 2.0$, an invariant mass between 120 GeV and 220 GeV, and one of the small-R jets used to build the large-R jet must be a b-jet. If more than one large-R jet passes the selection the one with higher $p_{\rm T}$ is considered the hadronically decaying top-quark candidate. The particle-level $E_{\rm T}^{\rm miss}$ is the magnitude of the vector sum of the transverse momenta of all the neutrinos. The reconstruction of the leptonically decaying top-quark candidate is analogous to that in data, using the lepton, b-jet and neu-

trino (see section 3). The constraint on the W boson mass is used to calculate the neutrino p_z in the same way as in data. The particle-level events must pass selection requirements which are the same as in the data selection, but applied to the particle-level objects.

4.4 Corrections for detector effects

Top-quark pair events that fail the fiducial selection requirements detailed in section 4.3 can still pass the event selection requirements. For example, the top-quark large-R jet can fail the p_T requirement at particle level, but due to the limited detector resolution can be measured above the requirement at detector level. These effects are corrected for with the factor f_{acc}^j. An example of the distribution of this factor for $p_T^{t,h}$ is shown in figure 2a. The corrections are largest at low p_T due to the resolution effects. The iterative unfolding uses as input the migration matrix M which encodes the relationship between the particle-level and detector-level distributions. For the measurements performed as a function of two observables, the matrix spans the full two-dimensional space, such that all migrations are accounted for. The binning of the migration matrix is chosen such that the majority of the events lie on the diagonal and there are sufficient simulated events in each bin to achieve stable estimates of the systematic uncertainties. The migration matrix for $p_T^{t,h}$ is shown in figure 2b and good correspondence between particle level and detector level is observed. The number of iterations used in the unfolding is determined by minimising the average correlation factor as defined in ref. [103]. For a limited number of variables, the number of iterations is adjusted to ensure good closure of the method as discussed in the following subsection, resulting in either two, three or four iterations being used. The final correction, f_{eff}^i, is for events that pass the particle-level selection but fail the detector-level selection. This efficiency, shown in figure 2c for $p_T^{t,h}$, is around 0.3, with the largest effect being due to the efficiency of the b-tagging, which is approximately 77% per b-jet. The shape of f_{eff}^i originates from the fact that the selection efficiency depends on the kinematics of the events. For example, the efficiency of the b-tagging is highest for jets with $p_T \sim 100$ GeV and is lower at higher and lower p_T values.

4.5 Validation of the measurement technique

Tests are performed to ensure the measurement is unbiased within the expected statistical uncertainty. In order to check for biases due to the iterative procedure, the simulated samples are divided into two equally sized samples. One sample is used as pseudo-data and the other sample is used to derive the correction factors and migration matrix. Good closure is observed between the unfolded pseudo-data and the corresponding particle-level distributions. In order to check that there is no significant bias originating from the choice of model used to derive the corrections applied to the data, pseudo-data are created with distorted differential distributions and injected into the measurement procedure. To test that the unfolding is not sensitive to the differences seen between the data and the nominal expectation, modified distributions are derived by reweighting the nominal $t\bar{t}$ MC sample as a function of particle-level observables such that the reweighted detector-level distributions are similar to the observed data. To test that the unfolding would not be biased if new physics is present in the data, modified distributions are also created by adding EFT
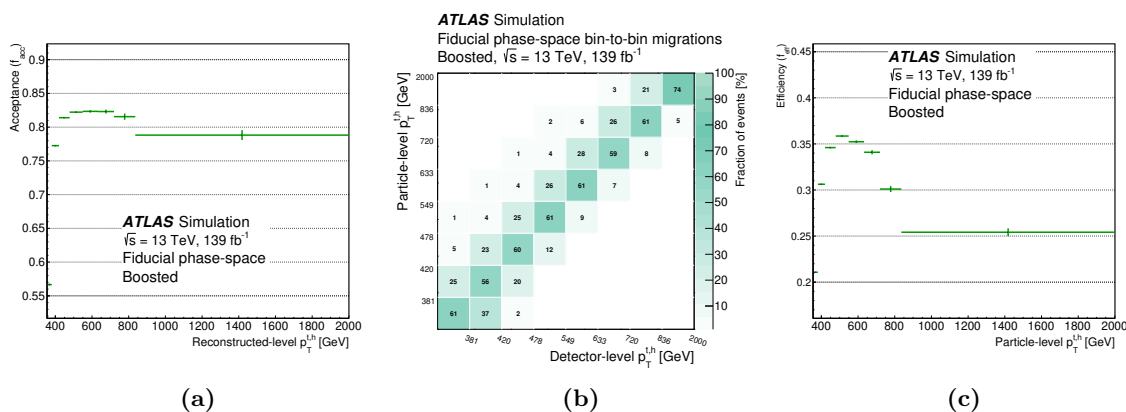
Figure 2. The acceptance and efficiency corrections for $p_T^{t,h}$ are shown in (a) and (c). The migration matrix for $p_T^{t,h}$ is shown in (b). For the migration matrix, the numerical value of the bin is displayed if it is $> 1\%$.

contributions to the nominal $t\bar{t}$ MC sample. Three separate tests are performed. In the first two tests, the MC samples that include terms up to Λ^{-2} are rescaled to produce pseudo-data equivalent to $(C_{tG}, C_{tq}^{(8)}) = (0.25, 0)$ and $(C_{tG}, C_{tq}^{(8)}) = (0, 0.25)$. The third test uses pseudo-data derived from the MC sample including terms up to Λ^{-4} with $(C_{tG}, C_{tq}^{(8)}) = (0.2, 0.2)$. Figure 3 shows the result of these tests for $p_T^{t,h}$. The figures display the ratio of the unfolded pseudo-data to the corresponding particle-level prediction. In each case, the ratio is found to be compatible with unity, demonstrating that there is no significant bias from the measurement technique. The size of the difference between the nominal MC sample and the pseudo-data at particle level is also shown in the figure by the dotted lines. The sample with $(C_{tG}, C_{tq}^{(8)}) = (0.2, 0.2)$ is also used to verify that the extracted JSF does not change significantly from the value extracted when using the nominal SM MC sample. The possible biases originating from systematic uncertainties are discussed in section 5.

4.6 Choice of observables

The measured observables can be split into two categories, those characterising the kinematics of the top quarks and those probing additional radiation in the events. In the first category are:

- $p_T^{t,h}$, $p_T^{t,\ell}$: the transverse momenta of the hadronically and leptonically decaying top quarks,

- $|y^{t,h}|$, $|y^{t,\ell}|$: the rapidity of the top quarks,

- $|y^{t\bar{t}}|$: the rapidity of the $t\bar{t}$ system,

- $m^{t\bar{t}}$: the invariant mass of the $t\bar{t}$ system,

- $\Delta\phi(b_\ell, t_h)$: the azimuthal separation between the hadronically decaying top quark and the b-tagged jet associated with the leptonically decaying top quark,

- $H_T^{t\bar{t}}$: the scalar sum of the transverse momenta of the top quarks.
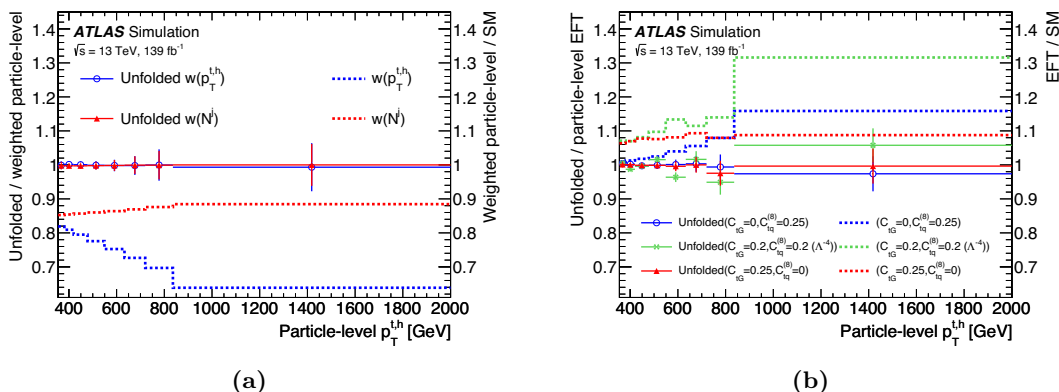
Figure 3. The ratio of unfolded pseudo-data to the corresponding particle-level prediction as a function of $p_T^{t,h}$ is shown in (a) for pseudo-data built by reweighting the MC sample to match the data in the $p_T^{t,h}$ (solid blue) and N^j (solid red) distributions. The equivalent ratio is shown in (b) for pseudo-data built from the nominal MC sample and adding contributions corresponding to $C_{tG} = 0.25$ (blue), $C_{tq}^{(8)} = 0.25$ (red, including only Λ^{-2} contributions) and $(C_{tG}, C_{tq}^{(8)} = 0.2, 0.2)$ (green, including Λ^{-2} and Λ^{-4} contributions). The dotted lines show in (a) the ratio of the weighted particle-level distribution to the particle-level distribution from the nominal $t\bar{t}$ MC sample and in (b) the ratio of the particle-level distribution of the EFT to the nominal $t\bar{t}$ sample. The y-axis on the right of each plot refers to these dotted lines.

The $H_T^{t\bar{t}}$, $m^{t\bar{t}}$ and top-quark p_T distributions are expected to be sensitive to new-physics effects. The rapidity distributions can potentially probe the parton distribution functions [104]. These variables were measured in previous publications [9, 11] but less precisely than in this analysis. In the second category are a set of variables that seek to probe the additional radiation in detail:

- $p_T^{t\bar{t}}$: the transverse momentum of the $t\bar{t}$ system,

- N^j: the number of additional jets,

- $p_T^{j,1}$, $p_T^{j,2}$: transverse momenta of the two leading additional jets,

- $\Delta\phi(j_1, t_h)$, $\Delta\phi(j_2, t_h)$: azimuthal angles between the two leading additional jets and the hadronically decaying top quark,

- $\Delta\phi(j_1, j_2)$: azimuthal angle between the two leading additional jets,

- $\Delta\phi(t_h, t_\ell)$: azimuthal angle between the two top quarks,

- $m(j_1, t_h)$: invariant mass of the leading additional jet and the hadronically decaying top quark,

- $H_T^{t\bar{t}+\text{jets}}$: scalar sum of the transverse momenta of the top quarks and the additional jets.

The variables involving one or two additional jets use the subsets of selected events that contain at least one or two additional jets. These eight variables were not measured previously for highly boosted $t\bar{t}$ events. Finally, a set of two-dimensional cross-section measurements that characterise the additional radiation as a function of $p_\mathrm{T}^{t,h}$ and N^j are presented:

- $p_\mathrm{T}^{j,1}$ in bins of $p_\mathrm{T}^{t,h}$,

- $p_\mathrm{T}^{j,1}$ in bins of N^j,

- $\Delta\phi(j_1, t_h)$ in bins of $p_\mathrm{T}^{t,h}$,

- $\Delta\phi(j_1, t_h)$ in bins of N^j.

4.7 Observed data distributions

A total of 75 743 events are observed after the JSF correction and data selection. The data are compared with the expectation from the simulation and background estimates in table 1. The uncertainties shown in the table are the combined effect of the statistical, detector systematic, and background modelling uncertainties (described in section 5). These uncertainties are shown because they do not change the predicted cross-section and hence directly impact the measured results. The selected sample is expected to be dominated by $t\bar{t}$ events and have a purity > 95%. The largest background contribution is from tW single top-quark production. The data yield is observed to be 14% lower than the expectation from the nominal signal and background predictions, which is consistent with the trend observed in the previous ATLAS measurement, where the cross-section at high top-quark p_T was found to be smaller than the expectation from POWHEG+PYTHIA [9]. Figures 4–6 show the data distributions for the selected observables at reconstruction level. In order to visualise the level of agreement in the shape of the distributions, the sum of the $t\bar{t}$ and expected background events is normalised to the data yield in these figures. The simulation is found to give a reasonable description of the data; however, in some distributions trends can be observed in the ratio between data and expectation. In particular, the $p_\mathrm{T}^{t,h}$ and $p_\mathrm{T}^{t,\ell}$ distributions are seen to be softer in data than predicted, and the shape of $\Delta\phi(t_h, t_\ell)$ differs between data and simulation. As discussed in section 4.5, these differences are used to check that the unfolding procedure is robust against potential mismodelling of the expected $t\bar{t}$ distributions. No significant biases are observed in these tests.

Process	Expected events
$t\bar{t}$	$84\,200 \pm 2600$
Single top quark	1710 ± 280
$t\bar{t}V$ ($t\bar{t}W + t\bar{t}Z + t\bar{t}H$)	850 ± 110
Multijet	560 ± 370
$W +$ jets	420 ± 160
$Z +$ jets	84 ± 43
Diboson	41 ± 21
Total prediction	$87\,900 \pm 2700$
Data	$75\,743$

Table 1. Event yields for measured data, simulated $t\bar{t}$ signal and background events. The uncertainty values are symmetrised and indicate the combined effect of statistical, detector and background modelling uncertainties.

5 Systematic uncertainties

Systematic uncertainties affect the measured cross-section through the unfolding corrections discussed in section 4. The systematic uncertainty from each source is evaluated by creating pseudo-data where the source of uncertainty was varied in the simulation and background model. The modified pseudo-data sample is treated as if it is data and differential cross-sections are extracted using the analysis procedure described in section 4. Of particular relevance is the JSF, which is extracted for each pseudo-data sample as described in section 4.2. In this way, correlations between the different aspects of the analysis methodology are fully accounted for. The difference between the cross-sections extracted from the varied pseudo-data and the cross-sections extracted from the nominal simulation is used as an estimate of the impact of that uncertainty source. For the signal modelling components, where alternative $t\bar{t}$ simulations are employed, the cross-sections extracted from the pseudo-data are compared with the corresponding particle-level distributions to assess the impact of the uncertainty. The total uncertainty is then calculated assuming all the systematic uncertainties are uncorrelated. A description of the different uncertainty components is given in the following subsections. Table 2 summarises the impact of the systematic uncertainties on the inclusive cross-section measurement. The benefit of the JSF correction procedure is evaluated by comparing the impact of each source for the case where no JSF correction is applied with the nominal analysis set-up. The precision of the measurement is seen to improve significantly due to the JSF correction. When examining the impact of the individual uncertainty sources, some distinct patterns are apparent. Uncertainty sources such as the b-tagging and lepton uncertainties are not affected by the JSF correction because they do not influence either the jet energy measurement or the $m^{t,h}$ distribution. The impact of the jet energy scale uncertainty is largely reduced because the JSF is able to absorb any overall jet energy scale differences between data and simulation. The top-quark mass uncertainty increases with the introduction of the JSF procedure be-
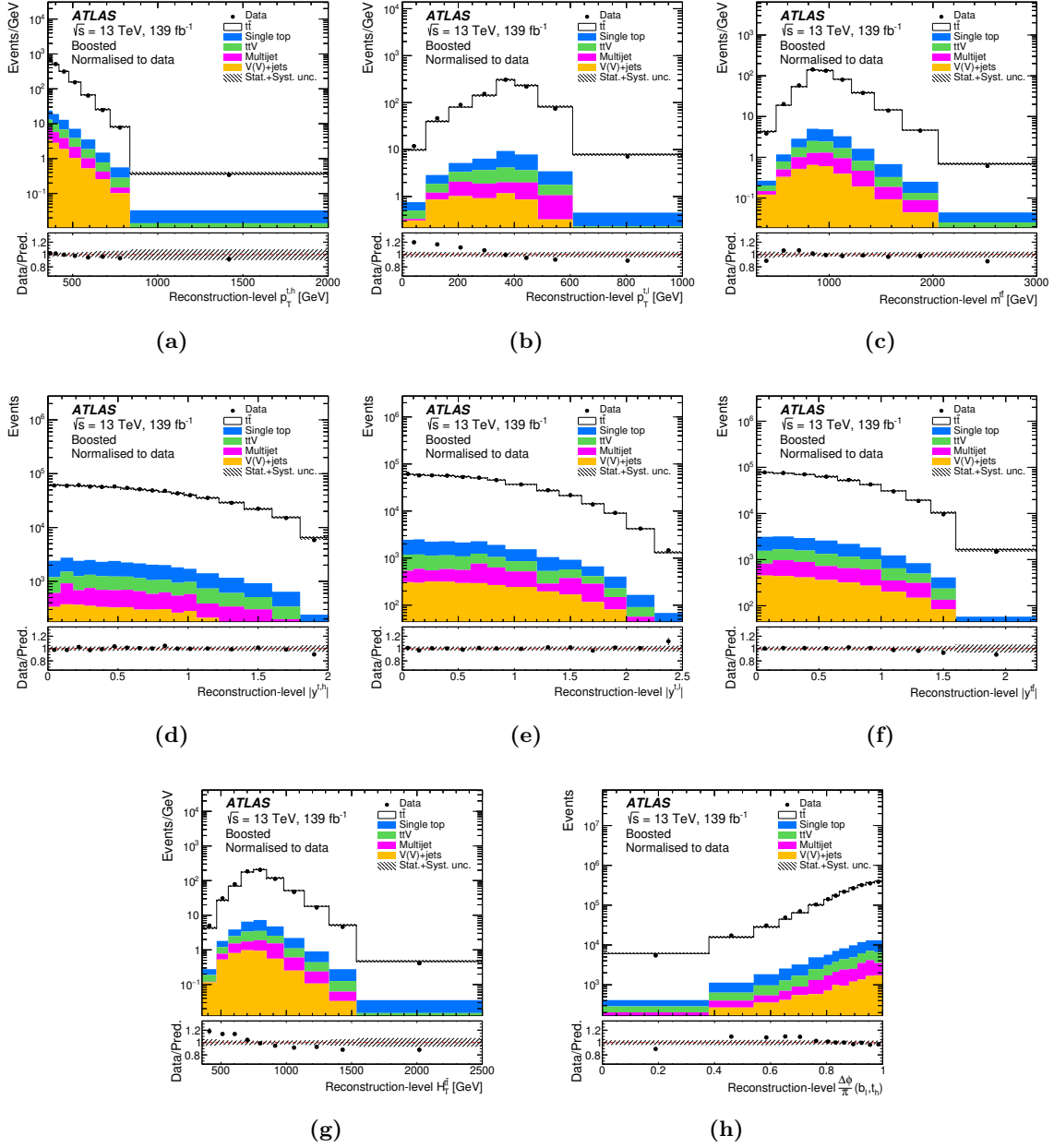
Figure 4. Distributions of the observables sensitive to the kinematics of the top quarks: (a) $p_\mathrm{T}^{t,h}$, (b) $p_\mathrm{T}^{t,\ell}$, (c) $m^{t\bar{t}}$, (d) $|y^{t,h}|$, (e) $|y^{t,\ell}|$, (f) $|y^{t\bar{t}}|$, (g) $H_\mathrm{T}^{t\bar{t}}$ and (h) $\Delta\phi(b_\ell, t_h)$. The data are compared with the expectation from the simulation and background estimates. The total prediction is normalised to the same number of entries as the data. The lower panel in each subfigure shows the ratio of the data to the normalised expectation. The shaded band represents the uncertainties originating from the limited data sample size and systematic uncertainties ($t\bar{t}$ modelling uncertainties are not included).

Figure 5. Distributions of observables sensitive to jets produced in association with the $t\bar{t}$ system: (a) $p_{\mathrm{T}}^{t\bar{t}}$, (b) $\Delta\phi(t_h, t_\ell)$, (c) $H_{\mathrm{T}}^{t\bar{t}+\mathrm{jets}}$, (d) N^j, (e) $p_{\mathrm{T}}^{j,1}$, (f) $m(j_1, t_h)$ and (g) $\Delta\phi(j_1, t_h)$. The data are compared with the expectation from the simulation and background estimates. The total prediction is normalised to the same number of entries as the data. The lower panel in each subfigure shows the ratio of the data to the normalised expectation. The shaded band represents the uncertainties originating from the limited data sample size and systematic uncertainties ($t\bar{t}$ modelling uncertainties are not included).
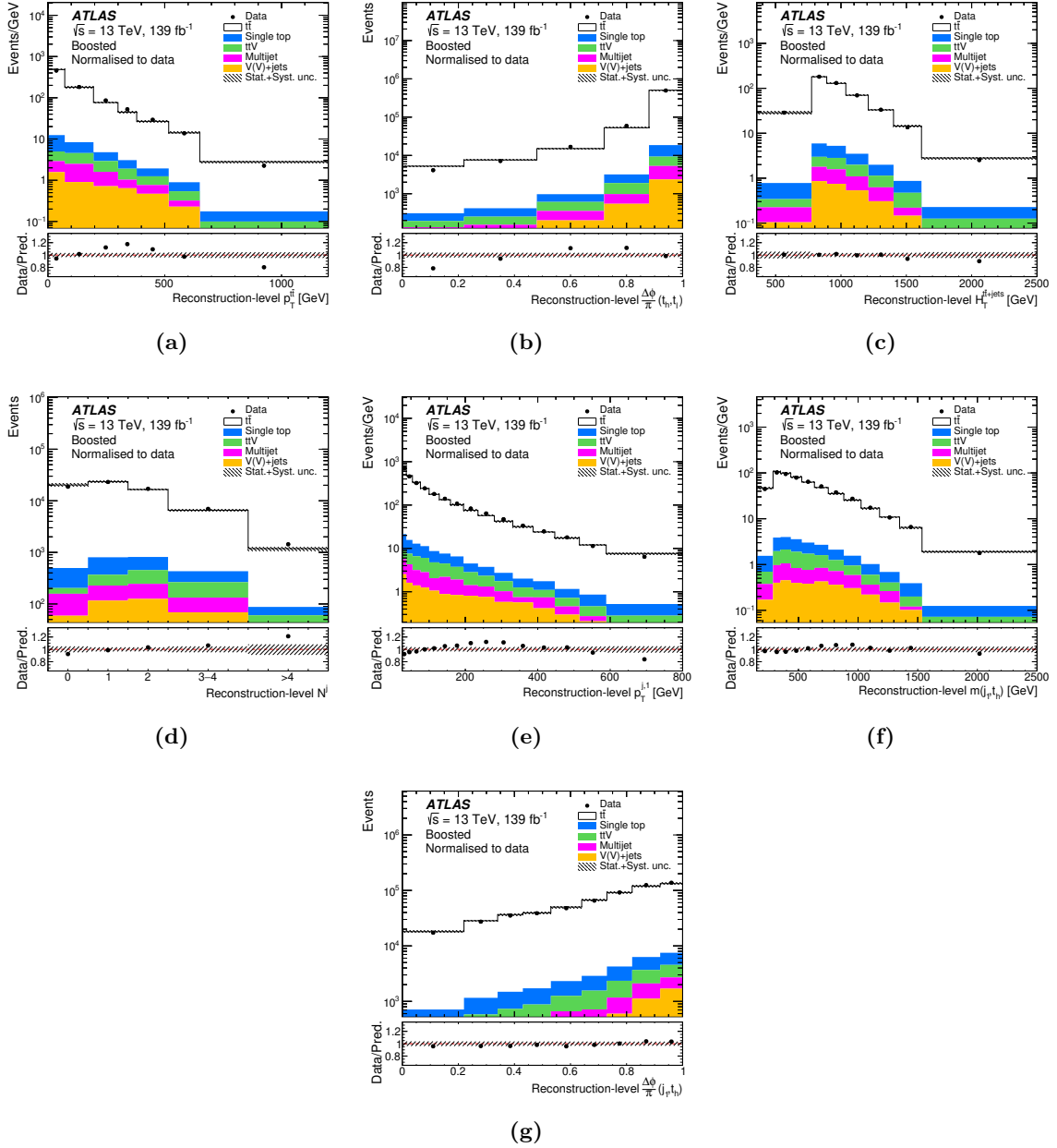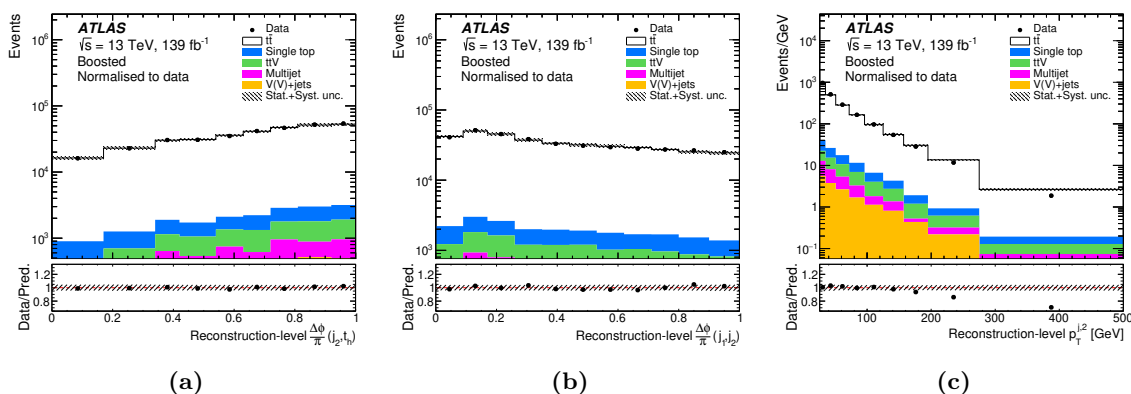
Figure 6. Distributions of observables sensitive to the second leading additional jet: (a) $\Delta\phi(j_2, t_h)$, (b) $\Delta\phi(j_1, j_2)$ and (c) $p_T^{j,2}$. The data are compared with the expectation from the simulation and background estimates. The total prediction is normalised to the same number of entries as the data. The lower panel in each subfigure shows the ratio of the data to the normalised expectation. The shaded band represents the uncertainties originating from the limited data sample size and systematic uncertainties ($t\bar{t}$ modelling uncertainties are not included).

cause the mean of the $m^{t,h}$ distribution is directly related to the top-quark mass. The data and MC statistical uncertainties are also increased by the use of $m^{t,h}$; the increased statistical uncertainty is traded for the reduced systematic uncertainties. The reduction of the uncertainties is also shown in figure 7, which displays the effect of the JSF correction on the uncertainty for three differential distributions, both for the total uncertainty and for the jet energy scale (JES) uncertainty. In most bins the JES uncertainty is reduced due to the introduction of the JSF. There are a small number of bins where the JES uncertainty increases due to the JSF; this occurs when the kinematics of the jets in these bins are very different from the average jet kinematics in the sample and hence the average correction provided by the JSF causes the systematic uncertainty from the JES to increase. Figure 8 summarises the impact of the systematic uncertainties on three example observables. The modelling uncertainties generally have the largest impact on the measurement, while the JES and b-tagging uncertainties are important in particular phase-space regions.

Source	Uncertainty [%]	Uncertainty [%] (no JSF)
Statistical (data)	±0.4	±0.4
JSF statistical (data)	±0.4	—
Statistical (MC)	±0.2	±0.1
Hard scatter	±0.5	±0.8
Hadronisation	±2.0	±1.8
Radiation (ISR/FSR + h_{damp})	+1.0 −1.6	+1.4 −2.3
PDF	±0.1	±0.1
Top-quark mass	+0.8 −1.1	±0.1
Jets	±0.7	±4.2
b-tagging	±2.4	±2.4
Leptons	±0.8	±0.8
$E_{\mathrm{T}}^{\mathrm{miss}}$	±0.1	±0.1
Pile-up	±0.4	±0.0
Luminosity	±1.8	±1.8
Background modelling	±0.6	±0.6
Total systematic uncertainty	+4.1 −4.3	+5.8 −6.0
Total	+4.1 −4.3	+5.8 −6.0

Table 2. Fractional uncertainty breakdown for the inclusive $t\bar{t}$ cross-section both with and without the JSF method applied.

5.1 Lepton reconstruction and identification

The uncertainty in the efficiency to reconstruct and identify electrons and muons was obtained by studying $Z \to ee/\mu\mu$ events as discussed in refs. [78, 79]. Similar studies were performed to determine the uncertainty in the trigger efficiencies for electrons and muons [26, 27]. The impact of these uncertainties on the analysis is small, but they are the largest part of the 'Leptons' entry in table 2. The uncertainties in the electron and muon energy / momentum scales and resolutions were determined using resonance decays [78, 105] and are found to have a negligible impact on the analysis.

5.2 Jet reconstruction and b-tagging

The JES and jet energy resolution of small-R jets were determined using a combination of simulation, test beam and in situ measurements [83]. The corresponding uncertainties are evaluated using a model with 30 independent components for the jet energy scale and 8 independent components for the jet energy resolution. The uncertainties are propagated to the large-R jets such that the correlations between the energies of small-R and large-R jets
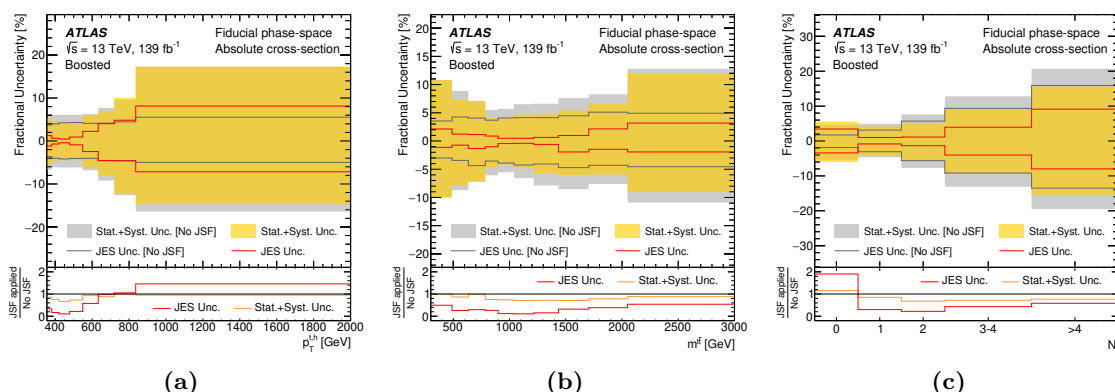
Figure 7. Effect of the JSF correction on the total uncertainty of the cross-section measurements as a function of (a) p_T of the hadronically decaying top quark ($p_T^{t,h}$), (b) invariant mass of the $t\bar{t}$ system ($m^{t\bar{t}}$) and (c) the number of additional jets in the event (N^j). The yellow (grey) bands represent the total uncertainty with (without) the JSF correction applied. The red (grey) line in the upper pad shows the JES uncertainty with (without) the JSF method. The bottom pad shows the ratios of the absolute size of the uncertainty with and without the JSF correction applied, in red for the JES uncertainty and in yellow for the total uncertainty.
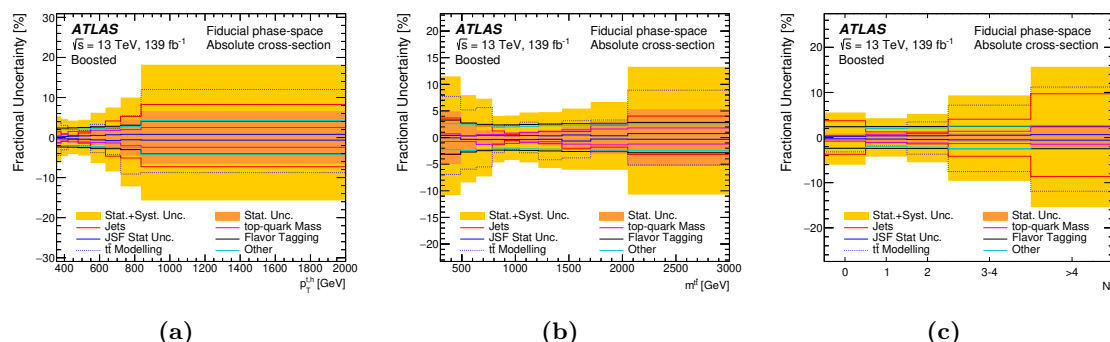

Figure 8. Fractional uncertainties of the absolute cross-section measurement as a function of (a) p_T of the hadronically decaying top quark ($p_T^{t,h}$), (b) invariant mass of the $t\bar{t}$ system ($m^{t\bar{t}}$) and (c) the number of additional jets in the event (N^j). The line labelled 'Jets' includes the uncertainties from the JES, JER and JVT requirements. The line labelled '$t\bar{t}$ Modelling' includes all the uncertainties discussed in section 5.4, with the exception of the uncertainty in the top-quark mass, which is shown separately.

are maintained. The impact of the JES uncertainties on the measurement is significantly reduced by the JSF procedure; for example, the uncertainty in the inclusive cross-section due to the JES is reduced from 4.0% to 0.4%. The JES uncertainties have their largest impact in regions with high jet multiplicity. The impact of the jet energy resolution uncertainty is generally smaller than that due to the jet energy scale uncertainty. The uncertainty in the efficiency of the JVT requirement for pile-up suppression is also considered [84].

The performance of the *b*-tagging algorithm has been calibrated in the data [85]. The corresponding uncertainties are propagated to the analysis by using an uncertainty model

containing 9/4/4 independent variations for the b-/c-/light-jet calibrations and two components for the MC-based extrapolation to jets with very high p_{T}. These uncertainties have a moderate impact on the fiducial cross-section measurement as seen in table 2 and do not significantly vary in size as a function of the measured observables, as seen in figure 8.

5.3 JSF statistical uncertainty

The statistical uncertainty due to the limited number of data events in the determination of the JSF is evaluated by performing pseudo-experiments in which the data yields in the $m^{t,h}$ distribution are varied according to a Poisson distribution. As the $m^{t,h}$ distribution is found to be largely uncorrelated with all measured observables, this uncertainty is assumed to be uncorrelated with the statistical uncertainty of the cross-section measurement. A similar procedure is used to assess the statistical uncertainty of the JSF due to the limited size of the simulated event samples.

5.4 $t\bar{t}$ modelling

Uncertainties in the modelling of $t\bar{t}$ production affect the unfolding corrections as well as the $m^{t,h}$ distribution that is used to determine the JSF. Several separate variations of the $t\bar{t}$ model are considered in the analysis.

The uncertainty due to the choice of parton shower and hadronisation models is assessed by using the events generated by POWHEG+HERWIG to build pseudo-data, repeating the analysis, and comparing the unfolded distributions with the particle-level prediction of POWHEG+HERWIG. The impact of this uncertainty is quite important and largest at low $p_{\mathrm{T}}^{t,h}$. The uncertainty originating from the choice of generator is assessed by using pseudo-data created from the MADGRAPH5_AMC@NLO+PYTHIA sample. The impact of this uncertainty is relatively small. The uncertainty originating from the scales used in the matrix elements and the parton shower is evaluated by using pseudo-data built from the samples with variations of the h_{damp} parameter, and by using pseudo-data created by reweighting the nominal sample to correspond to different values of the μ_{r} and μ_{f} scales in the matrix elements, the parameters in the showering tune [41], and the μ_{r} scale in the final-state parton shower. The reweighted samples using the changes in the scales in the matrix elements and the changes in the parameter values in the showering tune are referred to as the ISR variations. The reweighted samples using the varied scale in the final-state parton shower are referred to as the FSR variations. These modelling uncertainties are found to be particularly important at high $p_{\mathrm{T}}^{t,h}$ (figure 8a).

The extraction of the JSF relies on the measured value of the top-quark mass, which is known to a precision of around 0.5 GeV [100, 101]. This uncertainty is evaluated by using pseudo-data built from MC samples where the top-quark mass is varied from its nominal value of 172.5 GeV. Thanks to the high precision of the top-quark mass measurements, the impact on the analysis is small, although the use of the JSF method increases the impact of this uncertainty, as seen in table 2.

The uncertainty in the parton distribution functions is evaluated using the 30 eigenvectors of PDF4LHC30 [53]. The impact of the uncertainty is found to be very small.

5.5 Background modelling

The uncertainty in the modelling of single top-quark production is assessed by using samples where the scales are varied in a similar way to the $t\bar{t}$ samples described above. The uncertainty in the subtraction of the $t\bar{t}$ events from the tW sample is assessed by using an alternative sample that uses the diagram subtraction scheme [75] instead of the diagram removal scheme. Uncertainties in the cross-sections of the single-top-quark processes are also included.

The uncertainties in the W + jets background are evaluated by reweighting the MC samples to correspond to different values of the scales in the matrix elements and the parton shower [106]. The small Z + jets and diboson backgrounds are assigned uncertainties of 50% to cover potential mismodelling of these backgrounds. The $t\bar{t}V$ and $t\bar{t}H$ processes are assigned an uncertainty of 13% [107].

The uncertainty in the multijet background is assessed by comparing the estimate from the matrix method with the estimate from an alternative method based on fitting MC templates to the E_T^{miss} and $E_T^{\text{miss}} + m_T^W$ distributions. These comparisons result in an uncertainty of 65% in the multijet background estimate.

The impact of the background uncertainties on the measurements is generally small, and less than in the previous ATLAS measurement thanks to the tighter selection requirements (particularly the one on $m_{\ell b}$).

5.6 Luminosity and other uncertainties

The calibration of the integrated luminosity has an uncertainty of 1.7% [24]. The uncertainty is important for the inclusive cross-section measurement but less so for the differential measurements. The uncertainty in the pile-up modelling is evaluated by varying the mean number of interactions in the simulation and this uncertainty is found to be small. The uncertainty in the E_T^{miss} originates from the possible miscalibration of the tracks in the soft term and it was derived from the p_T imbalance between the soft and hard components in data-simulation comparisons [89]. The uncertainty due to the limited number of simulated events is evaluated by varying the number of events according to the statistical uncertainties of the simulated samples and is found to be smaller than the statistical uncertainty of the data.

6 Results

The fiducial cross-section (as defined in section 4.3) is measured to be $1.267 \pm 0.005 \pm 0.053$ pb, where the first uncertainty is due to the size of the data sample and the second originates from the systematic uncertainties. This cross-section is measured to a relative precision of 4.2%. This is smaller than the calculated uncertainty of 6.1% in the inclusive $t\bar{t}$ cross-section at NNLO+NNLL, which is composed of 4.2% from PDF uncertainties, 3% from scale variations and 2.8% from the uncertainty in the top-quark mass. A comparison with the SM predictions obtained with different MC set-ups (each normalised to the inclusive NNLO+NNLL $t\bar{t}$ cross-section) is shown in figure 9. All MC
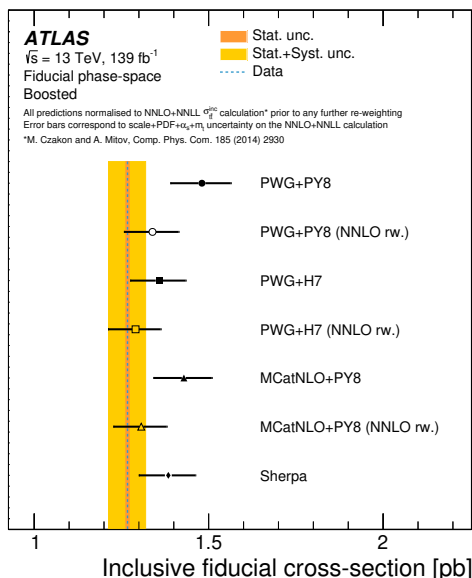
Figure 9. The fiducial cross-section at particle level for boosted $t\bar{t}$ production measured in data (dashed line) is compared with several NLO predictions (closed markers). All the MC samples are normalised to the NNLO+NNLL prediction for the total $t\bar{t}$ cross-section ($\sigma_{t\bar{t}}^{\text{inc}}$). The open markers show the predictions from the MC generators after they were reweighted at parton level to match NNLO predictions for $p_{\text{T}}(t)$, $m(t\bar{t})$ and $p_{\text{T}}(t\bar{t})$. The yellow band represents the total uncertainty of the measured cross-section, while the orange band shows the statistical component. The uncertainties in the predictions are evaluated as the quadrature sum of the α_{s}, PDF, m_t and scale uncertainties present in the NNLO+NNLL prediction. PWG+PY8 corresponds to the POWHEG+PYTHIA sample, PWG+H7 to the POWHEG+HERWIG sample, and MCatNLO+PY8 to the MADGRAPH5_AMC@NLO+PYTHIA sample.

set-ups give predictions that are higher than the data, with the POWHEG+PYTHIA and MADGRAPH5_AMC@NLO+PYTHIA predictions being around two standard deviations above the data.[4] Significantly better agreement is seen after reweighting the MC simulations to the differential NNLO predictions, indicating the corrections are relevant given the precision of the measurement.

The level of agreement for the differential cross-section measurements is quantified by calculating χ^2 values according to:

$$\chi^2 = V^{\text{T}} C^{-1} V$$

where V is the vector of residuals between the measured and predicted cross-sections and C is the covariance matrix of the measured data (including both the statistical and systematic uncertainties). No uncertainties in the theoretical predictions are included in the χ^2 calculation. The observed χ^2 and the number of degrees of freedom are used to calculate p-values. Table 3 shows the χ^2 values for the different NLO generators discussed in section 2. The effect of the NNLO reweighting is quantified in this table by also showing the

---

[4]The estimate of the uncertainty of the ratio between data and expectation includes the experimental uncertainty and the 6.1% uncertainty on the $t\bar{t}$ cross-section, assuming the two are uncorrelated.

Observable	PWG+PY8		PWG+PY8(NNLO weight)		MC@NLO+PY8		MC@NLO+PY8(NNLO weight)		PWG+H7		PWG+H7(NNLO weight)	
	χ^2/NDF	p-value	χ^2/NDF	p-value	χ^2/NDF	p-value	χ^2/NDF	p-value	χ^2/NDF	p-value	χ^2/NDF	p-value
$p_T^{t,h}$	26/8	<0.01	5/8	0.79	18/8	0.03	4/8	0.85	7/8	0.56	3/8	0.94
$p_T^{t,\ell}$	78/8	<0.01	28/8	<0.01	144/8	<0.01	10/8	0.27	43/8	<0.01	18/8	0.02
$p_T^{t\bar{t}}$	162/7	<0.01	46/7	<0.01	171/7	<0.01	22/7	<0.01	122/7	<0.01	39/7	<0.01
$H_T^{t\bar{t}+\text{jets}}$	36/7	<0.01	7/7	0.42	17/7	0.02	23/7	<0.01	21/7	<0.01	12/7	0.10
$H_T^{t\bar{t}}$	86/10	<0.01	37/10	<0.01	110/10	<0.01	16/10	0.10	47/10	<0.01	28/10	<0.01
$|y^{t,h}|$	47/17	<0.01	27/17	0.06	37/17	<0.01	23/17	0.15	30/17	0.03	26/17	0.07
$|y^{t,\ell}|$	40/14	<0.01	17/14	0.26	29/14	0.01	12/14	0.58	28/14	0.01	19/14	0.16
$|y^{t\bar{t}}|$	30/10	<0.01	8/10	0.58	23/10	0.01	6/10	0.81	14/10	0.19	7/10	0.74
$m^{t\bar{t}}$	52/10	<0.01	24/10	<0.01	81/10	<0.01	7/10	0.74	29/10	<0.01	22/10	0.02
$p_T^{j,1}$	115/15	<0.01	38/15	<0.01	413/15	<0.01	194/15	<0.01	143/15	<0.01	69/15	<0.01
$p_T^{j,2}$	46/9	<0.01	19/9	0.02	25/9	<0.01	74/9	<0.01	42/9	<0.01	29/9	<0.01
N^j	32/5	<0.01	12/5	0.03	76/5	<0.01	78/5	<0.01	57/5	<0.01	62/5	<0.01
$\Delta\phi(j_1,t_h)$	17/9	0.05	8/9	0.53	150/9	<0.01	80/9	<0.01	42/9	<0.01	30/9	<0.01
$\Delta\phi(j_2,t_h)$	8/9	0.56	5/9	0.84	8/9	0.57	25/9	<0.01	85/9	<0.01	76/9	<0.01
$\Delta\phi(b_\ell,t_h)$	95/13	<0.01	34/13	<0.01	145/13	<0.01	16/13	0.23	52/13	<0.01	25/13	0.02
$\Delta\phi(t_h,t_\ell)$	111/5	<0.01	36/5	<0.01	134/5	<0.01	82/5	<0.01	90/5	<0.01	36/5	<0.01
$\Delta\phi(j_1,j_2)$	24/11	0.01	16/11	0.13	31/11	<0.01	69/11	<0.01	237/11	<0.01	215/11	<0.01
$m(j_1,t_h)$	50/12	<0.01	20/12	0.06	221/12	<0.01	48/12	<0.01	41/12	<0.01	19/12	0.08
$p_T^{j,1}$ vs N^j	355/21	<0.01	205/21	<0.01	633/21	<0.01	316/21	<0.01	263/21	<0.01	159/21	<0.01
$p_T^{j,1}$ vs $p_T^{t,h}$	115/17	<0.01	53/17	<0.01	383/17	<0.01	152/17	<0.01	121/17	<0.01	74/17	<0.01
$\Delta\phi(j_1,t_h)$ vs $p_T^{t,h}$	69/21	<0.01	43/21	<0.01	427/21	<0.01	223/21	<0.01	78/21	<0.01	60/21	<0.01
$\Delta\phi(j_1,t_h)$ vs N^j	109/19	<0.01	64/19	<0.01	545/19	<0.01	250/19	<0.01	85/19	<0.01	60/19	<0.01

Table 3. χ^2 and p-values quantifying the level of agreement between the absolute unfolded spectra, several NLO+PS predictions and the respective NNLO reweighted spectrum. PWG+PY8 corresponds to the POWHEG+PYTHIA sample, PWG+H7 to the POWHEG+HERWIG sample and MC@NLO+PY8 to the MADGRAPH5_AMC@NLO+PYTHIA sample.

Observable	PWG+PY8		PWG+PY8(ISR Down)		PWG+PY8(ISR Up)		PWG+PY8($h_{\text{damp}} = 3m_t$)		SHERPA		SHERPA (NLO norm.)	
	χ^2/NDF	p-value	χ^2/NDF	p-value	χ^2/NDF	p-value	χ^2/NDF	p-value	χ^2/NDF	p-value	χ^2/NDF	p-value
$p_T^{t,h}$	26/8	<0.01	26/8	<0.01	25/8	<0.01	36/8	<0.01	12/8	0.15	11/8	0.19
$p_T^{t,\ell}$	78/8	<0.01	144/8	<0.01	20/8	0.01	50/8	<0.01	12/8	0.13	11/8	0.22
$p_T^{t\bar{t}}$	162/7	<0.01	243/7	<0.01	340/7	<0.01	108/7	<0.01	70/7	<0.01	57/7	<0.01
$H_T^{t\bar{t}+\text{jets}}$	36/7	<0.01	38/7	<0.01	96/7	<0.01	52/7	<0.01	39/7	<0.01	34/7	<0.01
$H_T^{t\bar{t}}$	86/10	<0.01	119/10	<0.01	46/10	<0.01	72/10	<0.01	28/10	<0.01	22/10	0.01
$|y^{t,h}|$	47/17	<0.01	46/17	<0.01	46/17	<0.01	55/17	<0.01	25/17	0.10	20/17	0.29
$|y^{t,\ell}|$	40/14	<0.01	45/14	<0.01	34/14	<0.01	45/14	<0.01	24/14	0.05	18/14	0.19
$|y^{t\bar{t}}|$	30/10	<0.01	32/10	<0.01	23/10	<0.01	35/10	<0.01	22/10	0.02	20/10	0.03
$m^{t\bar{t}}$	52/10	<0.01	78/10	<0.01	75/10	<0.01	53/10	<0.01	31/10	<0.01	25/10	<0.01
$p_T^{j,1}$	115/15	<0.01	136/15	<0.01	272/15	<0.01	74/15	<0.01	140/15	<0.01	98/15	<0.01
$p_T^{j,2}$	46/9	<0.01	12/9	0.23	196/9	<0.01	81/9	<0.01	41/9	<0.01	19/9	0.02
N^j	32/5	<0.01	51/5	<0.01	27/5	<0.01	41/5	<0.01	23/5	<0.01	16/5	<0.01
$\Delta\phi(j_1,t_h)$	17/9	0.05	34/9	<0.01	22/9	<0.01	23/9	<0.01	10/9	0.38	11/9	0.25
$\Delta\phi(j_2,t_h)$	8/9	0.56	7/9	0.67	22/9	0.01	19/9	0.03	6/9	0.74	3/9	0.96
$\Delta\phi(b_\ell,t_h)$	95/13	<0.01	116/13	<0.01	294/13	<0.01	119/13	<0.01	51/13	<0.01	28/13	0.01
$\Delta\phi(t_h,t_\ell)$	111/5	<0.01	164/5	<0.01	207/5	<0.01	79/5	<0.01	36/5	<0.01	39/5	<0.01
$\Delta\phi(j_1,j_2)$	24/11	0.01	17/11	0.12	41/11	<0.01	38/11	<0.01	26/11	<0.01	20/11	0.05
$m(j_1,t_h)$	50/12	<0.01	111/12	<0.01	93/12	<0.01	43/12	<0.01	65/12	<0.01	40/12	<0.01
$p_T^{j,1}$ vs N^j	355/21	<0.01	495/21	<0.01	488/21	<0.01	254/21	<0.01	193/21	<0.01	137/21	<0.01
$p_T^{j,1}$ vs $p_T^{t,h}$	115/17	<0.01	192/17	<0.01	256/17	<0.01	87/17	<0.01	133/17	<0.01	87/17	<0.01
$\Delta\phi(j_1,t_h)$ vs $p_T^{t,h}$	69/21	<0.01	104/21	<0.01	56/21	<0.01	73/21	<0.01	42/21	<0.01	32/21	0.06
$\Delta\phi(j_1,t_h)$ vs N^j	109/19	<0.01	201/19	<0.01	66/19	<0.01	91/19	<0.01	35/19	0.01	26/19	0.14

Table 4. χ^2 and p-values quantifying the level of agreement between the absolute unfolded spectra and several NLO+PS predictions. PWG+PY8 corresponds to the POWHEG+PYTHIA sample. SHERPA (NLO norm.) refers to the SHERPA sample with its default normalisation. All other samples are normalised to the inclusive NNLO+NNLL $t\bar{t}$ cross-section prediction.

χ^2 values for the different generators with the NNLO reweighting applied. Table 4 shows the observed χ^2 values for the different POWHEG+PYTHIA set-ups discussed in section 2.

Figure 10 shows the measured top-quark transverse momentum distributions, the invariant mass of the $t\bar{t}$ system, the rapidities of the top quarks and the $t\bar{t}$ system, $H_T^{t\bar{t}}$ and $\Delta\phi(b_\ell,t_h)$. In this figure, the distributions are compared with those from the nominal MC sample (with and without NNLO reweighting), the variations of the nominal MC sam-

ple used for the systematic uncertainties, and the alternative NLO generators. Figure 11 shows the same distributions, this time compared with the three NLO generator set-ups, in each case showing the impact of the NNLO reweighting. As observed in previous measurements, the p_{T} distributions of the top quarks are seen to be softer in data than in simulation. Reweighting the MC predictions to the NNLO parton-level prediction gives significantly better agreement between data and predictions. This is because the NNLO prediction has a softer top-quark p_{T} distribution than the MC set-ups predict and hence results in a lower predicted cross-section in the fiducial region as seen in figure 9. It is worth noting that the $p_{\mathrm{T}}^{t,\ell}$ distribution is somewhat anti-correlated with $p_{\mathrm{T}}^{t\bar{t}}$ (correlation coefficient of -0.55) due to the selection requirements and hence differences in this distribution and the corresponding large χ^2 values seen in tables 3 and 4 may originate from mismodelling of the $p_{\mathrm{T}}^{t\bar{t}}$ distribution rather than the $p_{\mathrm{T}}^{t,\ell}$ distribution. The measured $m^{t\bar{t}}$ distribution has a relatively poor χ^2 for all the MC models and in this case the impact of the NNLO reweighting is largest for the MADGRAPH5_AMC@NLO+PYTHIA set-up, where it brings the prediction into agreement with the data. The shapes of the top-quark rapidity distributions show good agreement between the data and the MC models. There is a small slope in the ratio of MC simulation to data in $|y^{t\bar{t}}|$; however, this disagreement is not found to be significant. The NNLO reweighting is found to have a very small impact on the level of agreement in the shapes of the rapidity distributions.

The modelling of the additional radiation is probed by the $p_{\mathrm{T}}^{t\bar{t}}$, $\Delta\phi(t_h, t_\ell)$ and $H_{\mathrm{T}}^{t\bar{t}+\mathrm{jets}}$ observables, and the observables involving the additional jets (defined in section 4.6). These are shown in figures 12 and 13. None of the tested models provides a good description of all the measured observables. The SHERPA sample provides the best description of the number of additional jets (figure 12d), indicating that matrix elements for the additional jets need to be included to model this distribution accurately. The shape of the leading additional jet's p_{T} distribution (figure 12e) is observed to be noticeably different between the MAD-GRAPH5_AMC@NLO and POWHEG set-ups, indicating that the technique for matching the matrix element and the parton shower is a relevant issue. The difficulty of accurately modelling the extra jet radiation is illustrated in figures 12e and 13c by the leading and sub-leading additional jets' p_{T} distributions, where using the POWHEG+PYTHIA sample with less ISR radiation gives better agreement than the nominal sample in $p_{\mathrm{T}}^{j,2}$ but worse agreement in $p_{\mathrm{T}}^{j,1}$. The observables that involve the sub-leading additional jet are expected to have sensitivity to the parton shower in the tested MC models. Differences between the models using PYTHIA and HERWIG are seen in the $\Delta\phi(j_1, j_2)$ and $\Delta\phi(j_2, t_h)$ distributions, where the POWHEG+HERWIG set-up is seen to have worse agreement with the data than the set-ups using PYTHIA.

The two-dimensional cross-section measurement results are shown in figures 14–17. The disagreement in the leading additional jet p_{T} is observed to be larger for events with high $p_{\mathrm{T}}^{t,h}$, and the $\Delta\phi(j_1, t_h)$ distribution is also seen to be poorly modelled at high $p_{\mathrm{T}}^{t,h}$ by all the tested models. The differences between the NLO models are often larger than the precision of the measurements, which indicates that comparisons with generators with higher precision would be beneficial. Higher precision could be obtained with a full NNLO plus parton shower MC model that may become available in the future [108].
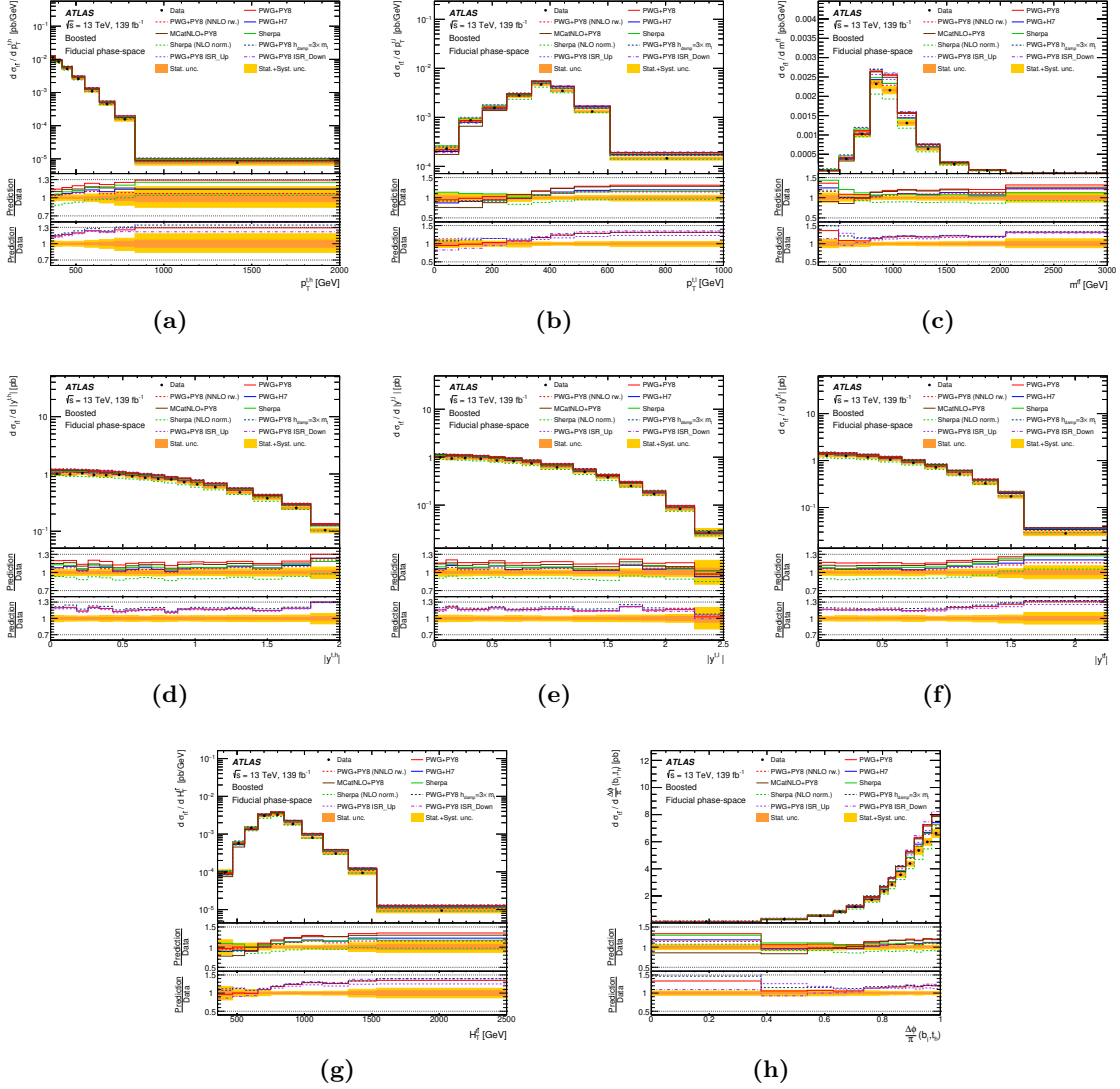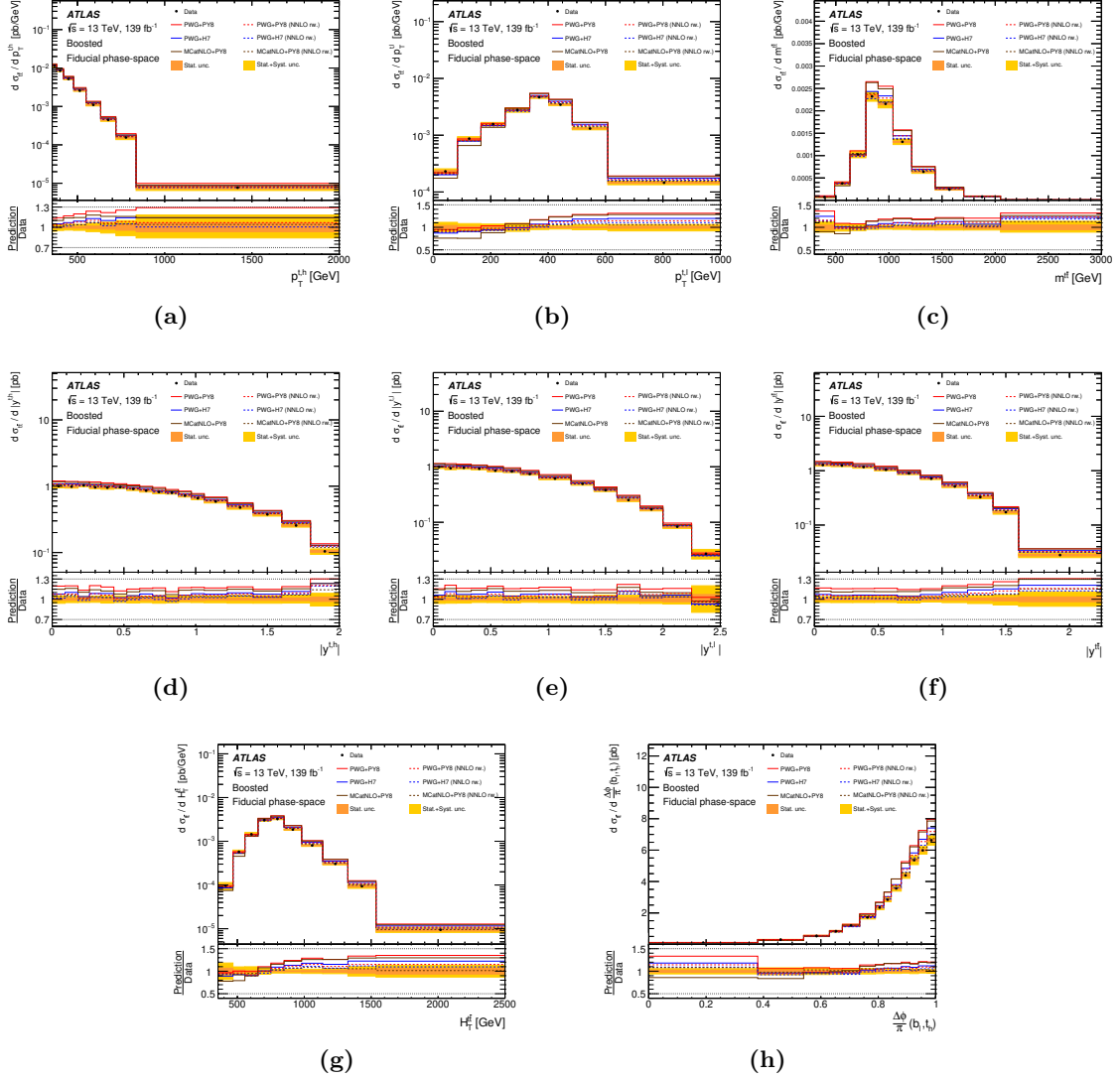
Figure 10. Differential cross-section measurements for the observables related to the kinematics of the top quarks. The cross-section is shown as a function of (a) $p_T^{t,h}$, (b) $p_T^{t,\ell}$, (c) $m^{t\bar{t}}$, (d) $|y^{t,h}|$, (e) $|y^{t,\ell}|$, (f) $|y^{t\bar{t}}|$, (g) $H_T^{t\bar{t}}$ and (h) $\Delta\phi(b_\ell, t_h)$. In each plot the data are compared with predictions from various MC generators. PWG+PY8 corresponds to the POWHEG+PYTHIA sample, PWG+H7 to the POWHEG+HERWIG sample and MCatNLO+PY8 to the MADGRAPH5_AMC@NLO+PYTHIA sample. The orange band shows the size of the statistical uncertainty and the yellow band shows the size of the total uncertainty. The lower two panels in each subfigure display the ratios of the different predictions to the data.

Figure 11. Differential cross-section measurements for the observables related to the kinematics of the top quarks. The cross-section is shown as a function of (a) $p_T^{t,h}$, (b) $p_T^{t,\ell}$, (c) $m^{t\bar{t}}$, (d) $|y^{t,h}|$, (e) $|y^{t,\ell}|$, (f) $|y^{t\bar{t}}|$, (g) $H_T^{t\bar{t}}$ and (h) $\Delta\phi(b_\ell, t_h)$. In each plot the data are compared with predictions from the NLO generators with and without the NNLO reweighting. PWG+PY8 corresponds to the POWHEG+PYTHIA sample, PWG+H7 to the POWHEG+HERWIG sample and MCatNLO+PY8 to the MADGRAPH5_AMC@NLO+PYTHIA sample. The orange band shows the size of the statistical uncertainty and the yellow band shows the size of the total uncertainty. The lower panel in each subfigure displays the ratios of the different predictions to the data.
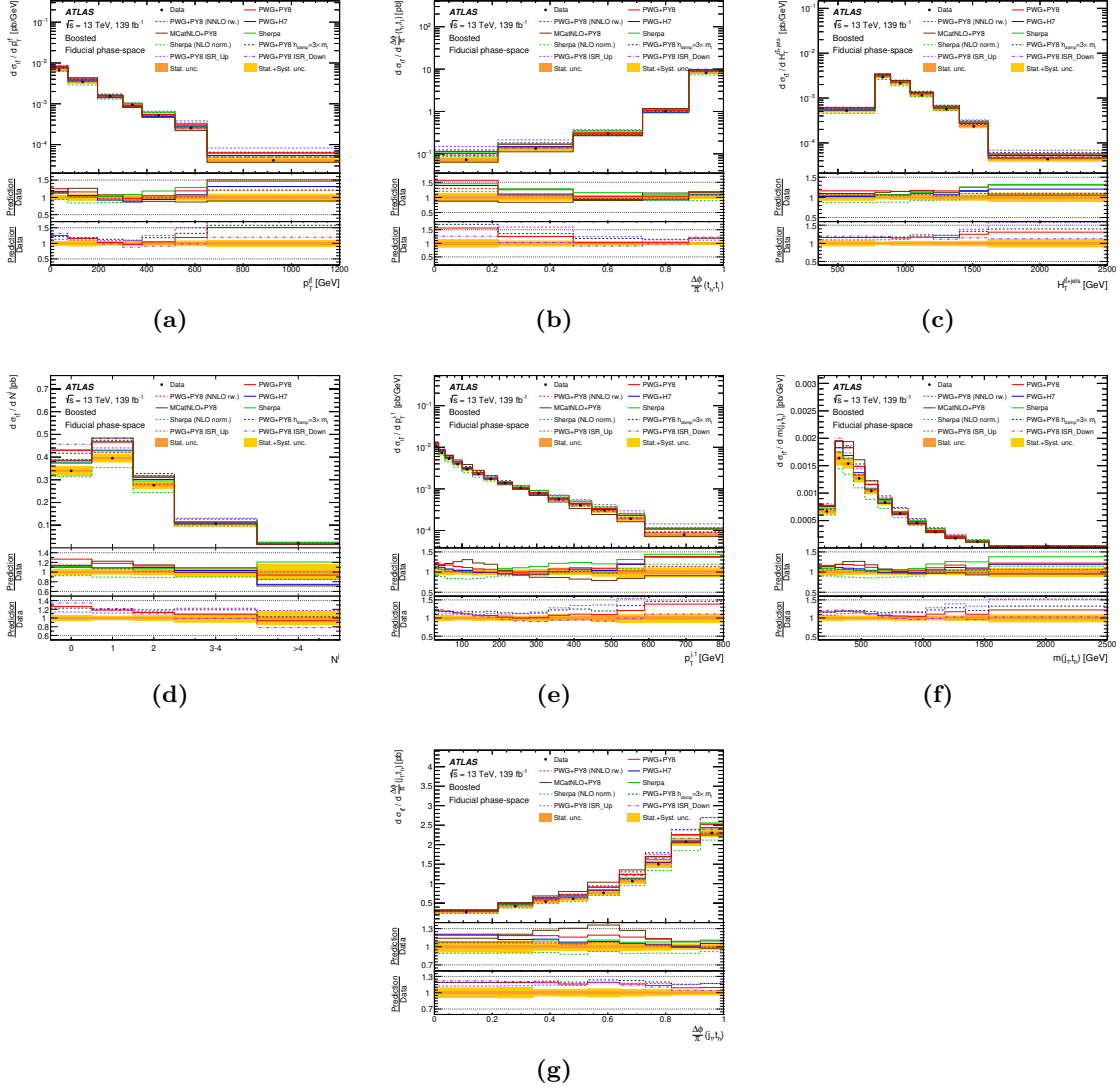
Figure 12. Differential cross-section measurements for the observables related to jets produced in association with the $t\bar{t}$ system. The cross-section is shown as a function of (a) $p_{\mathrm{T}}^{t\bar{t}}$, (b) $\Delta\phi(t_h, t_\ell)$, (c) $H_{\mathrm{T}}^{t\bar{t}+\mathrm{jets}}$, (d) N^j, (e) $p_{\mathrm{T}}^{j,1}$, (f) $m(j_1, t_h)$ and (g) $\Delta\phi(j_1, t_h)$. In each plot the data are compared with predictions from various MC generators. PWG+PY8 corresponds to the POWHEG+PYTHIA sample, PWG+H7 to the POWHEG+HERWIG sample and MCatNLO+PY8 to the MADGRAPH5_AMC@NLO+PYTHIA sample. The orange band shows the size of the statistical uncertainty and the yellow band shows the size of the total uncertainty. The lower two panels in each subfigure display the ratios of the different predictions to the data.
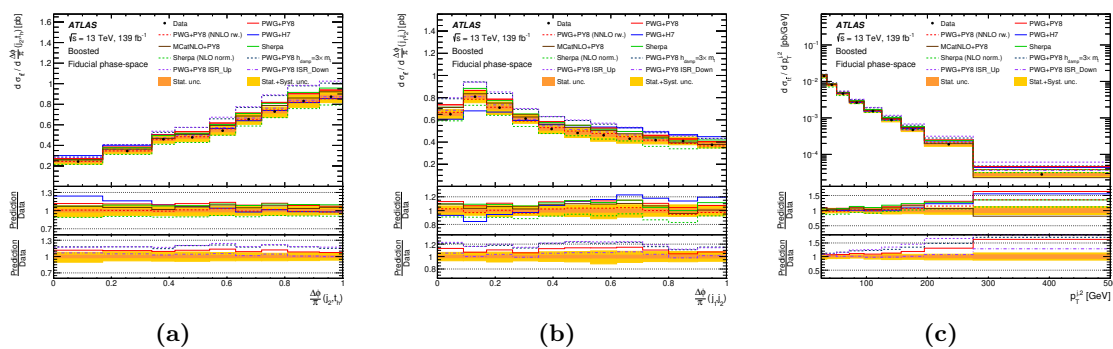
Figure 13. Differential cross-section measurements for the observables probing the second leading additional jet. The cross-section is shown as a function of (a) $\Delta\phi(j_2, t_h)$, (b) $\Delta\phi(j_1, j_2)$ and (c) $p_T^{j,2}$. In each plot the data are compared with predictions from various MC generators. PWG+PY8 corresponds to the POWHEG+PYTHIA sample, PWG+H7 to the POWHEG+HERWIG sample and MCatNLO+PY8 to the MADGRAPH5_AMC@NLO+PYTHIA sample. The orange band shows the size of the statistical uncertainty and the yellow band shows the size of the total uncertainty. The lower two panels in each subfigure display the ratios of the different predictions to the data.
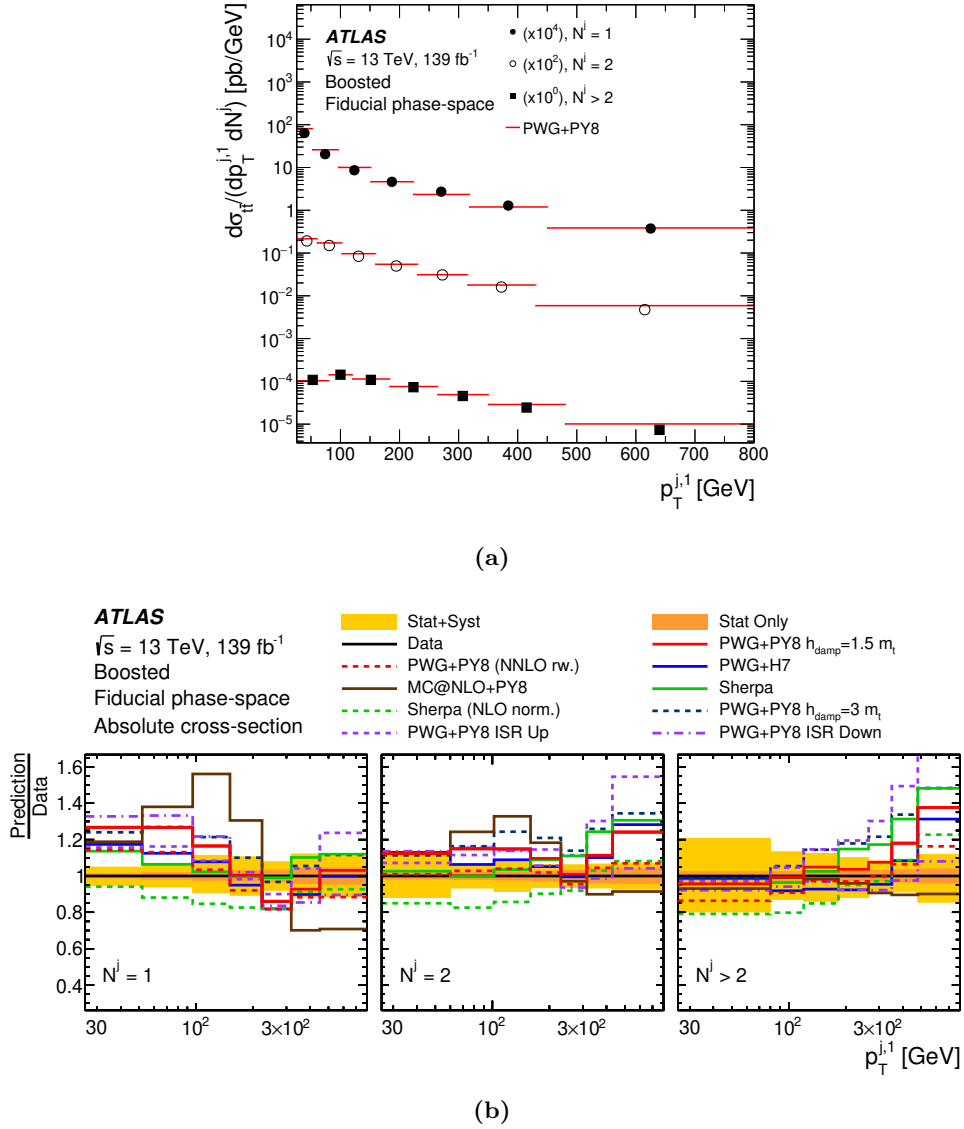
(a)

(b)

Figure 14. (a) Differential cross-section measurements as a function of the p_T of the leading additional jet in bins of additional jet multiplicity are compared with the prediction from the POWHEG+PYTHIA MC generator. The measurement and the predictions are normalised by the factors shown in parentheses to aid visibility. (b) Ratio of the measured absolute cross-section to different NLO, and NLO reweighted to NNLO, predictions of $t\bar{t}$ signal for the same differential variables. PWG+PY8 corresponds to the POWHEG+PYTHIA sample, PWG+H7 to the POWHEG+HERWIG sample and MCatNLO+PY8 to the MADGRAPH5_AMC@NLO+PYTHIA sample. The yellow band represents the total uncertainty of the measured differential cross-section while the orange band shows the statistical component.
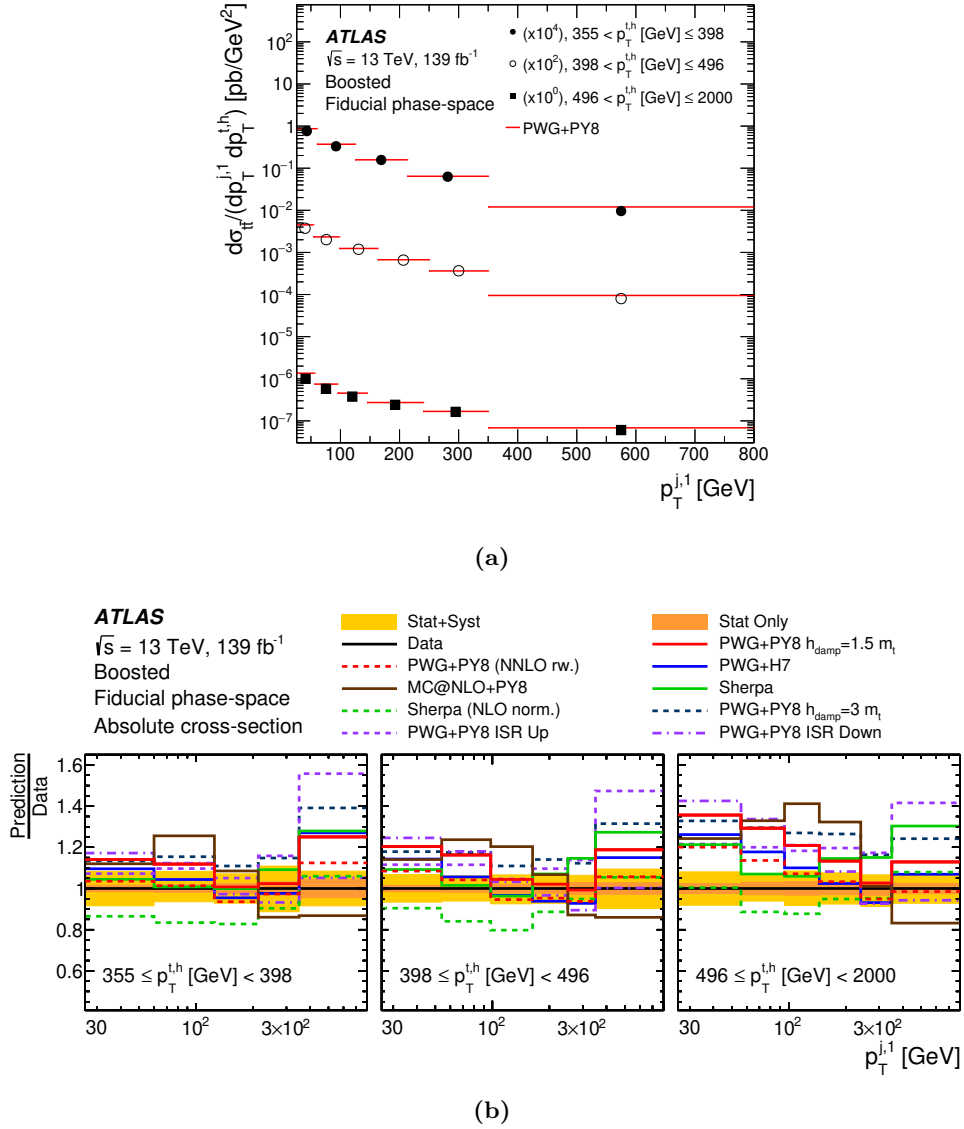
(a)

(b)

Figure 15. (a) Differential cross-section measurements as a function of the p_T of the leading additional jet in bins of $p_T^{t,h}$ are compared with the prediction from the POWHEG+PYTHIA MC generator. The measurement and the predictions are normalised by the factors shown in parentheses to aid visibility. (b) Ratio of the measured absolute cross-section to different NLO, and NLO reweighted to NNLO, predictions of $t\bar{t}$ signal for the same differential variables. PWG+PY8 corresponds to the POWHEG+PYTHIA sample, PWG+H7 to the POWHEG+HERWIG sample and MCatNLO+PY8 to the MADGRAPH5_AMC@NLO+PYTHIA sample. The yellow band represents the total uncertainty of the measured differential cross-section while the orange band shows the statistical component.
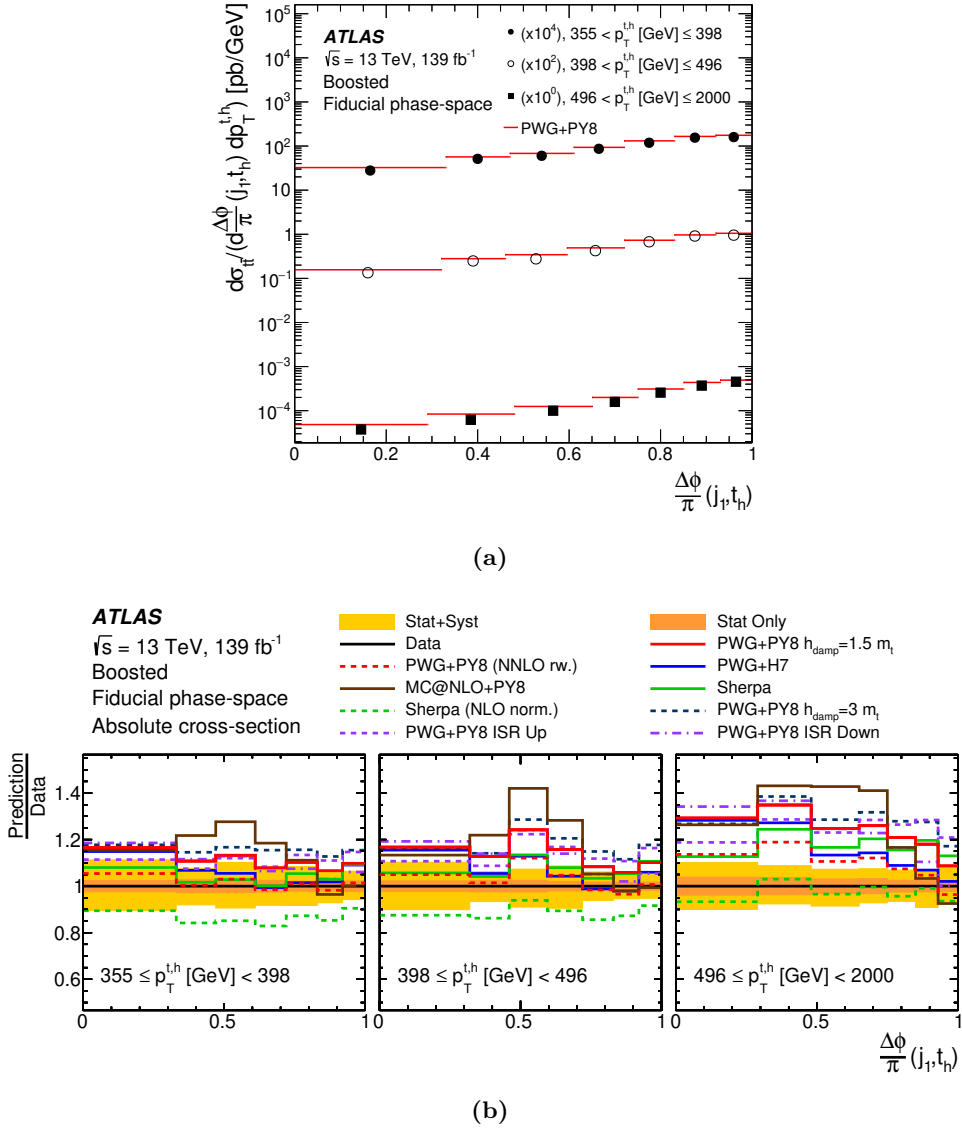
(a)

(b)

Figure 16. (a) Differential cross-section measurements as a function of the $\Delta\phi$ angle between the leading additional jet and the hadronically decaying top quark in bins of $p_T^{t,h}$ are compared with the prediction from the POWHEG+PYTHIA MC generator. The measurement and the predictions are normalised by the factors shown in parentheses to aid visibility. (b) Ratio of the measured absolute cross-section to different NLO, and NLO reweighted to NNLO, predictions of $t\bar{t}$ signal for the same differential variables. PWG+PY8 corresponds to the POWHEG+PYTHIA sample, PWG+H7 to the POWHEG+HERWIG sample and MCatNLO+PY8 to the MADGRAPH5_AMC@NLO+PYTHIA sample. The yellow band represents the total uncertainty of the measured differential cross-section while the orange band shows the statistical component.
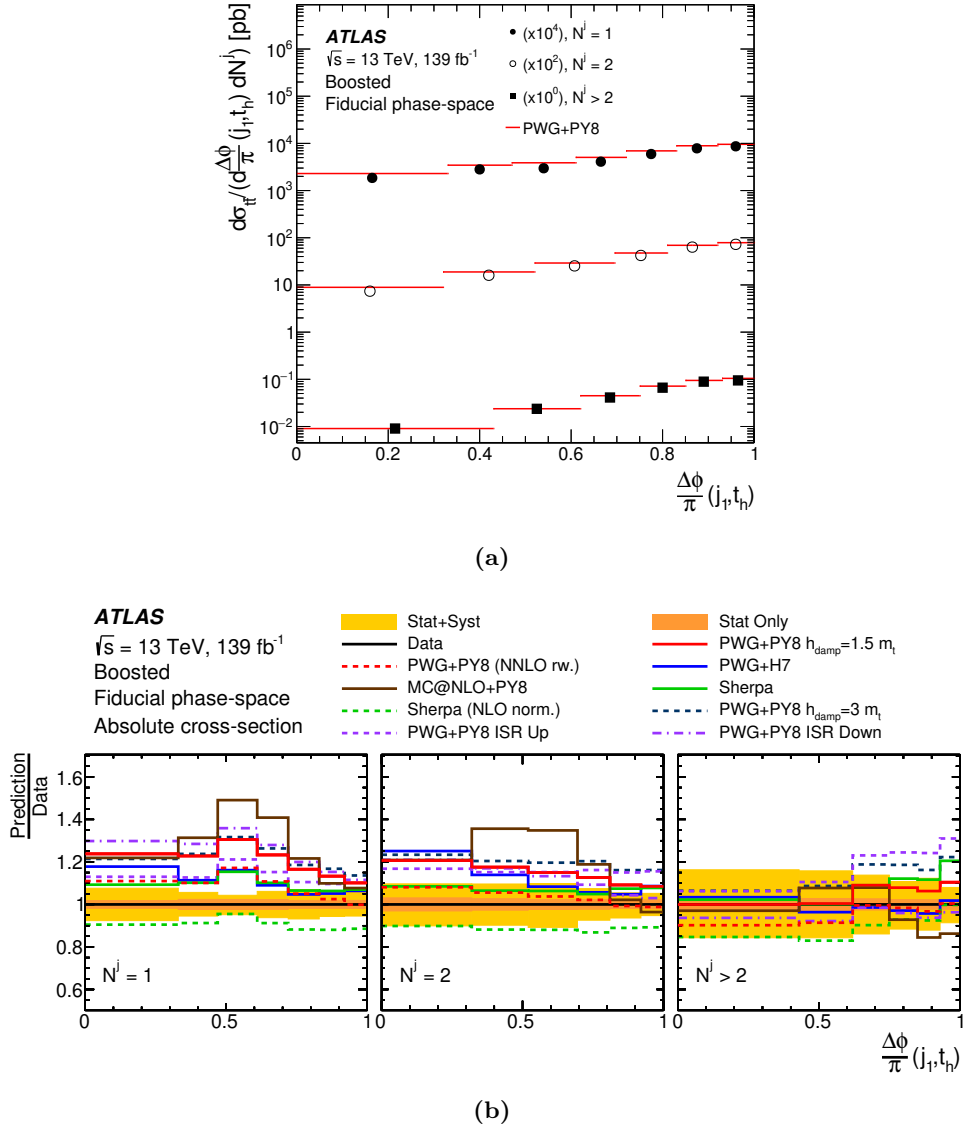
(a)

(b)

Figure 17. (a) Differential cross-section measurements as a function of the $\Delta\phi$ angle between the leading additional jet and the hadronically decaying top quark in bins of additional jet multiplicity are compared with the prediction from the Powheg+Pythia MC generator. The measurement and the predictions are normalised by the factors shown in parentheses to aid visibility. (b) Ratio of the measured absolute cross-section to different NLO, and NLO reweighted to NNLO, predictions of $t\bar{t}$ signal for the same differential variables. PWG+PY8 corresponds to the Powheg+Pythia sample, PWG+H7 to the Powheg+Herwig sample and MCatNLO+PY8 to the MadGraph5_aMC@NLO+Pythia sample. The yellow band represents the total uncertainty of the measured differential cross-section while the orange band shows the statistical component.

7 Limits on EFT operators

The sensitivity of the analysis to potential new physics in $t\bar{t}$ production is explored by interpreting the measured $p_T^{t,h}$ distribution in terms of dimension-six operators within the effective field theory framework. The interpretation allows two Wilson coefficients that are sensitive to $t\bar{t}$ production to be non-zero: C_{tG} and $C_{tq}^{(8)}$. All other Wilson coefficients, for both the dimension-six and higher-dimensional operators, are assumed to be zero. The O_{tG} operator primarily changes the overall rate of $t\bar{t}$ production while the $O_{tq}^{(8)}$ operator results in additional $t\bar{t}$ events at high energy. Example LO Feynman diagrams for the two operators are shown in figure 18. The two operators can be disentangled by fitting a differential cross-section measurement. The $p_T^{t,h}$ distribution, shown in figure 10a, is chosen as the observable, based on simulation studies that considered the sensitivity of the variables as well as the stability of the variables when going from LO to NLO QCD.

The differential cross-section is parameterised as a polynomial of second degree in the two Wilson coefficients under consideration:

$$\sigma^j(C_{tG}, C_{tq}^{(8)}) = p_0^j + p_1^j \cdot C_{tG} + p_2^j \cdot C_{tq}^{(8)} + p_3^j \cdot (C_{tG})^2 + p_4^j \cdot (C_{tq}^{(8)})^2 + p_5^j \cdot C_{tG} \cdot C_{tq}^{(8)}$$

where the index j labels the bins of the differential distribution. The parameters p_i^j with $i \geq 1$ are extracted from fits to the EFT samples with $(C_{tG}, C_{tq}^{(8)}) = (\pm 1 \text{ or } 0, \ \pm 1 \text{ or } 0)$; see section 2 for a description of the samples. Two separate fits are performed, one using samples containing the full EFT contributions (i.e. proportional to Λ^{-2} and Λ^{-4}), and the second containing only EFT contributions proportional to Λ^{-2}. This allows the impact of the Λ^{-4} terms on the sensitivity of the results to be examined and the two set-ups are referred to as the Λ^{-4} and Λ^{-2} models in the rest of this section.

The parameters p_0^j determine the Standard Model prediction and are taken from the POWHEG+PYTHIA sample after reweighting it to the NNLO prediction. The parameterisation of the EFT effects assumes that the background estimate is independent of the tested operators, which is reasonable given the high purity of the selected event sample.

The EFT*fitter* [109] package is used to extract the limits on the Wilson coefficients by minimising the likelihood:

$$-2\ln p(C_{tG}, C_{tq}^{(8)}|\boldsymbol{m}) = \left(\boldsymbol{m} - \boldsymbol{\sigma}(C_{tG}, C_{tq}^{(8)})\right)^T M^{-1} \left(\boldsymbol{m} - \boldsymbol{\sigma}(C_{tG}, C_{tq}^{(8)})\right)$$
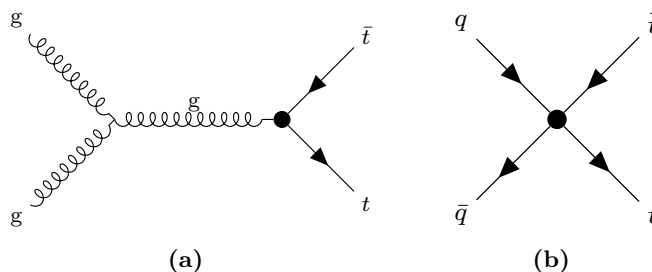

Figure 18. Example LO Feynman diagrams for EFT contributions from (a) C_{tG} and (b) $C_{tq}^{(8)}$. Couplings affected by EFT contributions are marked by the black dots.

where $\boldsymbol{m}$ is the vector of measurements of each bin of the observed distribution and $\boldsymbol{\sigma}(C_{tG}, C_{tq}^{(8)})$ is the vector of corresponding predictions for each bin that depends on the two Wilson coefficients of interest $(C_{tG}, C_{tq}^{(8)})$. The covariance matrix, M, is a sum of the matrices corresponding to the experimental and theoretical uncertainties, $M = M_e + M_t$. This procedure assumes that the theoretical uncertainties in the predicted cross-section are not correlated with the theoretical uncertainties in the experimental measurement (described in section 5.4). The covariance matrix for the experimental uncertainties corresponds exactly to the uncertainties described in section 5. The theoretical uncertainties are determined using the POWHEG+PYTHIA $t\bar{t}$ sample reweighted to NNLO. The scales μ_r and μ_f are varied to 2μ and $\mu/2$, with the condition $1/2 \leq \mu_r/\mu_f \leq 2$, giving seven variations. The envelope of those variations is used to define alternative shapes for the three parton-level distributions used in the NNLO reweighting procedure. The difference between each alternative prediction and the nominal one gives an estimate of the uncertainty in the shape of the distributions provided by the NNLO calculations. The uncertainty in all three distributions is included and assumed to be uncorrelated with the uncertainty in the other distributions. The uncertainty due to the choice of PDF set is also included. Since all these uncertainties cover only the shape differences, an additional 6% uncertainty is included for the uncertainty in the inclusive $t\bar{t}$ cross-section, covering the variations of the scales, PDFs, α_s and m_t. The posterior probability distribution for the Wilson coefficients is extracted using the equation of Bayes and Laplace, as implemented in the Bayesian Analysis Toolkit [110]. The prior probability distribution for the Wilson coefficients is taken to be uniform. To make the dependence of the sensitivity to the Wilson coefficients on the energy scale of the new physics explicit, the results are presented for the product $C_i(\text{TeV}/\Lambda)^2$. This also facilitates straightforward comparisons with results where $\Lambda = 1$ TeV. The credible interval for each Wilson coefficient is extracted by marginalising over the other coefficient. The fit is also performed with only one Wilson coefficient as a free parameter and the other fixed to zero; these are referred to as individual fits.

The measured $p_T^{t,h}$ differential cross-section is compared with the SM prediction and uncertainty in figure 19. The figure also displays the best fit for the EFT models, where the fitted Wilson coefficients are $C_{tG} = -0.11^{+0.16}_{-0.25}$ $(\Lambda/\text{TeV})^2$, $C_{tq}^{(8)} = -0.43^{+0.40}_{-0.06}$ $(\Lambda/\text{TeV})^2$ for Λ^{-4} and $C_{tG} = -0.24 \pm 0.23$ $(\Lambda/\text{TeV})^2$, $C_{tq}^{(8)} = 0.03 \pm 0.17$ $(\Lambda/\text{TeV})^2$ for Λ^{-2}. These values agree with zero within two standard deviations, indicating there is no evidence of new physics in the data. The fit prefers negative values for C_{tG} because the measured cross-section is lower than the SM prediction. Table 5 shows the expected and observed marginalised credible intervals for the nominal fit and the individual fits. The expected and observed posterior distributions are shown in figure 20. The expected and observed credible intervals are asymmetric in the Λ^{-4} model because the linear and quadratic terms can cancel out to some extent when the Wilson coefficients are negative. The impact of the different bins in the distribution is investigated by repeating the fit with a subset of the measured bins. Figure 21 shows the evolution of the posterior distribution as bins are added to the interpretation. With only a single bin, the operators are largely degenerate and the fit can only constrain the combination of the two. As bins are added to the fit, the
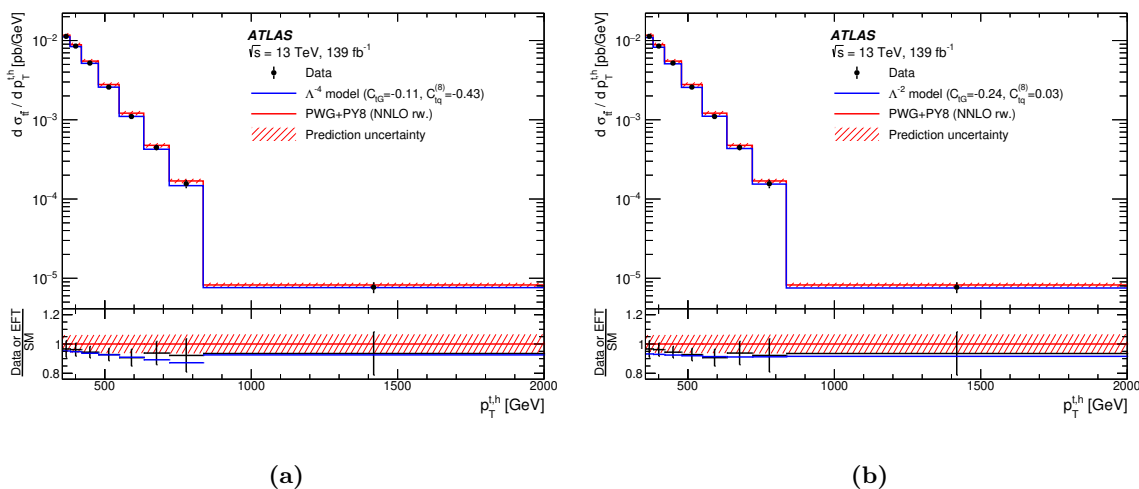
Figure 19. Differential cross-section measurement of $p_T^{t,h}$ used in the EFT interpretation. The data are compared with the SM prediction in red and the EFT model prediction in blue at the respective global modes for (a) the Λ^{-4} model and (b) the Λ^{-2} model. The lower panel in each plot displays the ratio of the data or EFT model to the SM prediction. The shaded red band shows the uncertainty in the SM prediction used in the EFT fit.

| Model | C_i $(\Lambda/\text{TeV})^2$ | Marginalised 95% intervals | | Individual 95% intervals | | Global fit 95% |
		Expected	Observed	Expected	Observed	limits [111]
Λ^{-4}	C_{tG}	$[-0.44, 0.35]$	$[-0.53, 0.21]$	$[-0.44, 0.28]$	$[-0.52, 0.15]$	$[0.006, 0.107]$
	$C_{tq}^{(8)}$	$[-0.57, 0.17]$	$[-0.60, 0.13]$	$[-0.57, 0.18]$	$[-0.64, 0.12]$	$[-0.48, 0.39]$
Λ^{-2}	C_{tG}	$[-0.44, 0.44]$	$[-0.68, 0.21]$	$[-0.41, 0.42]$	$[-0.63, 0.20]$	$[0.007, 0.111]$
	$C_{tq}^{(8)}$	$[-0.35, 0.35]$	$[-0.30, 0.36]$	$[-0.35, 0.36]$	$[-0.34, 0.27]$	$[-0.40, 0.61]$

Table 5. Expected and observed 95% intervals for the Wilson coefficients (C_i). The marginalised results show the intervals extracted from the nominal fit where both Wilson coefficients are allowed to vary. The individual intervals are extracted from fits where only the Wilson coefficient under study is allowed to differ from zero. The results are compared with the individual limits obtained in ref. [111].

ability of the fit to distinguish between the operators is improved. The figure also shows that the constraint on $C_{tq}^{(8)}$ is dominated by the measurements at high $p_T^{t,h}$. The observed constraints are compared in table 5 with the individual limits obtained in a recent global analysis based on multiple measurements [111]. The limits on C_{tG} obtained in this paper are significantly weaker than these, but the limits on $C_{tq}^{(8)}$ are more stringent than those obtained in the global fit, which, given the use of only a single dataset, indicates that the data presented here can provide important constraining power in future global EFT fits.
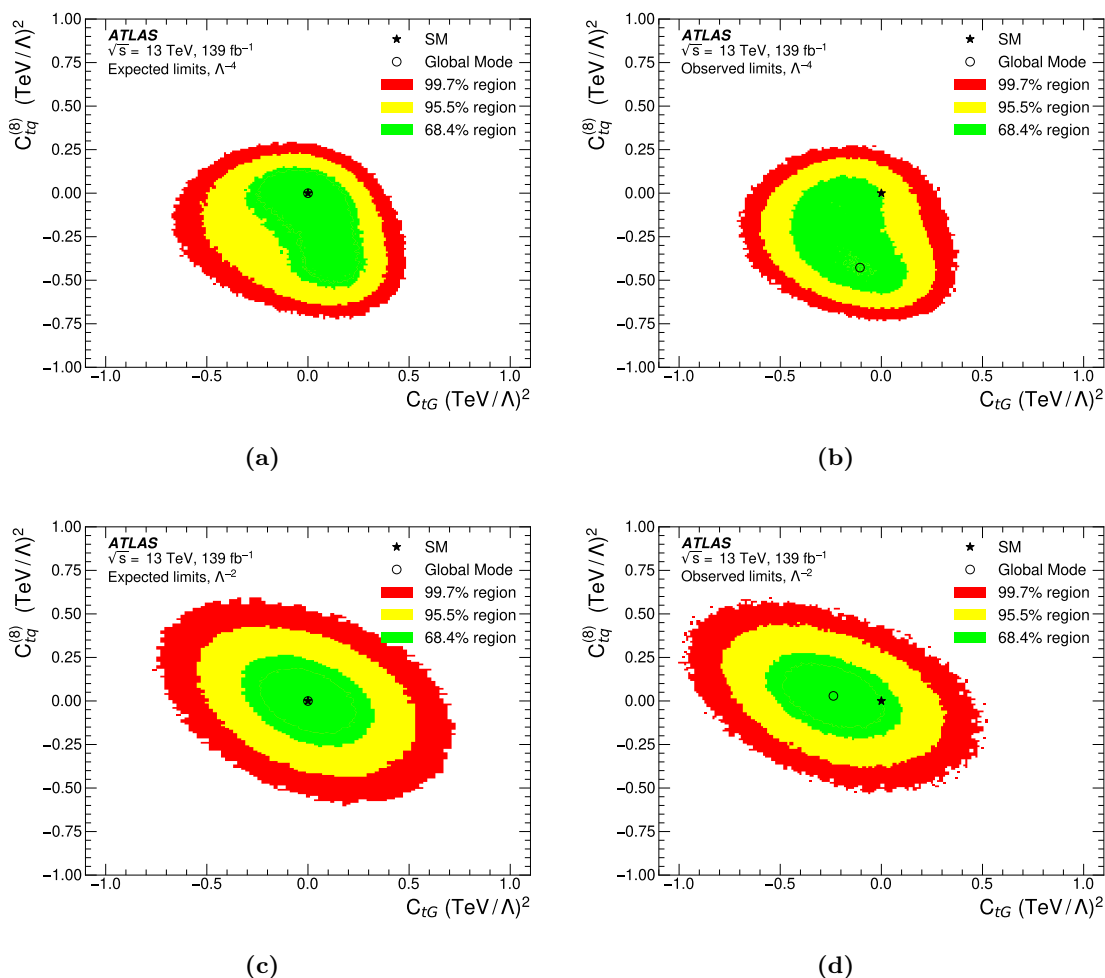
Figure 20. Two-dimensional posterior distributions for the two Wilson coefficients C_{tG} and $C_{tq}^{(8)}$ obtained from fitting the $p_T^{t,h}$ distribution. (a) Shows the posterior distribution expected from the SM prediction and (b) shows the distribution obtained from the data, both for the Λ^{-4} model. The same distributions are shown in (c) and (d) for the Λ^{-2} model. The 68.4 %, 95.5 % and 99.7 % regions are shown in green, yellow and red respectively.

8 Conclusions

This article presents precise cross-section measurements of $t\bar{t}$ events containing a high transverse momentum top quark that has decayed hadronically ($p_T^{t,h} > 355$ GeV). The events were selected from the full 139 fb^{-1} Run-2 ATLAS dataset of 13 TeV proton-proton collisions at the LHC and the cross-sections were extracted by unfolding the reconstructed distributions. The precision of the results is significantly better than in previous measurements. This improvement in precision is largely driven by the introduction of a novel technique to use the invariant mass of the selected large-radius jet from the hadronically decaying top quark to reduce the impact of jet energy scale uncertainties. In addition, the background from $W + $ jets and single top-quark production is reduced compared to the
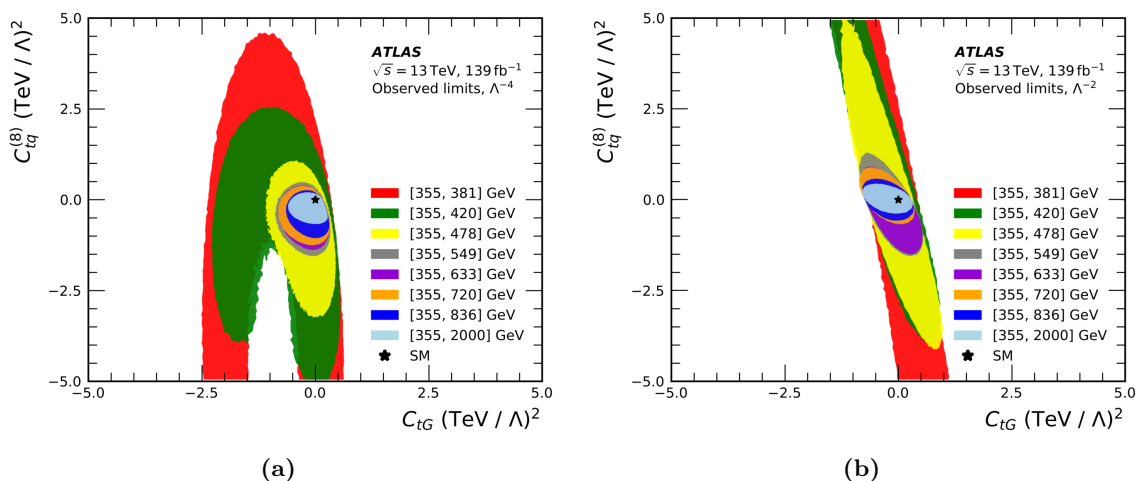
Figure 21. Evolution of the 95% observed credible region when adding the bins of the measured $p_{\mathrm{T}}^{t,h}$ distribution to the interpretation one-by-one for (a) the Λ^{-4} model and (b) the Λ^{-2} model. The coloured ellipses show the 95% regions obtained from fitting the $p_{\mathrm{T}}^{t,h}$ range indicated in the legend.

previous ATLAS measurement by requiring at least two b-tagged jets and $m_{\ell b} < 180$ GeV, which reduces the impact of the background uncertainties on the measurements. The fiducial cross-section is measured to be 1.267 ± 0.005 (stat.) ± 0.053 (syst.) pb. The measurements are compared with predictions from NLO+PS MC generators. No single generator is able to describe all the measured variables well. Applying parton-level reweighting to match NNLO QCD predictions gives better agreement with the data for all generators, indicating that these corrections are relevant given the precision of the measurements. The number of additional jets is best modelled by the SHERPA generator, which provides NLO accuracy for the first additional jet, but the details of the additional radiation are not well described by any of the MC predictions. The sensitivity of the measurement to new physics beyond the Standard Model is illustrated by using the transverse momentum distribution of the hadronically decaying top quark to set limits in the context of effective field theory. No evidence of new physics is seen and the 95% credible intervals of the Wilson coefficients are $C_{tG} \in [-0.53, 0.21]$ $(\Lambda/\mathrm{TeV})^2$ and $C_{tq}^{(8)} \in [-0.60, 0.13]$ $(\Lambda/\mathrm{TeV})^2$ when including EFT contributions proportional to Λ^{-2} and Λ^{-4}. The results demonstrate that the analysis can disentangle the O_{tG} and $O_{tq}^{(8)}$ operators, and the stringent limits placed on $C_{tq}^{(8)}$ demonstrate the data will be highly relevant in future global fits.

Acknowledgments

Observable	PWG+PY8		PWG+PY8(NNLO WEIGHT)		MC@NLO+PY8		MC@NLO+PY8(NNLO WEIGHT)		PWG+H7		PWG+H7(NNLO WEIGHT)	
	χ^2/NDF	p-value	χ^2/NDF	p-value	χ^2/NDF	p-value	χ^2/NDF	p-value	χ^2/NDF	p-value	χ^2/NDF	p-value
$p_{\mathrm{T}}^{t,h}$	3/7	0.84	2/7	0.95	3/7	0.85	3/7	0.89	3/7	0.90	3/7	0.92
$p_{\mathrm{T}}^{t,\ell}$	24/7	<0.01	15/7	0.03	76/7	<0.01	7/7	0.39	24/7	<0.01	13/7	0.07
$p_{\mathrm{T}}^{t\bar{t}}$	95/6	<0.01	34/6	<0.01	109/6	<0.01	20/6	<0.01	96/6	<0.01	35/6	<0.01
$H_{\mathrm{T}}^{t\bar{t}+\mathrm{jets}}$	9/6	0.17	4/6	0.71	5/6	0.57	21/6	<0.01	14/6	0.03	11/6	0.08
$H_{\mathrm{T}}^{t\bar{t}}$	39/9	<0.01	28/9	<0.01	63/9	<0.01	13/9	0.14	33/9	<0.01	26/9	<0.01
$|y^{t,h}|$	21/16	0.18	23/16	0.12	21/16	0.20	21/16	0.17	23/16	0.10	25/16	0.06
$|y^{t,\ell}|$	14/13	0.40	13/13	0.44	12/13	0.50	11/13	0.63	20/13	0.09	18/13	0.16
$|y^{t\bar{t}}|$	7/9	0.61	6/9	0.77	8/9	0.51	5/9	0.85	8/9	0.51	6/9	0.72
$m^{t\bar{t}}$	18/9	0.03	19/9	0.02	51/9	<0.01	6/9	0.74	20/9	0.02	21/9	0.01
$p_{\mathrm{T}}^{j,1}$	84/14	<0.01	35/14	<0.01	318/14	<0.01	168/14	<0.01	125/14	<0.01	65/14	<0.01
$p_{\mathrm{T}}^{j,2}$	29/8	<0.01	18/8	0.02	20/8	<0.01	51/8	<0.01	37/8	<0.01	28/8	<0.01
N^j	7/4	0.12	8/4	0.08	48/4	<0.01	72/4	<0.01	47/4	<0.01	58/4	<0.01
$\Delta\phi(j_1,t_h)$	9/8	0.32	7/8	0.51	113/8	<0.01	68/8	<0.01	37/8	<0.01	29/8	<0.01
$\Delta\phi(j_2,t_h)$	5/8	0.78	5/8	0.80	6/8	0.67	15/8	0.06	67/8	<0.01	61/8	<0.01
$\Delta\phi(b_\ell,t_h)$	35/12	<0.01	21/12	0.06	92/12	<0.01	13/12	0.35	32/12	<0.01	19/12	0.08
$\Delta\phi(t_h,t_\ell)$	62/4	<0.01	28/4	<0.01	74/4	<0.01	76/4	<0.01	71/4	<0.01	33/4	<0.01
$\Delta\phi(j_1,j_2)$	16/10	0.11	16/10	0.10	26/10	<0.01	51/10	<0.01	197/10	<0.01	186/10	<0.01
$m(j_1,t_h)$	30/11	<0.01	19/11	0.06	166/11	<0.01	34/11	<0.01	34/11	<0.01	18/11	0.07
$p_{\mathrm{T}}^{j,1}$ vs N^j	261/20	<0.01	194/20	<0.01	470/20	<0.01	273/20	<0.01	231/20	<0.01	154/20	<0.01
$p_{\mathrm{T}}^{j,1}$ vs $p_{\mathrm{T}}^{t,h}$	80/16	<0.01	50/16	<0.01	291/16	<0.01	127/16	<0.01	105/16	<0.01	71/16	<0.01
$\Delta\phi(j_1,t_h)$ vs $p_{\mathrm{T}}^{t,h}$	48/20	<0.01	39/20	<0.01	333/20	<0.01	196/20	<0.01	68/20	<0.01	56/20	<0.01
$\Delta\phi(j_1,t_h)$ vs N^j	68/18	<0.01	58/18	<0.01	404/18	<0.01	210/18	<0.01	73/18	<0.01	58/18	<0.01

Table 6. χ^2 and p-values quantifying the level of agreement between the relative unfolded spectra, several NLO+PS predictions and the respective NNLO reweighted spectrum. PWG+PY8 corresponds to the POWHEG+PYTHIA sample, PWG+H7 to the POWHEG+HERWIG sample and MC@NLO+PY8 to the MADGRAPH5_AMC@NLO+PYTHIA sample.

A   Normalised differential cross-section results

In this appendix, the differential cross-section results after normalising to the cross-section measured in the fiducial region are presented. These results allow comparisons of the shape of the measured observables with MC predictions. Tables 6 and 7 show the χ^2 values for the normalised distributions for the different MC models. Figure 22 shows the differential cross-section measurements of $p_{\mathrm{T}}^{t,h}$, $p_{\mathrm{T}}^{t,\ell}$, $m^{t\bar{t}}$, $|y^{t,h}|$, $|y^{t,\ell}|$, $|y^{t\bar{t}}|$, $H_{\mathrm{T}}^{t\bar{t}}$ and $\Delta\phi(b_\ell,t_h)$ compared with the predictions from different NLO generator set-ups. The same variables are compared in figure 23 with the MC generators with and without the reweighting to the NNLO prediction. The variables sensitive to additional radiation are shown in figures 24 and 25. The double-differential measurements are shown in figures 26–29.
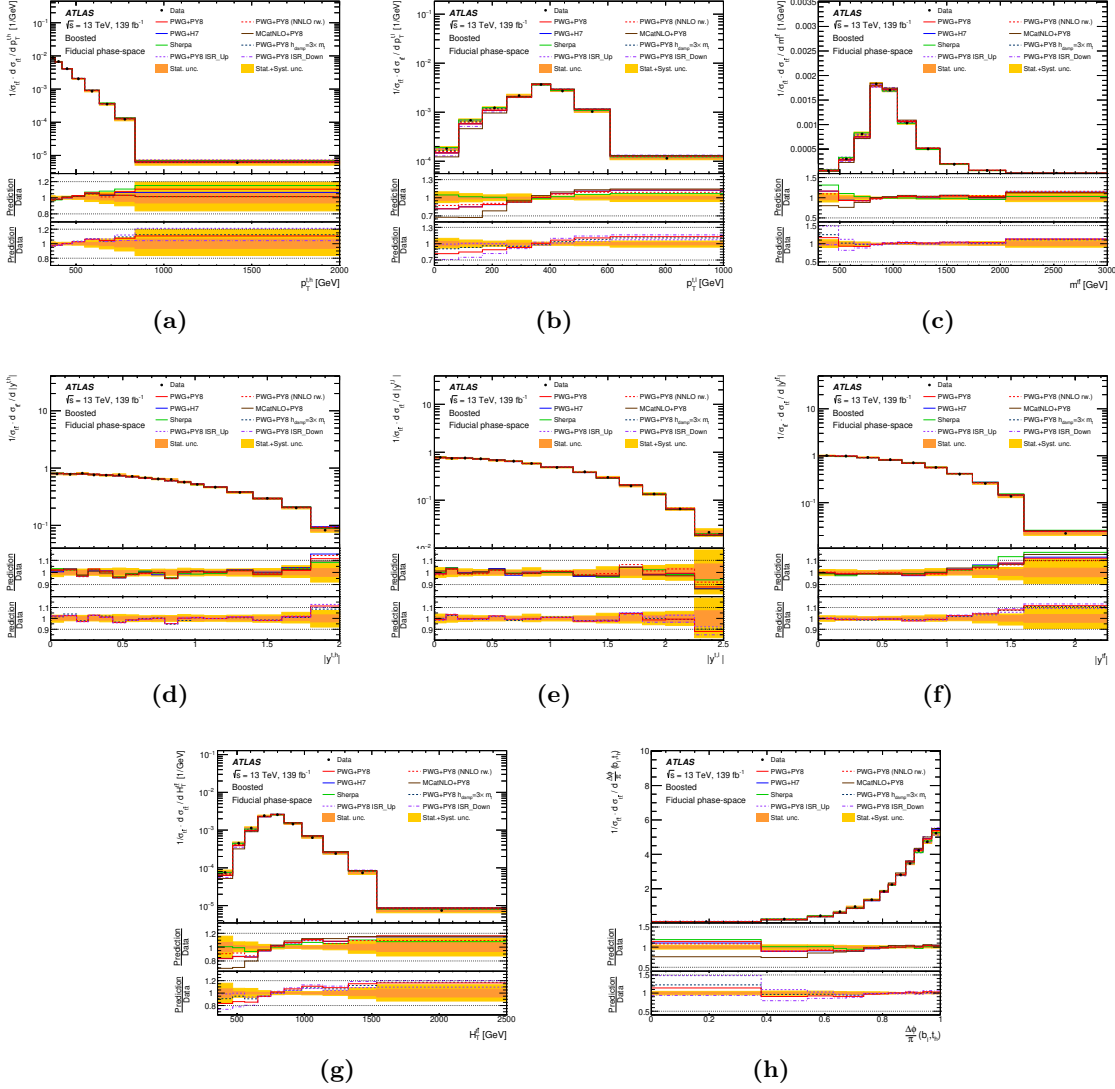
Figure 22. Normalised differential cross-section measurements for the observables related to the kinematics of the top quarks. The cross-section is shown as a function of (a) $p_T^{t,h}$, (b) $p_T^{t,\ell}$, (c) $m^{t\bar{t}}$, (d) $|y^{t,h}|$, (e) $|y^{t,\ell}|$, (f) $|y^{t\bar{t}}|$, (g) $H_T^{t\bar{t}}$ and (h) $\Delta\phi(b_\ell, t_h)$, In each plot the data are compared with predictions from various MC generators. PWG+PY8 corresponds to the POWHEG+PYTHIA sample, PWG+H7 to the POWHEG+HERWIG sample and MCatNLO+PY8 to the MADGRAPH5_AMC@NLO+PYTHIA sample. The orange band shows the size of the statistical uncertainty and the yellow band shows the size of the total uncertainty. The lower two panels in each subfigure display the ratios of the different predictions to the data.

Figure 23. Normalised differential cross-section measurements for the observables related to the kinematics of the top quarks. The cross-section is shown as a function of (a) $p_T^{t,h}$, (b) $p_T^{t,\ell}$, (c) $m^{t\bar{t}}$, (d) $|y^{t,h}|$, (e) $|y^{t,\ell}|$, (f) $|y^{t\bar{t}}|$, (g) $H_T^{t\bar{t}}$ and (h) $\Delta\phi(b_\ell, t_h)$. In each plot the data are compared with predictions from the NLO generators with and without the NNLO reweighting. PWG+PY8 corresponds to the POWHEG+PYTHIA sample, PWG+H7 to the POWHEG+HERWIG sample and MCatNLO+PY8 to the MADGRAPH5_AMC@NLO+PYTHIA sample. The orange band shows the size of the statistical uncertainty and the yellow band shows the size of the total uncertainty. The lower panel in each subfigure displays the ratios of the different predictions to the data.

Figure 24. Normalised differential cross-section measurements for the observables related to jets produced in association with the $t\bar{t}$ system. The cross-section is shown as a function of (a) $p_T^{t\bar{t}}$, (b) $\Delta\phi(t_h, t_\ell)$, (c) $H_T^{t\bar{t}+\text{jets}}$, (d) N^j, (e) $p_T^{j,1}$, (f) $m(j_1, t_h)$ and (g) $\Delta\phi(j_1, t_h)$. In each plot the data are compared with predictions from various MC generators. PWG+PY8 corresponds to the POWHEG+PYTHIA sample, PWG+H7 to the POWHEG+HERWIG sample and MCatNLO+PY8 to the MADGRAPH5_AMC@NLO+PYTHIA sample. The orange band shows the size of the statistical uncertainty and the yellow band shows the size of the total uncertainty. The lower two panels in each subfigure display the ratios of the different predictions to the data.
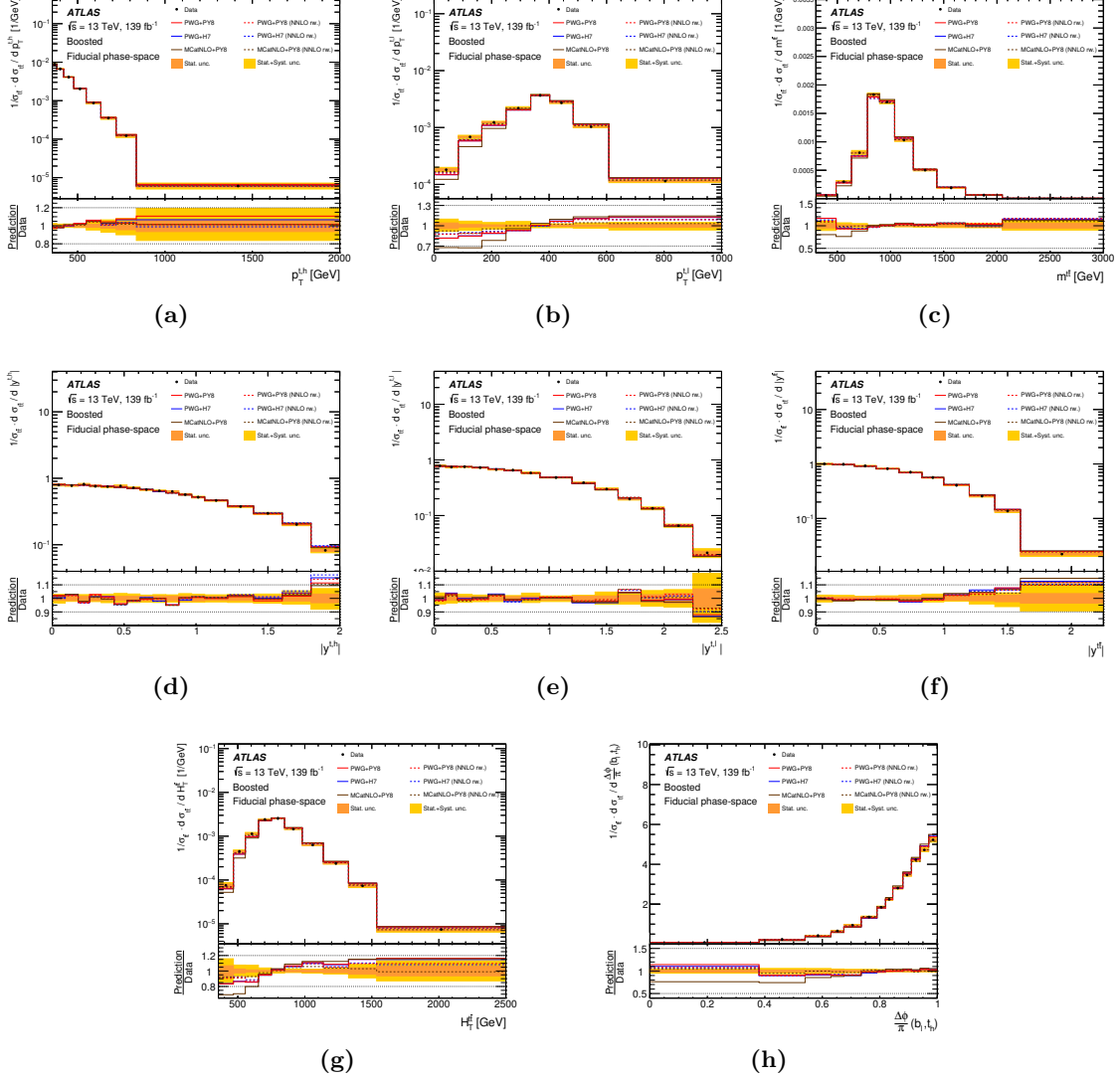
Observable	PWG+PY8		PWG+PY8(ISR Down)		PWG+PY8(ISR Up)		PWG+PY8(h_{damp}=3.0 m_t)		SHERPA		SHERPA (NLO norm.)	
	χ^2/NDF	p-value	χ^2/NDF	p-value	χ^2/NDF	p-value	χ^2/NDF	p-value	χ^2/NDF	p-value	χ^2/NDF	p-value
$p_{\mathrm{T}}^{t,h}$	3/7	0.84	3/7	0.90	6/7	0.57	5/7	0.63	5/7	0.69	5/7	0.69
$p_{\mathrm{T}}^{t,\ell}$	24/7	<0.01	57/7	<0.01	2/7	0.95	8/7	0.33	4/7	0.73	4/7	0.73
$p_{\mathrm{T}}^{t\bar{t}}$	95/6	<0.01	133/6	<0.01	258/6	<0.01	59/6	<0.01	57/6	<0.01	57/6	<0.01
$H_{\mathrm{T}}^{t\bar{t}+\mathrm{jets}}$	9/6	0.17	4/6	0.69	64/6	<0.01	20/6	<0.01	28/6	<0.01	28/6	<0.01
$H_{\mathrm{T}}^{t\bar{t}}$	39/9	<0.01	57/9	<0.01	22/9	0.01	26/9	<0.01	18/9	0.03	18/9	0.03
$|y^{t,h}|$	21/16	0.18	20/16	0.24	23/16	0.10	20/16	0.20	15/16	0.51	15/16	0.51
$|y^{t,\ell}|$	14/13	0.40	16/13	0.23	13/13	0.44	11/13	0.65	14/13	0.37	14/13	0.37
$|y^{t\bar{t}}|$	7/9	0.61	9/9	0.45	5/9	0.80	5/9	0.81	14/9	0.13	14/9	0.13
$m^{t\bar{t}}$	18/9	0.03	32/9	<0.01	43/9	<0.01	16/9	0.07	21/9	0.01	21/9	0.01
$p_{\mathrm{T}}^{j,1}$	84/14	<0.01	108/14	<0.01	187/14	<0.01	37/14	<0.01	113/14	<0.01	113/14	<0.01
$p_{\mathrm{T}}^{j,2}$	29/8	<0.01	11/8	0.21	96/8	<0.01	32/8	<0.01	23/8	<0.01	23/8	<0.01
N^j	7/4	0.12	16/4	<0.01	12/4	0.01	12/4	0.02	13/4	0.01	13/4	0.01
$\Delta\phi(j_1,t_h)$	9/8	0.32	27/8	<0.01	4/8	0.86	4/8	0.82	4/8	0.85	4/8	0.85
$\Delta\phi(j_2,t_h)$	5/8	0.78	6/8	0.64	6/8	0.69	6/8	0.63	1/8	1.00	1/8	1.00
$\Delta\phi(b_\ell,t_h)$	35/12	<0.01	48/12	<0.01	192/12	<0.01	46/12	<0.01	29/12	<0.01	29/12	<0.01
$\Delta\phi(t_h,t_\ell)$	62/4	<0.01	76/4	<0.01	156/4	<0.01	41/4	<0.01	29/4	<0.01	29/4	<0.01
$\Delta\phi(j_1,j_2)$	16/10	0.11	15/10	0.13	18/10	0.06	16/10	0.11	19/10	0.04	19/10	0.04
$m(j_1,t_h)$	30/11	<0.01	88/11	<0.01	46/11	<0.01	11/11	0.44	45/11	<0.01	45/11	<0.01
$p_{\mathrm{T}}^{j,1}$ vs N^j	261/20	<0.01	379/20	<0.01	363/20	<0.01	161/20	<0.01	161/20	<0.01	161/20	<0.01
$p_{\mathrm{T}}^{j,1}$ vs $p_{\mathrm{T}}^{t,h}$	80/16	<0.01	151/16	<0.01	170/16	<0.01	42/16	<0.01	103/16	<0.01	103/16	<0.01
$\Delta\phi(j_1,t_h)$ vs $p_{\mathrm{T}}^{t,h}$	48/20	<0.01	82/20	<0.01	27/20	0.13	37/20	0.01	30/20	0.07	30/20	0.07
$\Delta\phi(j_1,t_h)$ vs N^j	68/18	<0.01	146/18	<0.01	36/18	<0.01	40/18	<0.01	23/18	0.18	23/18	0.18

Table 7. χ^2 and p-values quantifying the level of agreement between the relative unfolded spectra and several NLO+PS predictions. PWG+PY8 corresponds to the POWHEG+PYTHIA sample. SHERPA (NLO norm.) refers to the SHERPA sample with its default normalisation. All other samples are normalised to the inclusive NNLO+NNLL $t\bar{t}$ cross-section prediction.
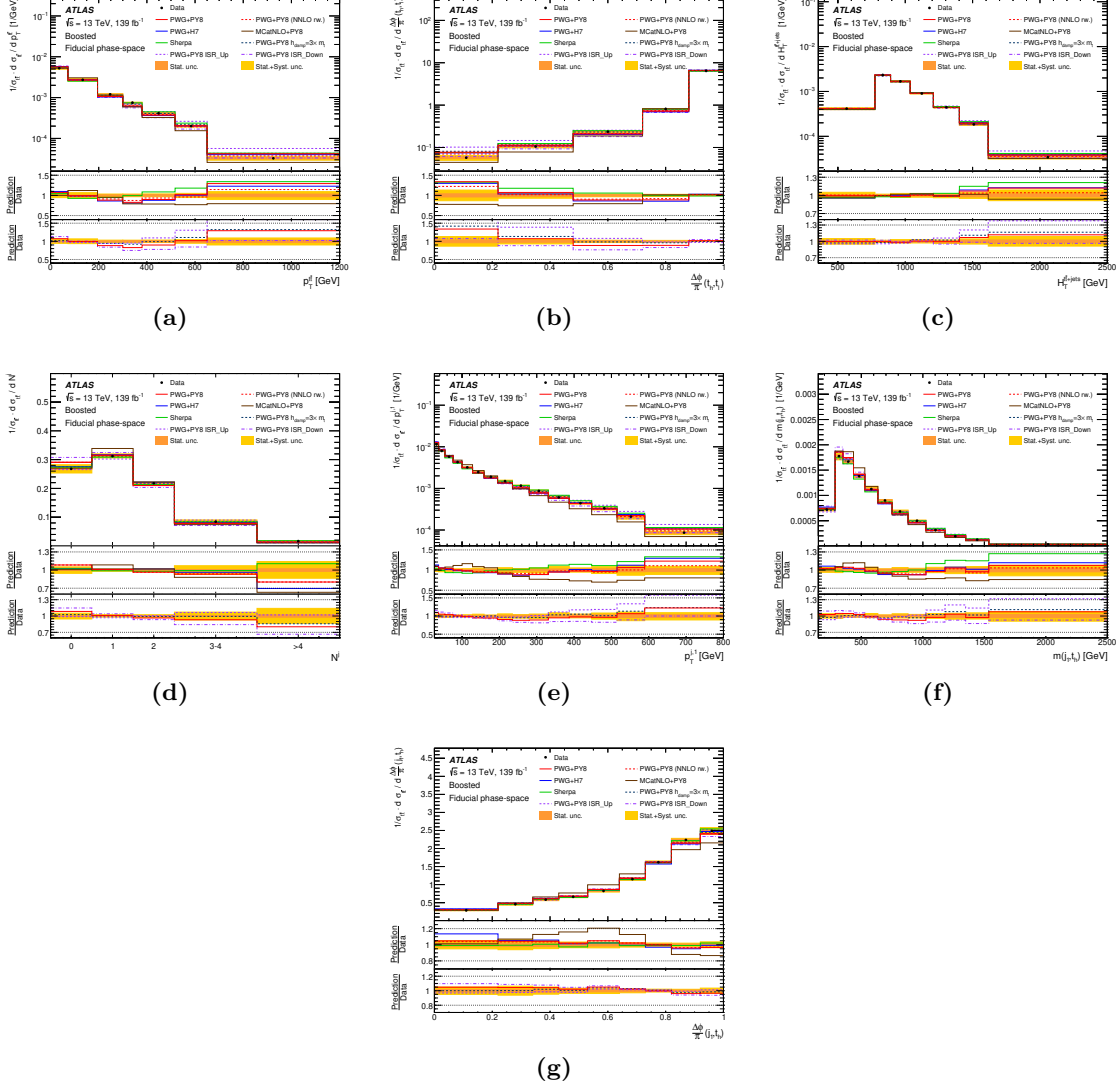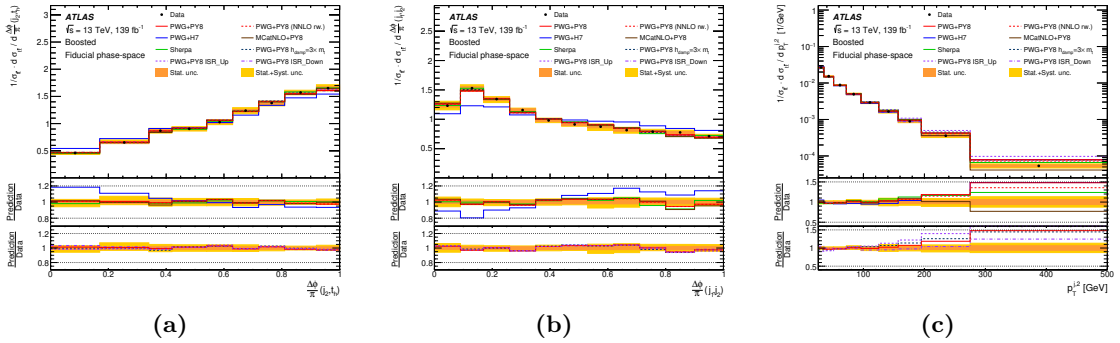

Figure 25. Normalised differential cross-section measurements for the observables related to jets produced in association with the $t\bar{t}$ system. The cross-section is shown as a function of (a) $\Delta\phi(j_2,t_h)$, (b) $\Delta\phi(j_1,j_2)$ and (c) $p_{\mathrm{T}}^{j,2}$.

(a)

(b)

Figure 26. (a) Normalised differential cross-section measurements as a function of the p_T of the leading additional jet in bins of additional jet multiplicity are compared with the prediction from the PowHEG+PYTHIA MC generator. The measurement and the predictions are further normalised by the factors shown in parentheses to aid visibility. (b) Ratio of the measured normalised cross-section to different NLO, and NLO reweighted to NNLO, predictions of $t\bar{t}$ signal for the same differential variables. PWG+PY8 corresponds to the PowHEG+PYTHIA sample, PWG+H7 to the PowHEG+HERWIG sample and MCatNLO+PY8 to the MadGraph5_aMC@NLO+PYTHIA sample. The yellow band represents the total uncertainty of the measured differential cross-section while the orange band shows the statistical component.

(a)

(b)

Figure 27. (a) Normalised differential cross-section measurements as a function of the p_T of the leading additional jet in bins of $p_T^{t,h}$ are compared with the prediction from the POWHEG+PYTHIA MC generator. The measurement 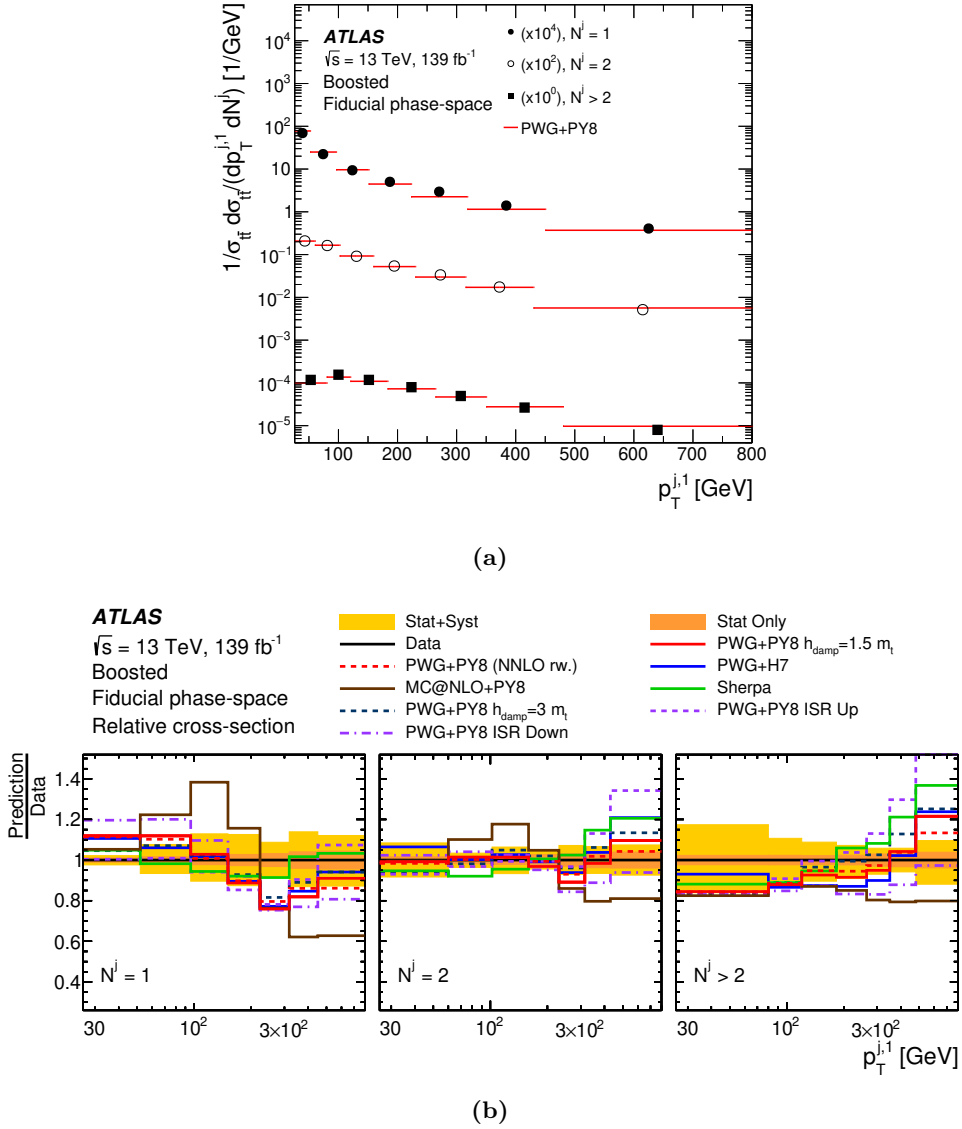and the predictions are further normalised by the factors shown in parentheses to aid visibility. (b) Ratio of the measured normalised cross-section to different NLO, and NLO reweighted to NNLO, predictions of $t\bar{t}$ signal for the same differential variables. PWG+PY8 corresponds to the POWHEG+PYTHIA sample, PWG+H7 to the POWHEG+HERWIG sample and MCatNLO+PY8 to the MADGRAPH5_AMC@NLO+PYTHIA sample. The yellow band represents the total uncertainty of the measured differential cross-section while the orange band shows the statistical component.

(a)

(b)

Figure 28. (a) Normalised differential cross-section measurements as a function of the $\Delta\phi$ angle between the leading additional jet and the hadronically decaying top quark in bins of $p_T^{t,h}$ are compared with the prediction from the POWHEG+PYTHIA MC generator. The measurement and the predictions are further normalised by the factors shown in parentheses to aid visibility. (b) Ratio of the measured normalised cross-section to different NLO, and NLO reweighted to NNLO, predictions of $t\bar{t}$ signal for the same differential variables. PWG+PY8 corresponds to the POWHEG+PYTHIA sample, PWG+H7 to the POWHEG+HERWIG sample and MCatNLO+PY8 to the MADGRAPH5_AMC@NLO+PYTHIA sample. The yellow band represents the total uncertainty of the measured differential cross-section while the orange band shows the statistical component.
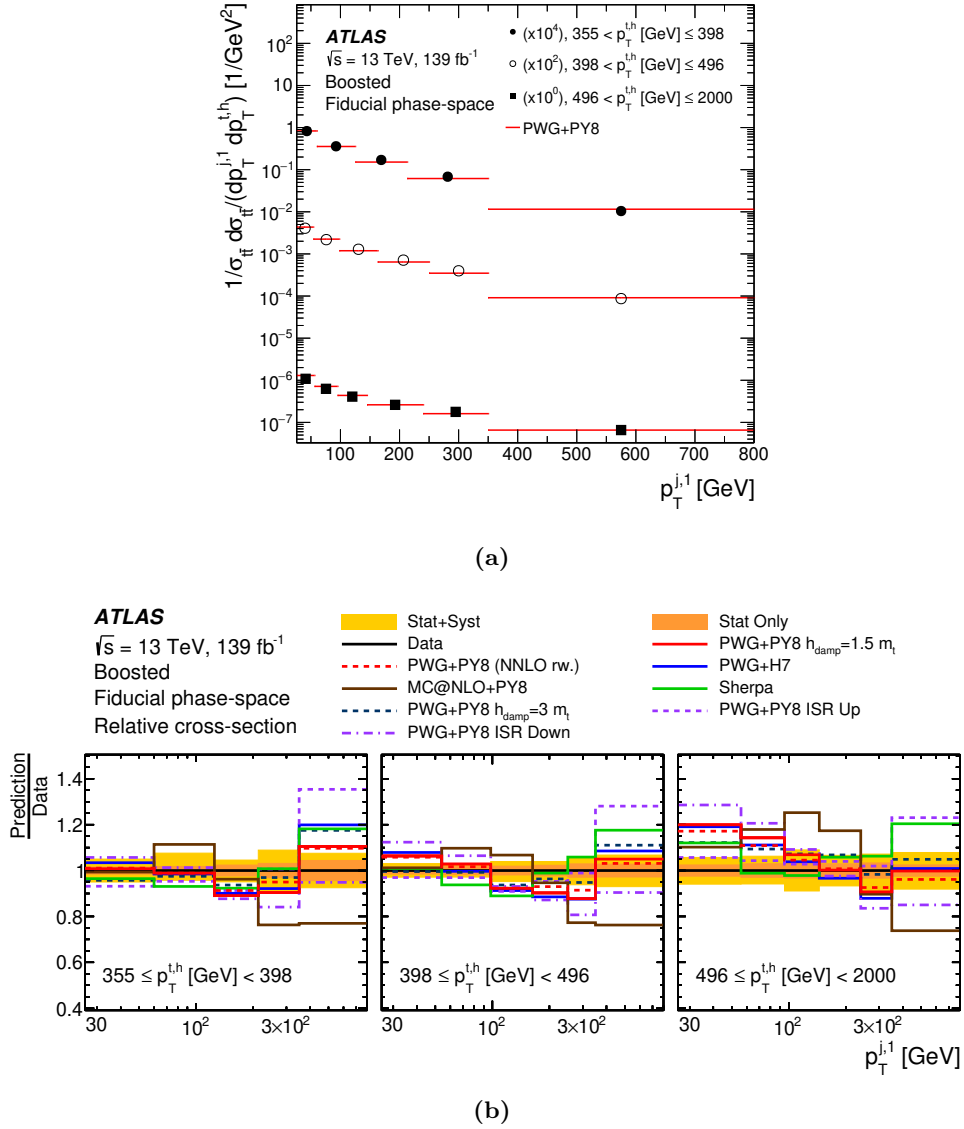
(a)

(b)

Figure 29. (a) Normalised differential cross-section measurements as a function of the $\Delta\phi$ angle between the leading additional jet and the hadronically decaying top quark in bins of additional jet multiplicity are compared with the prediction from the Powheg+Pythia MC generator. The measurement and the predictions are further normalised by the factors shown in parentheses to aid visibility. (b) Ratio of the measured normalised cross-section to different NLO, and NLO reweighted to NNLO, predictions of $t\bar{t}$ signal for the same differential variables. PWG+PY8 corresponds to the Powheg+Pythia sample, PWG+H7 to the Powheg+Herwig sample and MCatNLO+PY8 to the MadGraph5_aMC@NLO+Pythia sample. The yellow band represents the total uncertainty of the measured differential cross-section while the orange band shows the statistical component.
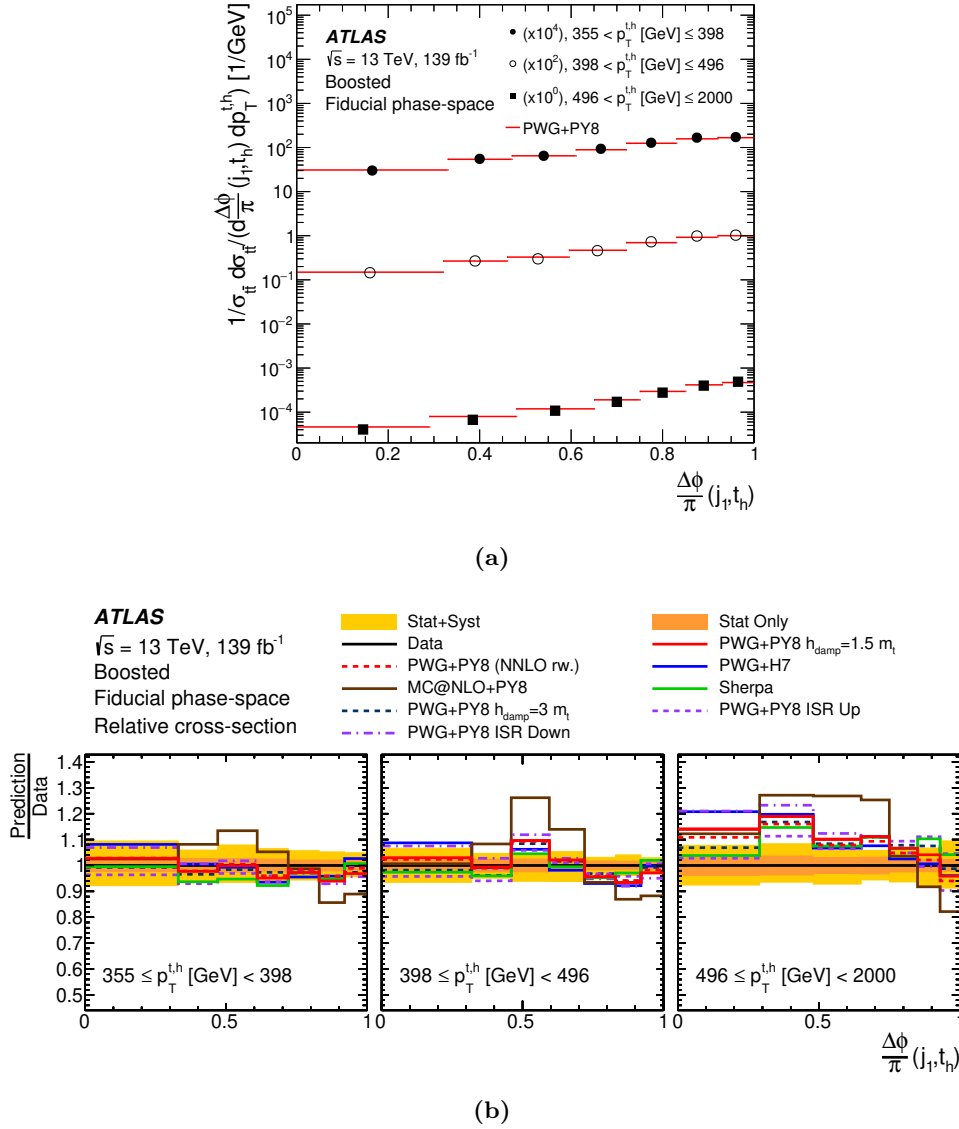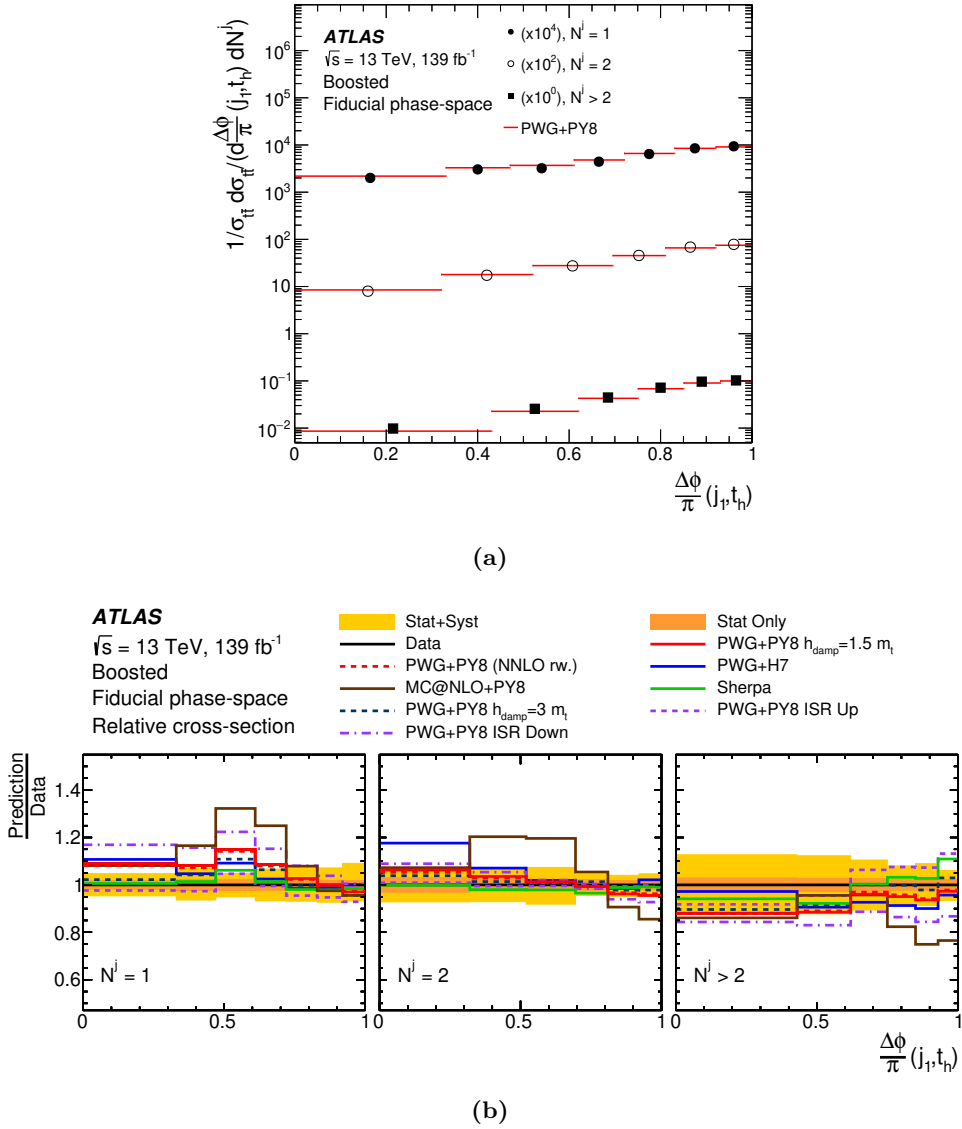
References

[1] S. Weinberg, *Phenomenological Lagrangians*, *Physica A* **96** (1979) 327 [INSPIRE].

[2] W. Buchmüller and D. Wyler, *Effective Lagrangian analysis of new interactions and flavor conservation*, *Nucl. Phys. B* **268** (1986) 621 [INSPIRE].

[3] C.J.C. Burges and H.J. Schnitzer, *Virtual effects of excited quarks as probes of a possible new hadronic mass scale*, *Nucl. Phys. B* **228** (1983) 464 [INSPIRE].

[4] C.N. Leung, S.T. Love and S. Rao, *Low-energy manifestations of a new interaction scale: operator analysis*, *Z. Phys. C* **31** (1986) 433 [INSPIRE].

[5] C. Degrande, J.-M. Gerard, C. Grojean, F. Maltoni and G. Servant, *Non-resonant new physics in top pair production at hadron colliders*, *JHEP* **03** (2011) 125 [arXiv:1010.6304] [INSPIRE].

[6] A. Buckley et al., *Constraining top quark effective theory in the LHC run II era*, *JHEP* **04** (2016) 015 [arXiv:1512.03360] [INSPIRE].

[7] M.P. Rosello and M. Vos, *Constraints on four-fermion interactions from the $t\bar{t}$ charge asymmetry at hadron colliders*, *Eur. Phys. J. C* **76** (2016) 200 [arXiv:1512.07542] [INSPIRE].

[8] C. Englert, L. Moore, K. Nordström and M. Russell, *Giving top quark effective operators a boost*, *Phys. Lett. B* **763** (2016) 9 [arXiv:1607.04304] [INSPIRE].

[9] ATLAS collaboration, *Measurements of top-quark pair differential and double-differential cross-sections in the ℓ+jets channel with pp collisions at $\sqrt{s} = 13$ TeV using the ATLAS detector*, *Eur. Phys. J. C* **79** (2019) 1028 [*Erratum ibid.* **80** (2020) 1092] [arXiv:1908.07305] [INSPIRE].

[10] ATLAS collaboration, *Measurements of $t\bar{t}$ differential cross-sections of highly boosted top quarks decaying to all-hadronic final states in pp collisions at $\sqrt{s} = 13$ TeV using the ATLAS detector*, *Phys. Rev. D* **98** (2018) 012003 [arXiv:1801.02052] [INSPIRE].

[11] CMS collaboration, *Measurement of differential $t\bar{t}$ production cross sections using top quarks at large transverse momenta in pp collisions at $\sqrt{s} = 13$ TeV*, *Phys. Rev. D* **103** (2021) 052008 [arXiv:2008.07860] [INSPIRE].

[12] ATLAS collaboration, *Measurement of the differential cross-section of highly boosted top quarks as a function of their transverse momentum in $\sqrt{s} = 8$ TeV proton-proton collisions using the ATLAS detector*, *Phys. Rev. D* **93** (2016) 032009 [arXiv:1510.03818] [INSPIRE].

[13] CMS collaboration, *Measurement of the integrated and differential $t\bar{t}$ production cross sections for high-p_t top quarks in pp collisions at $\sqrt{s} = 8$ TeV*, *Phys. Rev. D* **94** (2016) 072002 [arXiv:1605.00116] [INSPIRE].

[14] M. Czakon, D. Heymes and A. Mitov, *High-precision differential predictions for top-quark pairs at the LHC*, *Phys. Rev. Lett.* **116** (2016) 082003 [arXiv:1511.00549] [INSPIRE].

[15] M. Czakon, D. Heymes, A. Mitov, D. Pagani, I. Tsinikos and M. Zaro, *Top-pair production at the LHC through NNLO QCD and NLO EW*, *JHEP* **10** (2017) 186 [arXiv:1705.04105] [INSPIRE].

[16] S. Catani, S. Devoto, M. Grazzini, S. Kallweit and J. Mazzitelli, *Top-quark pair production at the LHC: fully differential QCD predictions at NNLO*, *JHEP* **07** (2019) 100 [arXiv:1906.06535] [INSPIRE].

[17] A. Behring, M. Czakon, A. Mitov, A.S. Papanastasiou and R. Poncelet, *Higher order corrections to spin correlations in top quark pair production at the LHC*, *Phys. Rev. Lett.* **123** (2019) 082001 [arXiv:1901.05407] [INSPIRE].

[18] B. Grzadkowski, M. Iskrzynski, M. Misiak and J. Rosiek, *Dimension-six terms in the Standard Model Lagrangian*, *JHEP* **10** (2010) 085 [arXiv:1008.4884] [INSPIRE].

[19] ATLAS collaboration, *The ATLAS experiment at the CERN Large Hadron Collider*, 2008 *JINST* **3** S08003 [INSPIRE].

[20] ATLAS IBL collaboration, *Production and integration of the ATLAS insertable B-layer*, 2018 *JINST* **13** T05008 [arXiv:1803.00844] [INSPIRE].

[21] ATLAS collaboration, *ATLAS insertable B-layer technical design report*, Tech. Rep. CERN-LHCC-2010-013, CERN, Geneva, Switzerland (2010) [ATLAS-TDR-19].

[22] ATLAS collaboration, *The ATLAS collaboration software and firmware*, Tech. Rep. ATL-SOFT-PUB-2021-001, CERN, Geneva, Switzerland (2021).

[23] ATLAS collaboration, *ATLAS data quality operations and performance for* 2015–2018 *data-taking*, 2020 *JINST* **15** P04003 [arXiv:1911.04632] [INSPIRE].

[24] ATLAS collaboration, *Luminosity determination in pp collisions at* $\sqrt{s} = 13$ *TeV using the ATLAS detector at the LHC*, Tech. Rep. ATLAS-CONF-2019-021, CERN, Geneva, Switzerland (2019).

[25] G. Avoni et al., *The new LUCID-2 detector for luminosity measurement and monitoring in ATLAS*, 2018 *JINST* **13** P07017 [INSPIRE].

[26] ATLAS collaboration, *Performance of electron and photon triggers in ATLAS during LHC run* 2, *Eur. Phys. J. C* **80** (2020) 47 [arXiv:1909.00761] [INSPIRE].

[27] ATLAS collaboration, *Performance of the ATLAS muon triggers in run* 2, 2020 *JINST* **15** P09015 [arXiv:2004.13447] [INSPIRE].

[28] ATLAS collaboration, *The ATLAS simulation infrastructure*, *Eur. Phys. J. C* **70** (2010) 823 [arXiv:1005.4568] [INSPIRE].

[29] GEANT4 collaboration, *GEANT4 — a simulation toolkit*, *Nucl. Instrum. Meth. A* **506** (2003) 250 [INSPIRE].

[30] ATLAS collaboration, *The simulation principle and performance of the ATLAS fast calorimeter simulation FastCaloSim*, Tech. Rep. ATL-PHYS-PUB-2010-013, CERN, Geneva, Switzerland (2010).

[31] T. Sjöstrand et al., *An introduction to PYTHIA* 8.2, *Comput. Phys. Commun.* **191** (2015) 159 [arXiv:1410.3012] [INSPIRE].

[32] ATLAS collaboration, *The PYTHIA* 8 *A3 tune description of ATLAS minimum bias and inelastic measurements incorporating the Donnachie-Landshoff diffractive model*, Tech. Rep. ATL-PHYS-PUB-2016-017, CERN, Geneva, Switzerland (2016).

[33] S. Frixione, P. Nason and G. Ridolfi, *A positive-weight next-to-leading-order Monte Carlo for heavy flavour hadroproduction*, *JHEP* **09** (2007) 126 [arXiv:0707.3088] [INSPIRE].

[34] P. Nason, *A new method for combining NLO QCD with shower Monte Carlo algorithms*, *JHEP* **11** (2004) 040 [hep-ph/0409146] [INSPIRE].

[35] S. Frixione, P. Nason and C. Oleari, *Matching NLO QCD computations with parton shower simulations: the POWHEG method*, *JHEP* **11** (2007) 070 [arXiv:0709.2092] [INSPIRE].

[36] S. Alioli, P. Nason, C. Oleari and E. Re, *A general framework for implementing NLO calculations in shower Monte Carlo programs: the POWHEG BOX*, *JHEP* **06** (2010) 043 [arXiv:1002.2581] [INSPIRE].

[37] NNPDF collaboration, *Parton distributions for the LHC run II*, *JHEP* **04** (2015) 040 [arXiv:1410.8849] [INSPIRE].

[38] ATLAS collaboration, *Studies on top-quark Monte Carlo modelling for Top*2016, Tech. Rep. ATL-PHYS-PUB-2016-020, CERN, Geneva, Switzerland (2016).

[39] *ATLAS PYTHIA* 8 *tunes to* 7 *TeV data*, Tech. Rep. ATL-PHYS-PUB-2014-021, CERN, Geneva, Switzerland (2014).

[40] R.D. Ball et al., *Parton distributions with LHC data*, *Nucl. Phys. B* **867** (2013) 244 [arXiv:1207.1303] [INSPIRE].

[41] ATLAS collaboration, *Studies on top-quark Monte Carlo modelling with Sherpa and MG5_aMC@NLO*, Tech. Rep. ATL-PHYS-PUB-2017-007, CERN, Geneva, Switzerland (2017).

[42] M. Bähr et al., *HERWIG++ physics and manual*, *Eur. Phys. J. C* **58** (2008) 639 [arXiv:0803.0883] [INSPIRE].

[43] J. Bellm et al., *HERWIG* 7.0/*HERWIG++* 3.0 *release note*, *Eur. Phys. J. C* **76** (2016) 196 [arXiv:1512.01178] [INSPIRE].

[44] L.A. Harland-Lang, A.D. Martin, P. Motylinski and R.S. Thorne, *Parton distributions in the LHC era: MMHT* 2014 *PDFs*, *Eur. Phys. J. C* **75** (2015) 204 [arXiv:1412.3989] [INSPIRE].

[45] J. Alwall et al., *The automated computation of tree-level and next-to-leading order differential cross sections, and their matching to parton shower simulations*, *JHEP* **07** (2014) 079 [arXiv:1405.0301] [INSPIRE].

[46] M. Beneke, P. Falgari, S. Klein and C. Schwinn, *Hadronic top-quark pair production with NNLL threshold resummation*, *Nucl. Phys. B* **855** (2012) 695 [arXiv:1109.1536] [INSPIRE].

[47] M. Cacciari, M. Czakon, M. Mangano, A. Mitov and P. Nason, *Top-pair production at hadron colliders with next-to-next-to-leading logarithmic soft-gluon resummation*, *Phys. Lett. B* **710** (2012) 612 [arXiv:1111.5869] [INSPIRE].

[48] P. Bärnreuther, M. Czakon and A. Mitov, *Percent level precision physics at the Tevatron: first genuine NNLO QCD corrections to $q\bar{q} \to t\bar{t} + X$*, *Phys. Rev. Lett.* **109** (2012) 132001 [arXiv:1204.5201] [INSPIRE].

[49] M. Czakon and A. Mitov, *NNLO corrections to top-pair production at hadron colliders: the all-fermionic scattering channels*, *JHEP* **12** (2012) 054 [arXiv:1207.0236] [INSPIRE].

[50] M. Czakon and A. Mitov, *NNLO corrections to top pair production at hadron colliders: the quark-gluon reaction*, *JHEP* **01** (2013) 080 [arXiv:1210.6832] [INSPIRE].

[51] M. Czakon, P. Fiedler and A. Mitov, *Total top-quark pair-production cross section at hadron colliders through $O(\alpha_S^4)$*, *Phys. Rev. Lett.* **110** (2013) 252004 [arXiv:1303.6254] [INSPIRE].

[52] M. Czakon and A. Mitov, *Top++: a program for the calculation of the top-pair cross-section at hadron colliders*, *Comput. Phys. Commun.* **185** (2014) 2930 [arXiv:1112.5675] [INSPIRE].

[53] J. Butterworth et al., *PDF4LHC recommendations for LHC run II*, *J. Phys. G* **43** (2016) 023001 [arXiv:1510.03865] [INSPIRE].

[54] A.D. Martin, W.J. Stirling, R.S. Thorne and G. Watt, *Parton distributions for the LHC*, *Eur. Phys. J. C* **63** (2009) 189 [arXiv:0901.0002] [INSPIRE].

[55] A.D. Martin, W.J. Stirling, R.S. Thorne and G. Watt, *Uncertainties on α_s in global PDF analyses and implications for predicted hadronic cross sections*, *Eur. Phys. J. C* **64** (2009) 653 [arXiv:0905.3531] [INSPIRE].

[56] H.-L. Lai et al., *New parton distributions for collider physics*, *Phys. Rev. D* **82** (2010) 074024 [arXiv:1007.2241] [INSPIRE].

[57] J. Gao et al., *CT10 next-to-next-to-leading order global analysis of QCD*, *Phys. Rev. D* **89** (2014) 033009 [arXiv:1302.6246] [INSPIRE].

[58] M. Grazzini, S. Kallweit and M. Wiesemann, *Fully differential NNLO computations with MATRIX*, *Eur. Phys. J. C* **78** (2018) 537 [arXiv:1711.06631] [INSPIRE].

[59] ATLAS, CMS collaboration, *Treatment of top-quark backgrounds in extreme phase spaces: the "top p_T reweighting" and novel data-driven estimations in ATLAS and CMS*, in 13$^{\text{th}}$ *international workshop on top quark physics*, (2021) [arXiv:2105.03977] [INSPIRE].

[60] SHERPA collaboration, *Event generation with Sherpa 2.2*, *SciPost Phys.* **7** (2019) 034 [arXiv:1905.09127] [INSPIRE].

[61] T. Gleisberg and S. Höche, *Comix, a new matrix element generator*, *JHEP* **12** (2008) 039 [arXiv:0808.3674] [INSPIRE].

[62] F. Buccioni et al., *OpenLoops 2*, *Eur. Phys. J. C* **79** (2019) 866 [arXiv:1907.13071] [INSPIRE].

[63] F. Cascioli, P. Maierhöfer and S. Pozzorini, *Scattering amplitudes with open loops*, *Phys. Rev. Lett.* **108** (2012) 111601 [arXiv:1111.5206] [INSPIRE].

[64] A. Denner, S. Dittmaier and L. Hofer, *Collier: a fortran-based Complex One-Loop LIbrary in Extended Regularizations*, *Comput. Phys. Commun.* **212** (2017) 220 [arXiv:1604.06792] [INSPIRE].

[65] S. Schumann and F. Krauss, *A parton shower algorithm based on Catani-Seymour dipole factorisation*, *JHEP* **03** (2008) 038 [arXiv:0709.1027] [INSPIRE].

[66] S. Höche, F. Krauss, M. Schönherr and F. Siegert, *A critical appraisal of NLO+PS matching methods*, *JHEP* **09** (2012) 049 [arXiv:1111.1220] [INSPIRE].

[67] S. Höche, F. Krauss, M. Schönherr and F. Siegert, *QCD matrix elements + parton showers: the NLO case*, *JHEP* **04** (2013) 027 [arXiv:1207.5030] [INSPIRE].

[68] S. Catani, F. Krauss, R. Kuhn and B.R. Webber, *QCD matrix elements + parton showers*, *JHEP* **11** (2001) 063 [hep-ph/0109231] [INSPIRE].

[69] S. Höche, F. Krauss, S. Schumann and F. Siegert, *QCD matrix elements and truncated showers*, *JHEP* **05** (2009) 053 [arXiv:0903.1219] [INSPIRE].

[70] G. D'Ambrosio, G.F. Giudice, G. Isidori and A. Strumia, *Minimal flavor violation: an effective field theory approach*, *Nucl. Phys. B* **645** (2002) 155 [hep-ph/0207036] [INSPIRE].

[71] C. Degrande, G. Durieux, F. Maltoni, K. Mimasu, E. Vryonidou and C. Zhang, *Automated one-loop computations in the standard model effective field theory*, *Phys. Rev. D* **103** (2021) 096024 [arXiv:2008.11743] [INSPIRE].

[72] I. Brivio et al., *Electroweak input parameters*, Tech. Rep. CERN-LPCC-2021-002, CERN, Geneva, Switzerland (2021) [CERN-LHCEFTWG-2021-001].

[73] E. Re, *Single-top Wt-channel production matched with parton showers using the POWHEG method*, *Eur. Phys. J. C* **71** (2011) 1547 [arXiv:1009.2450] [INSPIRE].

[74] S. Alioli, P. Nason, C. Oleari and E. Re, *NLO single-top production matched with shower in POWHEG: s- and t-channel contributions*, *JHEP* **09** (2009) 111 [*Erratum ibid.* **02** (2010) 011] [arXiv:0907.4076] [INSPIRE].

[75] S. Frixione, E. Laenen, P. Motylinski, B.R. Webber and C.D. White, *Single-top hadroproduction in association with a W boson*, *JHEP* **07** (2008) 029 [arXiv:0805.3067] [INSPIRE].

[76] R. Frederix, E. Re and P. Torrielli, *Single-top t-channel hadroproduction in the four-flavour scheme with POWHEG and aMC@NLO*, *JHEP* **09** (2012) 130 [arXiv:1207.5391] [INSPIRE].

[77] C. Anastasiou, L.J. Dixon, K. Melnikov and F. Petriello, *High precision QCD at hadron colliders: electroweak gauge boson rapidity distributions at NNLO*, *Phys. Rev. D* **69** (2004) 094008 [hep-ph/0312266] [INSPIRE].

[78] ATLAS collaboration, *Electron and photon performance measurements with the ATLAS detector using the* 2015–2017 *LHC proton-proton collision data*, 2019 *JINST* **14** P12006 [arXiv:1908.00005] [INSPIRE].

[79] ATLAS collaboration, *Muon reconstruction and identification efficiency in ATLAS using the full run* 2 *pp collision data set at* $\sqrt{s} = 13$ *TeV*, *Eur. Phys. J. C* **81** (2021) 578 [arXiv:2012.00578] [INSPIRE].

[80] M. Cacciari, G.P. Salam and G. Soyez, *The anti-k_t jet clustering algorithm*, *JHEP* **04** (2008) 063 [arXiv:0802.1189] [INSPIRE].

[81] M. Cacciari, G.P. Salam and G. Soyez, *FastJet user manual*, *Eur. Phys. J. C* **72** (2012) 1896 [arXiv:1111.6097] [INSPIRE].

[82] ATLAS collaboration, *Jet reconstruction and performance using particle flow with the ATLAS detector*, *Eur. Phys. J. C* **77** (2017) 466 [arXiv:1703.10485] [INSPIRE].

[83] ATLAS collaboration, *Jet energy scale and resolution measured in proton-proton collisions at* $\sqrt{s} = 13$ *TeV with the ATLAS detector*, *Eur. Phys. J. C* **81** (2021) 689 [arXiv:2007.02645] [INSPIRE].

[84] ATLAS collaboration, *Performance of pile-up mitigation techniques for jets in pp collisions at* $\sqrt{s} = 8$ *TeV using the ATLAS detector*, *Eur. Phys. J. C* **76** (2016) 581 [arXiv:1510.03823] [INSPIRE].

[85] ATLAS collaboration, *ATLAS b-jet identification performance and efficiency measurement with $t\bar{t}$ events in pp collisions at* $\sqrt{s} = 13$ *TeV*, *Eur. Phys. J. C* **79** (2019) 970 [arXiv:1907.05120] [INSPIRE].

[86] ATLAS collaboration, *Optimisation and performance studies of the ATLAS b-tagging algorithms for the* 2017–18 *LHC run*, Tech. Rep. ATL-PHYS-PUB-2017-013, CERN, Geneva, Switzerland (2017).

[87] B. Nachman, P. Nef, A. Schwartzman, M. Swiatlowski and C. Wanotayaroj, *Jets from jets: re-clustering as a tool for large radius jet reconstruction and grooming at the LHC*, *JHEP* **02** (2015) 075 [arXiv:1407.2922] [ɪɴSPIRE].

[88] D. Krohn, J. Thaler and L.-T. Wang, *Jet trimming*, *JHEP* **02** (2010) 084 [arXiv:0912.1342] [ɪɴSPIRE].

[89] ATLAS collaboration, *Performance of missing transverse momentum reconstruction with the ATLAS detector using proton-proton collisions at* $\sqrt{s} = 13$ *TeV*, *Eur. Phys. J. C* **78** (2018) 903 [arXiv:1802.08168] [ɪɴSPIRE].

[90] ATLAS collaboration, *Probing the quantum interference between singly and doubly resonant top-quark production in pp collisions at* $\sqrt{s} = 13$ *TeV with the ATLAS detector*, *Phys. Rev. Lett.* **121** (2018) 152002 [arXiv:1806.04667] [ɪɴSPIRE].

[91] Particle Data Group collaboration, *Review of particle physics*, *Phys. Rev. D* **98** (2018) 030001 [ɪɴSPIRE].

[92] G. D'Agostini, *A multidimensional unfolding method based on Bayes' theorem*, *Nucl. Instrum. Meth. A* **362** (1995) 487 [ɪɴSPIRE].

[93] T. Adye, *Unfolding algorithms and tests using RooUnfold*, in *PHYSTAT* 2011, CERN-2011-006, CERN, Geneva, Switzerland (2011), p. 313 [arXiv:1105.1160] [ɪɴSPIRE].

[94] ATLAS collaboration, *Search for single production of vector-like quarks decaying into Wb in pp collisions at* $\sqrt{s} = 13$ *TeV with the ATLAS detector*, *JHEP* **05** (2019) 164 [arXiv:1812.07343] [ɪɴSPIRE].

[95] ATLAS collaboration, *Estimation of non-prompt and fake lepton backgrounds in final states with top quarks produced in proton-proton collisions at* $\sqrt{s} = 8$ *TeV with the ATLAS detector*, Tech. Rep. ATLAS-CONF-2014-058, CERN, Geneva, Switzerland (2014).

[96] ATLAS collaboration, *Measurement of the* $t\bar{t}$ *production cross-section in the lepton+jets channel at* $\sqrt{s} = 13$ *TeV with the ATLAS experiment*, *Phys. Lett. B* **810** (2020) 135797 [arXiv:2006.13076] [ɪɴSPIRE].

[97] ATLAS collaboration, *Measurements of top-quark pair single- and double-differential cross-sections in the all-hadronic channel in pp collisions at* $\sqrt{s} = 13$ *TeV using the ATLAS detector*, *JHEP* **01** (2021) 033 [arXiv:2006.09274] [ɪɴSPIRE].

[98] CMS collaboration, *Measurement of the cross section for* $t\bar{t}$ *production with additional jets and b jets in pp collisions at* $\sqrt{s} = 13$ *TeV*, *JHEP* **07** (2020) 125 [arXiv:2003.06467] [ɪɴSPIRE].

[99] CMS collaboration, *Measurement of differential cross sections for the production of top quark pairs and of additional jets in lepton+jets events from pp collisions at* $\sqrt{s} = 13$ *TeV*, *Phys. Rev. D* **97** (2018) 112003 [arXiv:1803.08856] [ɪɴSPIRE].

[100] CMS collaboration, *Measurement of the top quark mass using proton-proton data at* $\sqrt{s} = 7$ *and 8 TeV*, *Phys. Rev. D* **93** (2016) 072004 [arXiv:1509.04044] [ɪɴSPIRE].

[101] ATLAS collaboration, *Measurement of the top quark mass in the* $t\bar{t} \rightarrow$ *lepton+jets channel from* $\sqrt{s} = 8$ *TeV ATLAS data and combination with previous results*, *Eur. Phys. J. C* **79** (2019) 290 [arXiv:1810.01772] [ɪɴSPIRE].

[102] M. Cacciari, G.P. Salam and G. Soyez, *The catchment area of jets*, *JHEP* **04** (2008) 005 [arXiv:0802.1188] [INSPIRE].

[103] S. Schmitt, *Data unfolding methods in high energy physics*, *EPJ Web Conf.* **137** (2017) 11008 [arXiv:1611.01927] [INSPIRE].

[104] M. Czakon, N.P. Hartland, A. Mitov, E.R. Nocera and J. Rojo, *Pinning down the large-x gluon with NNLO top-quark pair differential distributions*, *JHEP* **04** (2017) 044 [arXiv:1611.08609] [INSPIRE].

[105] ATLAS collaboration, *Muon reconstruction performance of the ATLAS detector in proton-proton collision data at $\sqrt{s} = 13$ TeV*, *Eur. Phys. J. C* **76** (2016) 292 [arXiv:1603.05598] [INSPIRE].

[106] ATLAS collaboration, *ATLAS simulation of boson plus jets processes in run* 2, Tech. Rep. ATL-PHYS-PUB-2017-006, CERN, Geneva, Switzerland (2017).

[107] LHC HIGGS CROSS SECTION WORKING GROUP collaboration, *Handbook of LHC Higgs cross sections:* 4. *Deciphering the nature of the Higgs sector*, arXiv:1610.07922 [INSPIRE].

[108] J. Mazzitelli, P.F. Monni, P. Nason, E. Re, M. Wiesemann and G. Zanderighi, *Next-to-next-to-leading order event generation for top-quark pair production*, *Phys. Rev. Lett.* **127** (2021) 062001 [arXiv:2012.14267] [INSPIRE].

[109] N. Castro, J. Erdmann, C. Grunwald, K. Kröninger and N.-A. Rosien, *EFTfitter — a tool for interpreting measurements in the context of effective field theories*, *Eur. Phys. J. C* **76** (2016) 432 [arXiv:1605.05585] [INSPIRE].

[110] A. Caldwell, D. Kollár and K. Kroninger, *BAT: the Bayesian Analysis Toolkit*, *Comput. Phys. Commun.* **180** (2009) 2197 [arXiv:0808.2552] [INSPIRE].

[111] SMEFIT collaboration, *Combined SMEFT interpretation of Higgs, diboson, and top quark data from the LHC*, *JHEP* **11** (2021) 089 [arXiv:2105.00006] [INSPIRE].

[112] ATLAS collaboration, *ATLAS computing acknowledgements*, Tech. Rep. ATL-SOFT-PUB-2021-003, CERN, Geneva, Switzerland (2021).

The ATLAS collaboration

G. Aad[100], B. Abbott[126], D.C. Abbott[101], A. Abed Abud[36], K. Abeling[53], D.K. Abhayasinghe[93],
S.H. Abidi[29], A. Aboulhorma[35e], H. Abramowicz[158], H. Abreu[157], Y. Abulaiti[123],
A.C. Abusleme Hoffman[144a], B.S. Acharya[66a,66b,n], B. Achkar[53], L. Adam[98],
C. Adam Bourdarios[4], L. Adamczyk[83a], L. Adamek[163], S.V. Addepalli[26], J. Adelman[118],
A. Adiguzel[21c], S. Adorni[54], T. Adye[141], A.A. Affolder[143], Y. Afik[36], M.N. Agaras[13],
J. Agarwala[70a,70b], A. Aggarwal[98], C. Agheorghiesei[27c], J.A. Aguilar-Saavedra[137f,137a,x],
A. Ahmad[36], F. Ahmadov[79], W.S. Ahmed[102], X. Ai[46], G. Aielli[73a,73b], I. Aizenberg[176],
M. Akbiyik[98], T.P.A. Åkesson[96], A.V. Akimov[109], K. Al Khoury[39], G.L. Alberghi[23b],
J. Albert[172], P. Albicocco[51], M.J. Alconada Verzini[88], S. Alderweireldt[50], M. Aleksa[36],
I.N. Aleksandrov[79], C. Alexa[27b], T. Alexopoulos[10], A. Alfonsi[117], F. Alfonsi[23b], M. Alhroob[126],
B. Ali[139], S. Ali[155], M. Aliev[162], G. Alimonti[68a], C. Allaire[36], B.M.M. Allbrooke[153],
P.P. Allport[20], A. Aloisio[69a,69b], F. Alonso[88], C. Alpigiani[145], E. Alunno Camelia[73a,73b],
M. Alvarez Estevez[97], M.G. Alviggi[69a,69b], Y. Amaral Coutinho[80b], A. Ambler[102], L. Ambroz[132],
C. Amelung[36], D. Amidei[104], S.P. Amor Dos Santos[137a], S. Amoroso[46], K.R. Amos[170],
C.S. Amrouche[54], V. Ananiev[131], C. Anastopoulos[146], N. Andari[142], T. Andeen[11], J.K. Anders[19],
S.Y. Andrean[45a,45b], A. Andreazza[68a,68b], S. Angelidakis[9], A. Angerami[39],
A.V. Anisenkov[119b,119a], A. Annovi[71a], C. Antel[54], M.T. Anthony[146], E. Antipov[127],
M. Antonelli[51], D.J.A. Antrim[17], F. Anulli[72a], M. Aoki[81], J.A. Aparisi Pozo[170], M.A. Aparo[153],
L. Aperio Bella[46], C. Appelt[18], N. Aranzabal[36], V. Araujo Ferraz[80a], C. Arcangeletti[51],
A.T.H. Arce[49], E. Arena[90], J-F. Arguin[108], S. Argyropoulos[52], J.-H. Arling[46], A.J. Armbruster[36],
O. Arnaez[163], H. Arnold[117], Z.P. Arrubarrena Tame[112], G. Artoni[72a,72b], H. Asada[114],
K. Asai[124], S. Asai[160], N.A. Asbah[59], E.M. Asimakopoulou[168], J. Assahsah[35d], K. Assamagan[29],
R. Astalos[28a], R.J. Atkin[33a], M. Atkinson[169], N.B. Atlay[18], H. Atmani[60b], P.A. Atmasiddha[104],
K. Augsten[139], S. Auricchio[69a,69b], V.A. Austrup[178], G. Avner[157], G. Avolio[36], M.K. Ayoub[14c],
G. Azuelos[108,ae], D. Babal[28a], H. Bachacou[142], K. Bachas[159], A. Bachiu[34], F. Backman[45a,45b],
A. Badea[59], P. Bagnaia[72a,72b], M. Bahmani[18], A.J. Bailey[170], V.R. Bailey[169], J.T. Baines[141],
C. Bakalis[10], O.K. Baker[179], P.J. Bakker[117], E. Bakos[15], D. Bakshi Gupta[8], S. Balaji[154],
R. Balasubramanian[117], E.M. Baldin[119b,119a], P. Balek[140], E. Ballabene[68a,68b], F. Balli[142],
L.M. Baltes[61a], W.K. Balunas[32], J. Balz[98], E. Banas[84], M. Bandieramonte[136],
A. Bandyopadhyay[24], S. Bansal[24], L. Barak[158], E.L. Barberio[103], D. Barberis[55b,55a],
M. Barbero[100], G. Barbour[94], K.N. Barends[33a], T. Barillari[113], M-S. Barisits[36], J. Barkeloo[129],
T. Barklow[150], R.M. Barnett[17], P. Baron[128], A. Baroncelli[60a], G. Barone[29], A.J. Barr[132],
L. Barranco Navarro[45a,45b], F. Barreiro[97], J. Barreiro Guimarães da Costa[14a], U. Barron[158],
S. Barsov[135], F. Bartels[61a], R. Bartoldus[150], G. Bartolini[100], A.E. Barton[89], P. Bartos[28a],
A. Basalaev[46], A. Basan[98], M. Baselga[47], I. Bashta[74a,74b], A. Bassalat[64,ab], M.J. Basso[163],
C.R. Basson[99], R.L. Bates[57], S. Batlamous[35e], J.R. Batley[32], B. Batool[148], M. Battaglia[143],
M. Bauce[72a,72b], F. Bauer[142,*], P. Bauer[24], A. Bayirli[21a], J.B. Beacham[49], T. Beau[133],
P.H. Beauchemin[166], F. Becherer[52], P. Bechtle[24], H.P. Beck[19,p], K. Becker[174], C. Becot[46],
A.J. Beddall[21d], V.A. Bednyakov[79], C.P. Bee[152], L.J. Beemster[15], T.A. Beermann[36],
M. Begalli[80b], M. Begel[29], A. Behera[152], J.K. Behr[46], C. Beirao Da Cruz E Silva[36],
J.F. Beirer[53,36], F. Beisiegel[24], M. Belfkir[122b], G. Bella[158], L. Bellagamba[23b], A. Bellerive[34],
P. Bellos[20], K. Beloborodov[119b,119a], K. Belotskiy[110], N.L. Belyaev[110], D. Benchekroun[35a],
Y. Benhammou[158], D.P. Benjamin[29], M. Benoit[29], J.R. Bensinger[26], S. Bentvelsen[117],
L. Beresford[36], M. Beretta[51], D. Berge[18], E. Bergeaas Kuutmann[168], N. Berger[4],
B. Bergmann[139], J. Beringer[17], S. Berlendis[7], G. Bernardi[5], C. Bernius[150], F.U. Bernlochner[24],
T. Berry[93], P. Berta[140], I.A. Bertram[89], O. Bessidskaia Bylund[178], S. Bethke[113], A. Betti[42],

A.J. Bevan[92], S. Bhatta[152], D.S. Bhattacharya[173], P. Bhattarai[26], V.S. Bhopatkar[6], R. Bi[136], R. Bi[29], R.M. Bianchi[136], O. Biebel[112], R. Bielski[129], N.V. Biesuz[71a,71b], M. Biglietti[74a], T.R.V. Billoud[139], M. Bindi[53], A. Bingul[21b], C. Bini[72a,72b], S. Biondi[23b,23a], A. Biondini[90], C.J. Birch-sykes[99], G.A. Bird[20,141], M. Birman[176], T. Bisanz[36], J.P. Biswal[2], D. Biswas[177,j], A. Bitadze[99], K. Bjørke[131], I. Bloch[46], A. Blocker[26], A. Blue[57], U. Blumenschein[92], J. Blumenthal[98], G.J. Bobbink[117], V.S. Bobrovnikov[119b,119a], M. Boehler[52], D. Bogavac[13], A.G. Bogdanchikov[119b,119a], C. Bohm[45a], V. Boisvert[93], P. Bokan[46], T. Bold[83a], M. Bomben[5], M. Bona[92], M. Boonekamp[142], C.D. Booth[93], A.G. Borbély[57], H.M. Borecka-Bielska[108], L.S. Borgna[94], G. Borissov[89], D. Bortoletto[132], D. Boscherini[23b], M. Bosman[13], J.D. Bossio Sola[36], K. Bouaouda[35a], J. Boudreau[136], E.V. Bouhova-Thacker[89], D. Boumediene[38], R. Bouquet[5], A. Boveia[125], J. Boyd[36], D. Boye[29], I.R. Boyko[79], J. Bracinik[20], N. Brahimi[60d,60c], G. Brandt[178], O. Brandt[32], F. Braren[46], B. Brau[101], J.E. Brau[129], W.D. Breaden Madden[57], K. Brendlinger[46], R. Brener[176], L. Brenner[36], R. Brenner[168], S. Bressler[176], B. Brickwedde[98], D. Britton[57], D. Britzger[113], I. Brock[24], G. Brooijmans[39], W.K. Brooks[144f], E. Brost[29], P.A. Bruckman de Renstrom[84], B. Brüers[46], D. Bruncko[28b], A. Bruni[23b], G. Bruni[23b], M. Bruschi[23b], N. Bruscino[72a,72b], L. Bryngemark[150], T. Buanes[16], Q. Buat[145], P. Buchholz[148], A.G. Buckley[57], I.A. Budagov[79], M.K. Bugge[131], O. Bulekov[110], B.A. Bullard[59], S. Burdin[90], C.D. Burgard[46], A.M. Burger[38], B. Burghgrave[8], J.T.P. Burr[32], C.D. Burton[11], J.C. Burzynski[149], E.L. Busch[39], V. Büscher[98], P.J. Bussey[57], J.M. Butler[25], C.M. Buttar[57], J.M. Butterworth[94], W. Buttinger[141], C.J. Buxo Vazquez[105], A.R. Buzykaev[119b,119a], G. Cabras[23b], S. Cabrera Urbán[170], D. Caforio[56], H. Cai[136], Y. Cai[14a], V.M.M. Cairo[36], O. Cakir[3a], N. Calace[36], P. Calafiura[17], G. Calderini[133], P. Calfayan[65], G. Callea[57], L.P. Caloba[80b], D. Calvet[38], S. Calvet[38], T.P. Calvet[100], M. Calvetti[71a,71b], R. Camacho Toro[133], S. Camarda[36], D. Camarero Munoz[97], P. Camarri[73a,73b], M.T. Camerlingo[74a,74b], D. Cameron[131], C. Camincher[172], M. Campanelli[94], A. Camplani[40], V. Canale[69a,69b], A. Canesse[102], M. Cano Bret[77], J. Cantero[97], Y. Cao[169], F. Capocasa[26], M. Capua[41b,41a], A. Carbone[68a,68b], R. Cardarelli[73a], J.C.J. Cardenas[8], F. Cardillo[170], G. Carducci[41b,41a], T. Carli[36], G. Carlino[69a], B.T. Carlson[136], E.M. Carlson[172,164a], L. Carminati[68a,68b], M. Carnesale[72a,72b], S. Caron[116], E. Carquin[144f], S. Carrá[46], G. Carratta[23b,23a], J.W.S. Carter[163], T.M. Carter[50], D. Casadei[33c], M.P. Casado[13,g], A.F. Casha[163], E.G. Castiglia[179], F.L. Castillo[61a], L. Castillo Garcia[13], V. Castillo Gimenez[170], N.F. Castro[137a,137e], A. Catinaccio[36], J.R. Catmore[131], V. Cavaliere[29], N. Cavalli[23b,23a], V. Cavasinni[71a,71b], E. Celebi[21a], F. Celli[132], M.S. Centonze[67a,67b], K. Cerny[128], A.S. Cerqueira[80a], A. Cerri[153], L. Cerrito[73a,73b], F. Cerutti[17], A. Cervelli[23b], S.A. Cetin[21d], Z. Chadi[35a], D. Chakraborty[118], M. Chala[137f], J. Chan[177], W.S. Chan[117], W.Y. Chan[90], J.D. Chapman[32], B. Chargeishvili[156b], D.G. Charlton[20], T.P. Charman[92], M. Chatterjee[19], S. Chekanov[6], S.V. Chekulaev[164a], G.A. Chelkov[79,z], A. Chen[104], B. Chen[158], B. Chen[172], C. Chen[60a], H. Chen[14c], H. Chen[29], J. Chen[60c], J. Chen[26], S. Chen[134], S.J. Chen[14c], X. Chen[60c], X. Chen[14b], Y. Chen[60a], C.L. Cheng[177], H.C. Cheng[62a], A. Cheplakov[79], E. Cheremushkina[46], E. Cherepanova[79], R. Cherkaoui El Moursli[35e], E. Cheu[7], K. Cheung[63], L. Chevalier[142], V. Chiarella[51], G. Chiarelli[71a], G. Chiodini[67a], A.S. Chisholm[20], A. Chitan[27b], Y.H. Chiu[172], M.V. Chizhov[79], K. Choi[11], A.R. Chomont[72a,72b], Y. Chou[101], Y.S. Chow[117], T. Chowdhury[33g], L.D. Christopher[33g], M.C. Chu[62a], X. Chu[14a,14d], J. Chudoba[138], J.J. Chwastowski[84], D. Cieri[113], K.M. Ciesla[84], V. Cindro[91], A. Ciocio[17], F. Cirotto[69a,69b], Z.H. Citron[176,k], M. Citterio[68a], D.A. Ciubotaru[27b], B.M. Ciungu[163], A. Clark[54], P.J. Clark[50], J.M. Clavijo Columbie[46], S.E. Clawson[99], C. Clement[45a,45b], L. Clissa[23b,23a], Y. Coadou[100], M. Cobal[66a,66c], A. Coccaro[55b], R.F. Coelho Barrue[137a], R. Coelho Lopes De Sa[101], S. Coelli[68a], H. Cohen[158], A.E.C. Coimbra[36], B. Cole[39], J. Collot[58], P. Conde Muiño[137a,137g],

S.H. Connell[33c], I.A. Connelly[57], E.I. Conroy[132], F. Conventi[69a,af], H.G. Cooke[20],
A.M. Cooper-Sarkar[132], F. Cormier[171], L.D. Corpe[36], M. Corradi[72a,72b], E.E. Corrigan[96],
F. Corriveau[102,v], M.J. Costa[170], F. Costanza[4], D. Costanzo[146], B.M. Cote[125], G. Cowan[93],
J.W. Cowley[32], K. Cranmer[123], S. Crépé-Renaudin[58], F. Crescioli[133], M. Cristinziani[148],
M. Cristoforetti[75a,75b,b], V. Croft[166], G. Crosetti[41b,41a], A. Cueto[36],
T. Cuhadar Donszelmann[167], H. Cui[14a,14d], Z. Cui[7], A.R. Cukierman[150], W.R. Cunningham[57],
F. Curcio[41b,41a], P. Czodrowski[36], M.M. Czurylo[61b], M.J. Da Cunha Sargedas De Sousa[60a],
J.V. Da Fonseca Pinto[80b], C. Da Via[99], W. Dabrowski[83a], T. Dado[47], S. Dahbi[33g], T. Dai[104],
C. Dallapiccola[101], M. Dam[40], G. D'amen[29], V. D'Amico[74a,74b], J. Damp[98], J.R. Dandoy[134],
M.F. Daneri[30], M. Danninger[149], V. Dao[36], G. Darbo[55b], S. Darmora[6], A. Dattagupta[129],
S. D'Auria[68a,68b], C. David[164b], T. Davidek[140], D.R. Davis[49], B. Davis-Purcell[34], I. Dawson[92],
K. De[8], R. De Asmundis[69a], M. De Beurs[117], S. De Castro[23b,23a], N. De Groot[116], P. de Jong[117],
H. De la Torre[105], A. De Maria[14c], A. De Salvo[72a], U. De Sanctis[73a,73b], M. De Santis[73a,73b],
A. De Santo[153], J.B. De Vivie De Regie[58], D.V. Dedovich[79], J. Degens[117], A.M. Deiana[42],
J. Del Peso[97], F. Del Rio[61a], F. Deliot[142], C.M. Delitzsch[47], M. Della Pietra[69a,69b],
D. Della Volpe[54], A. Dell'Acqua[36], L. Dell'Asta[68a,68b], M. Delmastro[4], P.A. Delsart[58],
S. Demers[179], M. Demichev[79], S.P. Denisov[120], L. D'Eramo[118], D. Derendarz[84], F. Derue[133],
P. Dervan[90], K. Desch[24], K. Dette[163], C. Deutsch[24], P.O. Deviveiros[36], F.A. Di Bello[72a,72b],
A. Di Ciaccio[73a,73b], L. Di Ciaccio[4], A. Di Domenico[72a,72b], C. Di Donato[69a,69b],
A. Di Girolamo[36], G. Di Gregorio[71a,71b], A. Di Luca[75a,75b], B. Di Micco[74a,74b],
R. Di Nardo[74a,74b], C. Diaconu[100], F.A. Dias[117], T. Dias Do Vale[149], M.A. Diaz[144a],
F.G. Diaz Capriles[24], M. Didenko[170], E.B. Diehl[104], S. Díez Cornell[46], C. Diez Pardos[148],
C. Dimitriadi[24,168], A. Dimitrievska[17], W. Ding[14b], J. Dingfelder[24], I-M. Dinu[27b],
S.J. Dittmeier[61b], F. Dittus[36], F. Djama[100], T. Djobava[156b], J.I. Djuvsland[16], D. Dodsworth[26],
C. Doglioni[99,96], J. Dolejsi[140], Z. Dolezal[140], M. Donadelli[80c], B. Dong[60c], J. Donini[38],
A. D'onofrio[14c], M. D'Onofrio[90], J. Dopke[141], A. Doria[69a], M.T. Dova[88], A.T. Doyle[57],
E. Drechsler[149], E. Dreyer[176], A.S. Drobac[166], D. Du[60a], T.A. du Pree[117], F. Dubinin[109],
M. Dubovsky[28a], E. Duchovni[176], G. Duckeck[112], O.A. Ducu[36,27b], D. Duda[113], A. Dudarev[36],
M. D'uffizi[99], L. Duflot[64], M. Dührssen[36], C. Dülsen[178], A.E. Dumitriu[27b], M. Dunford[61a],
S. Dungs[47], K. Dunne[45a,45b], A. Duperrin[100], H. Duran Yildiz[3a], M. Düren[56],
A. Durglishvili[156b], B. Dutta[46], B.L. Dwyer[118], G.I. Dyckes[17], M. Dyndal[83a], S. Dysch[99],
B.S. Dziedzic[84], B. Eckerova[28a], M.G. Eggleston[49], E. Egidio Purcino De Souza[80b], L.F. Ehrke[54],
G. Eigen[16], K. Einsweiler[17], T. Ekelof[168], Y. El Ghazali[35b], H. El Jarrari[35e,155],
A. El Moussaouy[35a], V. Ellajosyula[168], M. Ellert[168], F. Ellinghaus[178], A.A. Elliot[92], N. Ellis[36],
J. Elmsheuser[29], M. Elsing[36], D. Emeliyanov[141], A. Emerman[39], Y. Enari[160], I. Ene[17],
J. Erdmann[47], A. Ereditato[19], P.A. Erland[84], M. Errenst[178], M. Escalier[64], C. Escobar[170],
E. Etzion[158], G. Evans[137a], H. Evans[65], M.O. Evans[153], A. Ezhilov[135], S. Ezzarqtouni[35a],
F. Fabbri[57], L. Fabbri[23b,23a], G. Facini[174], V. Fadeyev[143], R.M. Fakhrutdinov[120], S. Falciano[72a],
P.J. Falke[24], S. Falke[36], J. Faltova[140], Y. Fan[14a], Y. Fang[14a], G. Fanourakis[44], M. Fanti[68a,68b],
M. Faraj[60c], A. Farbin[8], A. Farilla[74a], T. Farooque[105], S.M. Farrington[50], F. Fassi[35e],
D. Fassouliotis[9], M. Faucci Giannelli[73a,73b], W.J. Fawcett[32], L. Fayard[64], O.L. Fedin[135,o],
G. Fedotov[135], M. Feickert[169], L. Feligioni[100], A. Fell[146], D.E. Fellers[129], C. Feng[60b], M. Feng[14b],
M.J. Fenton[167], A.B. Fenyuk[120], S.W. Ferguson[43], J.A. Fernandez Pretel[52], J. Ferrando[46],
A. Ferrari[168], P. Ferrari[117], R. Ferrari[70a], D. Ferrere[54], C. Ferretti[104], F. Fiedler[98], A. Filipčič[91],
E.K. Filmer[1], F. Filthaut[116], M.C.N. Fiolhais[137a,137c,a], L. Fiorini[170], F. Fischer[148],
W.C. Fisher[105], T. Fitschen[20,64], I. Fleck[148], P. Fleischmann[104], T. Flick[178], L. Flores[134],
M. Flores[33d], L.R. Flores Castillo[62a], F.M. Follega[75a,75b], N. Fomin[16], J.H. Foo[163],
B.C. Forland[65], A. Formica[142], A.C. Forti[99], E. Fortin[100], A.W. Fortman[59], M.G. Foti[17],

L. Fountas[9], D. Fournier[64], H. Fox[89], P. Francavilla[71a,71b], S. Francescato[59], M. Franchini[23b,23a],
S. Franchino[61a], D. Francis[36], L. Franco[4], L. Franconi[19], M. Franklin[59], G. Frattari[72a,72b],
A.C. Freegard[92], P.M. Freeman[20], W.S. Freund[80b], E.M. Freundlich[47], D. Froidevaux[36],
J.A. Frost[132], Y. Fu[60a], M. Fujimoto[124], E. Fullana Torregrosa[170], J. Fuster[170],
A. Gabrielli[23b,23a], A. Gabrielli[36], P. Gadow[46], G. Gagliardi[55b,55a], L.G. Gagnon[17],
G.E. Gallardo[132], E.J. Gallas[132], B.J. Gallop[141], R. Gamboa Goni[92], K.K. Gan[125],
S. Ganguly[160], J. Gao[60a], Y. Gao[50], F.M. Garay Walls[144a,144b], B. Garcia[29], C. García[170],
J.E. García Navarro[170], J.A. García Pascual[14a], M. Garcia-Sciveres[17], R.W. Gardner[37],
D. Garg[77], R.B. Garg[150], S. Gargiulo[52], C.A. Garner[163], V. Garonne[29], S.J. Gasiorowski[145],
P. Gaspar[80b], G. Gaudio[70a], P. Gauzzi[72a,72b], I.L. Gavrilenko[109], A. Gavrilyuk[121], C. Gay[171],
G. Gaycken[46], E.N. Gazis[10], A.A. Geanta[27b], C.M. Gee[143], J. Geisen[96], M. Geisen[98],
C. Gemme[55b], M.H. Genest[58], S. Gentile[72a,72b], S. George[93], W.F. George[20], T. Geralis[44],
L.O. Gerlach[53], P. Gessinger-Befurt[36], M. Ghasemi Bostanabad[172], A. Ghosal[148], A. Ghosh[167],
A. Ghosh[7], B. Giacobbe[23b], S. Giagu[72a,72b], N. Giangiacomi[163], P. Giannetti[71a], A. Giannini[60a],
S.M. Gibson[93], M. Gignac[143], D.T. Gil[83b], B.J. Gilbert[39], D. Gillberg[34], G. Gilles[117],
N.E.K. Gillwald[46], L. Ginabat[133], D.M. Gingrich[2,ae], M.P. Giordani[66a,66c], P.F. Giraud[142],
G. Giugliarelli[66a,66c], D. Giugni[68a], F. Giuli[73a,73b], I. Gkialas[9,h], P. Gkountoumis[10],
L.K. Gladilin[111], C. Glasman[97], G.R. Gledhill[129], M. Glisic[129], I. Gnesi[41b,d], Y. Go[29],
M. Goblirsch-Kolb[26], D. Godin[108], S. Goldfarb[103], T. Golling[54], M.G.D. Gololo[33g],
D. Golubkov[120], J.P. Gombas[105], A. Gomes[137a,137b], A.J. Gomez Delegido[170],
R. Goncalves Gama[53], R. Gonçalo[137a,137c], G. Gonella[129], L. Gonella[20], A. Gongadze[79],
F. Gonnella[20], J.L. Gonski[39], S. González de la Hoz[170], S. Gonzalez Fernandez[13],
R. Gonzalez Lopez[90], C. Gonzalez Renteria[17], R. Gonzalez Suarez[168], S. Gonzalez-Sevilla[54],
G.R. Gonzalvo Rodriguez[170], R.Y. González Andana[50], L. Goossens[36], N.A. Gorasia[20],
P.A. Gorbounov[121], H.A. Gordon[29], B. Gorini[36], E. Gorini[67a,67b], A. Gorišek[91], A.T. Goshaw[49],
M.I. Gostkin[79], C.A. Gottardo[116], M. Gouighri[35b], V. Goumarre[46], A.G. Goussiou[145],
N. Govender[33c], C. Goy[4], I. Grabowska-Bold[83a], K. Graham[34], E. Gramstad[131],
S. Grancagnolo[18], M. Grandi[153], V. Gratchev[135], P.M. Gravila[27f], F.G. Gravili[67a,67b],
H.M. Gray[17], C. Grefe[24], I.M. Gregor[46], P. Grenier[150], K. Grevtsov[46], C. Grieco[13],
A.A. Grillo[143], K. Grimm[31,l], S. Grinstein[13,t], J.-F. Grivaz[64], S. Groh[98], E. Gross[176],
J. Grosse-Knetter[53], C. Grud[104], A. Grummer[115], J.C. Grundy[132], L. Guan[104], W. Guan[177],
C. Gubbels[171], J.G.R. Guerrero Rojas[170], F. Guescini[113], D. Guest[18], R. Gugel[98], A. Guida[46],
T. Guillemin[4], S. Guindon[36], F. Guo[14a], J. Guo[60c], L. Guo[64], Y. Guo[104], R. Gupta[46],
S. Gurbuz[24], G. Gustavino[36], M. Guth[54], P. Gutierrez[126], L.F. Gutierrez Zagazeta[134],
C. Gutschow[94], C. Guyot[142], C. Gwenlan[132], C.B. Gwilliam[90], E.S. Haaland[131], A. Haas[123],
M. Habedank[46], C. Haber[17], H.K. Hadavand[8], A. Hadef[98], S. Hadzic[113], M. Haleem[173],
J. Haley[127], J.J. Hall[146], G.D. Hallewell[100], L. Halser[19], K. Hamano[172], H. Hamdaoui[35e],
M. Hamer[24], G.N. Hamity[50], J. Han[60b], K. Han[60a], L. Han[14c], L. Han[60a], S. Han[17], Y.F. Han[163],
K. Hanagaki[81,r], M. Hance[143], D.A. Hangal[39], M.D. Hank[37], R. Hankache[99], E. Hansen[96],
J.B. Hansen[40], J.D. Hansen[40], P.H. Hansen[40], K. Hara[165], D. Harada[54], T. Harenberg[178],
S. Harkusha[106], Y.T. Harris[132], P.F. Harrison[174], N.M. Hartman[150], N.M. Hartmann[112],
Y. Hasegawa[147], A. Hasib[50], S. Haug[19], R. Hauser[105], M. Havranek[139], C.M. Hawkes[20],
R.J. Hawkings[36], S. Hayashida[114], D. Hayden[105], C. Hayes[104], R.L. Hayes[171], C.P. Hays[132],
J.M. Hays[92], H.S. Hayward[90], F. He[60a], Y. He[161], Y. He[133], M.P. Heath[50], V. Hedberg[96],
A.L. Heggelund[131], N.D. Hehir[92], C. Heidegger[52], K.K. Heidegger[52], W.D. Heidorn[78],
J. Heilman[34], S. Heim[46], T. Heim[17], B. Heinemann[46,ac], J.G. Heinlein[134], J.J. Heinrich[129],
L. Heinrich[36], J. Hejbal[138], L. Helary[46], A. Held[123], C.M. Helling[143], S. Hellman[45a,45b],
C. Helsens[36], R.C.W. Henderson[89], L. Henkelmann[32], A.M. Henriques Correia[36], H. Herde[150],

Y. Hernández Jiménez[152], H. Herr[98], M.G. Herrmann[112], T. Herrmann[48], G. Herten[52],
R. Hertenberger[112], L. Hervas[36], N.P. Hessey[164a], H. Hibi[82], E. Higón-Rodriguez[170],
S.J. Hillier[20], I. Hinchliffe[17], F. Hinterkeuser[24], M. Hirose[130], S. Hirose[165], D. Hirschbuehl[178],
B. Hiti[91], O. Hladik[138], J. Hobbs[152], R. Hobincu[27e], N. Hod[176], M.C. Hodgkinson[146],
B.H. Hodkinson[32], A. Hoecker[36], J. Hofer[46], D. Hohn[52], T. Holm[24], M. Holzbock[113],
L.B.A.H. Hommels[32], B.P. Honan[99], J. Hong[60c], T.M. Hong[136], Y. Hong[53], J.C. Honig[52],
A. Hönle[113], B.H. Hooberman[169], W.H. Hopkins[6], Y. Horii[114], L.A. Horyn[37], S. Hou[155],
J. Howarth[57], J. Hoya[88], M. Hrabovsky[128], A. Hrynevich[107], T. Hryn'ova[4], P.J. Hsu[63],
S.-C. Hsu[145], Q. Hu[39], S. Hu[60c], Y.F. Hu[14a,14d,ag], D.P. Huang[94], X. Huang[14c], Y. Huang[60a],
Y. Huang[14a], Z. Hubacek[139], M. Huebner[24], F. Huegging[24], T.B. Huffman[132], M. Huhtinen[36],
S.K. Huiberts[16], R. Hulsken[58], N. Huseynov[12,y], J. Huston[105], J. Huth[59], R. Hyneman[150],
S. Hyrych[28a], G. Iacobucci[54], G. Iakovidis[29], I. Ibragimov[148], L. Iconomidou-Fayard[64],
P. Iengo[36], R. Iguchi[160], T. Iizawa[54], Y. Ikegami[81], A. Ilg[19], N. Ilic[163], H. Imam[35a],
T. Ingebretsen Carlson[45a,45b], G. Introzzi[70a,70b], M. Iodice[74a], V. Ippolito[72a,72b], M. Ishino[160],
W. Islam[177], C. Issever[18,46], S. Istin[21a,ah], H. Ito[175], J.M. Iturbe Ponce[62a], R. Iuppa[75a,75b],
A. Ivina[176], J.M. Izen[43], V. Izzo[69a], P. Jacka[138], P. Jackson[1], R.M. Jacobs[46], B.P. Jaeger[149],
C.S. Jagfeld[112], G. Jäkel[178], K. Jakobs[52], T. Jakoubek[176], J. Jamieson[57], K.W. Janas[83a],
G. Jarlskog[96], A.E. Jaspan[90], T. Javůrek[36], M. Javurkova[101], F. Jeanneau[142], L. Jeanty[129],
J. Jejelava[156a,w], P. Jenni[52,e], S. Jézéquel[4], J. Jia[152], X. Jia[59], Z. Jia[14c], Y. Jiang[60a],
S. Jiggins[50], J. Jimenez Pena[113], S. Jin[14c], A. Jinaru[27b], O. Jinnouchi[161], H. Jivan[33g],
P. Johansson[146], K.A. Johns[7], C.A. Johnson[65], D.M. Jones[32], E. Jones[174], R.W.L. Jones[89],
T.J. Jones[90], J. Jovicevic[15], X. Ju[17], J.J. Junggeburth[36], A. Juste Rozas[13,t], S. Kabana[144e],
A. Kaczmarska[84], M. Kado[72a,72b], H. Kagan[125], M. Kagan[150], A. Kahn[39], A. Kahn[134],
C. Kahra[98], T. Kaji[175], E. Kajomovitz[157], N. Kakati[176], C.W. Kalderon[29], A. Kamenshchikov[163],
N.J. Kang[143], Y. Kano[114], D. Kar[33g], K. Karava[132], M.J. Kareem[164b], E. Karentzos[52],
I. Karkanias[159], S.N. Karpov[79], Z.M. Karpova[79], V. Kartvelishvili[89], A.N. Karyukhin[120],
E. Kasimi[159], C. Kato[60d], J. Katzy[46], S. Kaur[34], K. Kawade[147], K. Kawagoe[87], T. Kawaguchi[114],
T. Kawamoto[142], G. Kawamura[53], E.F. Kay[172], F.I. Kaya[166], S. Kazakos[13],
V.F. Kazanin[119b,119a], Y. Ke[152], J.M. Keaveney[33a], R. Keeler[172], G.V. Kehris[59], J.S. Keller[34],
A.S. Kelly[94], D. Kelsey[153], J.J. Kempster[20], J. Kendrick[20], K.E. Kennedy[39], O. Kepka[138],
S. Kersten[178], B.P. Kerševan[91], S. Ketabchi Haghighat[163], M. Khandoga[133], A. Khanov[127],
A.G. Kharlamov[119b,119a], T. Kharlamova[119b,119a], E.E. Khoda[145], T.J. Khoo[18], G. Khoriauli[173],
E. Khramov[79], J. Khubua[156b], M. Kiehn[36], A. Kilgallon[129], E. Kim[161], Y.K. Kim[37],
N. Kimura[94], A. Kirchhoff[53], D. Kirchmeier[48], C. Kirfel[24], J. Kirk[141], A.E. Kiryunin[113],
T. Kishimoto[160], D.P. Kisliuk[163], C. Kitsaki[10], O. Kivernyk[24], M. Klassen[61a], C. Klein[34],
L. Klein[173], M.H. Klein[104], M. Klein[90], U. Klein[90], P. Klimek[36], A. Klimentov[29], F. Klimpel[113],
T. Klingl[24], T. Klioutchnikova[36], F.F. Klitzner[112], P. Kluit[117], S. Kluth[113], E. Kneringer[76],
T.M. Knight[163], A. Knue[52], D. Kobayashi[87], R. Kobayashi[85], M. Kocian[150], T. Kodama[160],
P. Kodys[140], D.M. Koeck[153], P.T. Koenig[24], T. Koffas[34], N.M. Köhler[36], M. Kolb[142],
I. Koletsou[4], T. Komarek[128], K. Köneke[52], A.X.Y. Kong[1], T. Kono[124], N. Konstantinidis[94],
B. Konya[96], R. Kopeliansky[65], S. Koperny[83a], K. Korcyl[84], K. Kordas[159], G. Koren[158],
A. Korn[94], S. Korn[53], I. Korolkov[13], N. Korotkova[111], B. Kortman[117], O. Kortner[113],
S. Kortner[113], W.H. Kostecka[118], V.V. Kostyukhin[148,162], A. Kotsokechagia[64], A. Kotwal[49],
A. Koulouris[36], A. Kourkoumeli-Charalampidi[70a,70b], C. Kourkoumelis[9], E. Kourlitis[6],
O. Kovanda[153], R. Kowalewski[172], W. Kozanecki[142], A.S. Kozhin[120], V.A. Kramarenko[111],
G. Kramberger[91], P. Kramer[98], M.W. Krasny[133], A. Krasznahorkay[36], J.A. Kremer[98],
J. Kretzschmar[90], K. Kreul[18], P. Krieger[163], F. Krieter[112], S. Krishnamurthy[101], A. Krishnan[61b],
M. Krivos[140], K. Krizka[17], K. Kroeninger[47], H. Kroha[113], J. Kroll[138], J. Kroll[134],

K.S. Krowpman[105], U. Kruchonak[79], H. Krüger[24], N. Krumnack[78], M.C. Kruse[49],
J.A. Krzysiak[84], A. Kubota[161], O. Kuchinskaia[162], S. Kuday[3a], D. Kuechler[46], J.T. Kuechler[46],
S. Kuehn[36], T. Kuhl[46], V. Kukhtin[79], Y. Kulchitsky[106,y], S. Kuleshov[144d,144b], M. Kumar[33g],
N. Kumari[100], M. Kuna[58], A. Kupco[138], T. Kupfer[47], O. Kuprash[52], H. Kurashige[82],
L.L. Kurchaninov[164a], Y.A. Kurochkin[106], A. Kurova[110], E.S. Kuwertz[36], M. Kuze[161],
A.K. Kvam[145], J. Kvita[128], T. Kwan[102], K.W. Kwok[62a], C. Lacasta[170], F. Lacava[72a,72b],
H. Lacker[18], D. Lacour[133], N.N. Lad[94], E. Ladygin[79], B. Laforge[133], T. Lagouri[144e], S. Lai[53],
I.K. Lakomiec[83a], N. Lalloue[58], J.E. Lambert[126], S. Lammers[65], W. Lampl[7], C. Lampoudis[159],
E. Lançon[29], U. Landgraf[52], M.P.J. Landon[92], V.S. Lang[52], J.C. Lange[53], R.J. Langenberg[101],
A.J. Lankford[167], F. Lanni[29], K. Lantzsch[24], A. Lanza[70a], A. Lapertosa[55b,55a], J.F. Laporte[142],
T. Lari[68a], F. Lasagni Manghi[23b], M. Lassnig[36], V. Latonova[138], T.S. Lau[62a], A. Laudrain[98],
A. Laurier[34], M. Lavorgna[69a,69b], S.D. Lawlor[93], Z. Lawrence[99], M. Lazzaroni[68a,68b], B. Le[99],
B. Leban[91], A. Lebedev[78], M. LeBlanc[36], T. LeCompte[150], F. Ledroit-Guillon[58], A.C.A. Lee[94],
G.R. Lee[16], L. Lee[59], S.C. Lee[155], L.L. Leeuw[33c], B. Lefebvre[164a], H.P. Lefebvre[93],
M. Lefebvre[172], C. Leggett[17], K. Lehmann[149], G. Lehmann Miotto[36], W.A. Leight[101],
A. Leisos[159,s], M.A.L. Leite[80c], C.E. Leitgeb[46], R. Leitner[140], K.J.C. Leney[42], T. Lenz[24],
S. Leone[71a], C. Leonidopoulos[50], A. Leopold[151], C. Leroy[108], R. Les[105], C.G. Lester[32],
M. Levchenko[135], J. Levêque[4], D. Levin[104], L.J. Levinson[176], D.J. Lewis[20], B. Li[14b], B. Li[60b],
C. Li[60a], C-Q. Li[60c,60d], H. Li[60a], H. Li[60b], H. Li[60b], J. Li[60c], K. Li[145], L. Li[60c], M. Li[14a,14d],
Q.Y. Li[60a], S. Li[60d,60c,c], T. Li[60b], X. Li[46], Z. Li[60b], Z. Li[132], Z. Li[102], Z. Li[90], Z. Liang[14a],
M. Liberatore[46], B. Liberti[73a], K. Lie[62c], J. Lieber Marin[80b], K. Lin[105], R.A. Linck[65],
R.E. Lindley[7], J.H. Lindon[2], A. Linss[46], E. Lipeles[134], A. Lipniacka[16], T.M. Liss[169,ad],
A. Lister[171], J.D. Little[4], B. Liu[14a], B.X. Liu[149], D. Liu[60d,60c], J.B. Liu[60a], J.K.K. Liu[32],
K. Liu[60d,60c], M. Liu[60a], M.Y. Liu[60a], P. Liu[14a], Q. Liu[60d,145,60c], X. Liu[60a], Y. Liu[46],
Y. Liu[14c,14d], Y.L. Liu[104], Y.W. Liu[60a], M. Livan[70a,70b], J. Llorente Merino[149], S.L. Lloyd[92],
E.M. Lobodzinska[46], P. Loch[7], S. Loffredo[73a,73b], T. Lohse[18], K. Lohwasser[146], M. Lokajicek[138],
J.D. Long[169], I. Longarini[72a,72b], L. Longo[67a,67b], R. Longo[169], I. Lopez Paz[36], A. Lopez Solis[46],
J. Lorenz[112], N. Lorenzo Martinez[4], A.M. Lory[112], A. Lösle[52], X. Lou[45a,45b], X. Lou[14a],
A. Lounis[64], J. Love[6], P.A. Love[89], J.J. Lozano Bahilo[170], G. Lu[14a], M. Lu[77], S. Lu[134],
Y.J. Lu[63], H.J. Lubatti[145], C. Luci[72a,72b], F.L. Lucio Alves[14c], A. Lucotte[58], F. Luehring[65],
I. Luise[152], O. Lundberg[151], B. Lund-Jensen[151], N.A. Luongo[129], M.S. Lutz[158], D. Lynn[29],
H. Lyons[90], R. Lysak[138], E. Lytken[96], F. Lyu[14a], V. Lyubushkin[79], T. Lyubushkina[79], H. Ma[29],
L.L. Ma[60b], Y. Ma[94], D.M. Mac Donell[172], G. Maccarrone[51], J.C. MacDonald[146], R. Madar[38],
W.F. Mader[48], J. Maeda[82], T. Maeno[29], M. Maerker[48], V. Magerl[52], J. Magro[66a,66c],
D.J. Mahon[39], C. Maidantchik[80b], A. Maio[137a,137b,137d], K. Maj[83a], O. Majersky[28a],
S. Majewski[129], N. Makovec[64], V. Maksimovic[15], B. Malaescu[133], Pa. Malecki[84], V.P. Maleev[135],
F. Malek[58], D. Malito[41b,41a], U. Mallik[77], C. Malone[32], S. Maltezos[10], S. Malyukov[79],
J. Mamuzic[170], G. Mancini[51], J.P. Mandalia[92], I. Mandić[91], L. Manhaes de Andrade Filho[80a],
I.M. Maniatis[159], M. Manisha[142], J. Manjarres Ramos[48], D.C. Mankad[176], K.H. Mankinen[96],
A. Mann[112], A. Manousos[76], B. Mansoulie[142], S. Manzoni[36], A. Marantis[159,s], G. Marchiori[5],
M. Marcisovsky[138], L. Marcoccia[73a,73b], C. Marcon[96], M. Marinescu[20], M. Marjanovic[126],
Z. Marshall[17], S. Marti-Garcia[170], T.A. Martin[174], V.J. Martin[50], B. Martin dit Latour[16],
L. Martinelli[72a,72b], M. Martinez[13,t], P. Martinez Agullo[170], V.I. Martinez Outschoorn[101],
P. Martinez Suarez[13], S. Martin-Haugh[141], V.S. Martoiu[27b], A.C. Martyniuk[94], A. Marzin[36],
S.R. Maschek[113], L. Masetti[98], T. Mashimo[160], J. Masik[99], A.L. Maslennikov[119b,119a],
L. Massa[23b], P. Massarotti[69a,69b], P. Mastrandrea[71a,71b], A. Mastroberardino[41b,41a],
T. Masubuchi[160], T. Mathisen[168], A. Matic[112], N. Matsuzawa[160], J. Maurer[27b], B. Maček[91],
D.A. Maximov[119b,119a], R. Mazini[155], I. Maznas[159], M. Mazza[105], S.M. Mazza[143], C. Mc Ginn[29],

J.P. Mc Gowan[102], S.P. Mc Kee[104], T.G. McCarthy[113], W.P. McCormack[17], E.F. McDonald[103],
A.E. McDougall[117], J.A. Mcfayden[153], G. Mchedlidze[156b], M.A. McKay[42], R.P. Mckenzie[33g],
D.J. Mclaughlin[94], K.D. McLean[172], S.J. McMahon[141], P.C. McNamara[103],
R.A. McPherson[172,v], J.E. Mdhluli[33g], S. Meehan[36], T. Megy[38], S. Mehlhase[112], A. Mehta[90],
B. Meirose[43], D. Melini[157], B.R. Mellado Garcia[33g], A.H. Melo[53], F. Meloni[46], A. Melzer[24],
E.D. Mendes Gouveia[137a], A.M. Mendes Jacques Da Costa[20], H.Y. Meng[163], L. Meng[89],
S. Menke[113], M. Mentink[36], E. Meoni[41b,41a], C. Merlassino[132], L. Merola[69a,69b], C. Meroni[68a],
G. Merz[104], O. Meshkov[109,111], J.K.R. Meshreki[148], J. Metcalfe[6], A.S. Mete[6], C. Meyer[65],
J-P. Meyer[142], M. Michetti[18], R.P. Middleton[141], L. Mijović[50], G. Mikenberg[176],
M. Mikestikova[138], M. Mikuž[91], H. Mildner[146], A. Milic[163], C.D. Milke[42], D.W. Miller[37],
L.S. Miller[34], A. Milov[176], D.A. Milstead[45a,45b], T. Min[14c], A.A. Minaenko[120],
I.A. Minashvili[156b], L. Mince[57], A.I. Mincer[123], B. Mindur[83a], M. Mineev[79], Y. Minegishi[160],
Y. Mino[85], L.M. Mir[13], M. Miralles Lopez[170], M. Mironova[132], T. Mitani[175], A. Mitra[174],
V.A. Mitsou[170], O. Miu[163], P.S. Miyagawa[92], Y. Miyazaki[87], A. Mizukami[81], J.U. Mjörnmark[96],
T. Mkrtchyan[61a], M. Mlynarikova[118], T. Moa[45a,45b], S. Mobius[53], K. Mochizuki[108], P. Moder[46],
P. Mogg[112], A.F. Mohammed[14a], S. Mohapatra[39], G. Mokgatitswane[33g], B. Mondal[148],
S. Mondal[139], K. Mönig[46], E. Monnier[100], L. Monsonis Romero[170], J. Montejo Berlingen[36],
M. Montella[125], F. Monticelli[88], N. Morange[64], A.L. Moreira De Carvalho[137a],
M. Moreno Llácer[170], C. Moreno Martinez[13], P. Morettini[55b], S. Morgenstern[174], D. Mori[149],
M. Morii[59], M. Morinaga[160], V. Morisbak[131], A.K. Morley[36], L. Morvaj[36], P. Moschovakos[36],
B. Moser[117], M. Mosidze[156b], T. Moskalets[52], P. Moskvitina[116], J. Moss[31,m], E.J.W. Moyse[101],
S. Muanza[100], J. Mueller[136], R. Mueller[19], D. Muenstermann[89], G.A. Mullier[96], J.J. Mullin[134],
D.P. Mungo[68a,68b], J.L. Munoz Martinez[13], F.J. Munoz Sanchez[99], M. Murin[99],
W.J. Murray[174,141], A. Murrone[68a,68b], J.M. Muse[126], M. Muškinja[17], C. Mwewa[29],
A.G. Myagkov[120,z], A.J. Myers[8], A.A. Myers[136], G. Myers[65], M. Myska[139], B.P. Nachman[17],
O. Nackenhorst[47], A.Nag Nag[48], K. Nagai[132], K. Nagano[81], J.L. Nagle[29], E. Nagy[100],
A.M. Nairz[36], Y. Nakahama[81], K. Nakamura[81], H. Nanjo[130], R. Narayan[42], E.A. Narayanan[115],
I. Naryshkin[135], M. Naseri[34], C. Nass[24], G. Navarro[22a], J. Navarro-Gonzalez[170], R. Nayak[158],
P.Y. Nechaeva[109], F. Nechansky[46], T.J. Neep[20], A. Negri[70a,70b], M. Negrini[23b], C. Nellist[116],
C. Nelson[102], K. Nelson[104], S. Nemecek[138], M. Nessi[36,f], M.S. Neubauer[169], F. Neuhaus[98],
J. Neundorf[46], R. Newhouse[171], P.R. Newman[20], C.W. Ng[136], Y.S. Ng[18], Y.W.Y. Ng[167],
B. Ngair[35e], H.D.N. Nguyen[108], R.B. Nickerson[132], R. Nicolaidou[142], D.S. Nielsen[40],
J. Nielsen[143], M. Niemeyer[53], N. Nikiforou[11], V. Nikolaenko[120,z], I. Nikolic-Audit[133],
K. Nikolopoulos[20], P. Nilsson[29], H.R. Nindhito[54], A. Nisati[72a], N. Nishu[2], R. Nisius[113],
S.J. Noacco Rosende[88], T. Nobe[160], D.L. Noel[32], Y. Noguchi[85], I. Nomidis[133], M.A. Nomura[29],
M.B. Norfolk[146], R.R.B. Norisam[94], J. Novak[91], T. Novak[46], O. Novgorodova[48], L. Novotny[139],
R. Novotny[115], L. Nozka[128], K. Ntekas[167], E. Nurse[94], F.G. Oakham[34,ae], J. Ocariz[133],
A. Ochi[82], I. Ochoa[137a], J.P. Ochoa-Ricoux[144a], S. Oda[87], S. Oerdek[168], A. Ogrodnik[83a],
A. Oh[99], C.C. Ohm[151], H. Oide[161], R. Oishi[160], M.L. Ojeda[46], Y. Okazaki[85], M.W. O'Keefe[90],
Y. Okumura[160], A. Olariu[27b], L.F. Oleiro Seabra[137a], S.A. Olivares Pino[144e],
D. Oliveira Damazio[29], D. Oliveira Goncalves[80a], J.L. Oliver[167], M.J.R. Olsson[167],
A. Olszewski[84], J. Olszowska[84], Ö.O. Öncel[52], D.C. O'Neil[149], A.P. O'neill[19], A. Onofre[137a,137e],
P.U.E. Onyisi[11], R.G. Oreamuno Madriz[118], M.J. Oreglia[37], G.E. Orellana[88], D. Orestano[74a,74b],
N. Orlando[13], R.S. Orr[163], V. O'Shea[57], R. Ospanov[60a], G. Otero y Garzon[30], H. Otono[87],
P.S. Ott[61a], G.J. Ottino[17], M. Ouchrif[35d], J. Ouellette[29], F. Ould-Saada[131], M. Owen[57],
R.E. Owen[141], K.Y. Oyulmaz[21a], V.E. Ozcan[21a], N. Ozturk[8], S. Ozturk[21d], J. Pacalt[128],
H.A. Pacey[32], K. Pachal[49], A. Pacheco Pages[13], C. Padilla Aranda[13], S. Pagan Griso[17],
G. Palacino[65], S. Palazzo[50], S. Palestini[36], M. Palka[83b], J. Pan[179], D.K. Panchal[11],

C.E. Pandini[117], J.G. Panduro Vazquez[93], P. Pani[46], G. Panizzo[66a,66c], L. Paolozzi[54],
C. Papadatos[108], S. Parajuli[42], A. Paramonov[6], C. Paraskevopoulos[10], D. Paredes Hernandez[62b],
B. Parida[176], T.H. Park[163], A.J. Parker[31], M.A. Parker[32], F. Parodi[55b,55a], E.W. Parrish[118],
V.A. Parrish[50], J.A. Parsons[39], U. Parzefall[52], B. Pascual Dias[108], L. Pascual Dominguez[158],
V.R. Pascuzzi[17], F. Pasquali[117], E. Pasqualucci[72a], S. Passaggio[55b], F. Pastore[93],
P. Pasuwan[45a,45b], J.R. Pater[99], A. Pathak[177], J. Patton[90], T. Pauly[36], J. Pearkes[150],
M. Pedersen[131], R. Pedro[137a], S.V. Peleganchuk[119b,119a], O. Penc[138], C. Peng[62b], H. Peng[60a],
M. Penzin[162], B.S. Peralva[80a], A.P. Pereira Peixoto[58], L. Pereira Sanchez[45a,45b],
D.V. Perepelitsa[29], E. Perez Codina[164a], M. Perganti[10], L. Perini[68a,68b], H. Pernegger[36],
S. Perrella[36], A. Perrevoort[116], O. Perrin[38], K. Peters[46], R.F.Y. Peters[99], B.A. Petersen[36],
T.C. Petersen[40], E. Petit[100], V. Petousis[139], C. Petridou[159], A. Petrukhin[148], M. Pettee[17],
N.E. Pettersson[36], K. Petukhova[140], A. Peyaud[142], R. Pezoa[144f], L. Pezzotti[36], G. Pezzullo[179],
T. Pham[103], P.W. Phillips[141], M.W. Phipps[169], G. Piacquadio[152], E. Pianori[17], F. Piazza[68a,68b],
R. Piegaia[30], D. Pietreanu[27b], A.D. Pilkington[99], M. Pinamonti[66a,66c], J.L. Pinfold[2],
C. Pitman Donaldson[94], D.A. Pizzi[34], L. Pizzimento[73a,73b], A. Pizzini[117], M.-A. Pleier[29],
V. Plesanovs[52], V. Pleskot[140], E. Plotnikova[79], G. Poddar[4], R. Poettgen[96], R. Poggi[54],
L. Poggioli[133], I. Pogrebnyak[105], D. Pohl[24], I. Pokharel[53], S. Polacek[140], G. Polesello[70a],
A. Poley[149,164a], R. Polifka[139], A. Polini[23b], C.S. Pollard[132], Z.B. Pollock[125],
V. Polychronakos[29], D. Ponomarenko[110], L. Pontecorvo[36], S. Popa[27a], G.A. Popeneciu[27d],
D.M. Portillo Quintero[164a], S. Pospisil[139], P. Postolache[27c], K. Potamianos[132], I.N. Potrap[79],
C.J. Potter[32], H. Potti[1], T. Poulsen[46], J. Poveda[170], G. Pownall[46], M.E. Pozo Astigarraga[36],
A. Prades Ibanez[170], P. Pralavorio[100], M.M. Prapa[44], D. Price[99], M. Primavera[67a],
M.A. Principe Martin[97], M.L. Proffitt[145], N. Proklova[110], K. Prokofiev[62c], F. Prokoshin[79],
G. Proto[73a,73b], S. Protopopescu[29], J. Proudfoot[6], M. Przybycien[83a], D. Pudzha[135], P. Puzo[64],
D. Pyatiizbyantseva[110], J. Qian[104], Y. Qin[99], T. Qiu[92], A. Quadt[53], M. Queitsch-Maitland[24],
G. Rabanal Bolanos[59], D. Rafanoharana[52], F. Ragusa[68a,68b], J.A. Raine[54], S. Rajagopalan[29],
K. Ran[14a,14d], V. Raskina[133], D.F. Rassloff[61a], S. Rave[98], B. Ravina[57], I. Ravinovich[176],
M. Raymond[36], A.L. Read[131], N.P. Readioff[146], D.M. Rebuzzi[70a,70b], G. Redlinger[29],
K. Reeves[43], D. Reikher[158], A. Reiss[98], A. Rej[148], C. Rembser[36], A. Renardi[46], M. Renda[27b],
M.B. Rendel[113], A.G. Rennie[57], S. Resconi[68a], M. Ressegotti[55b,55a], E.D. Resseguie[17],
S. Rettie[94], B. Reynolds[125], E. Reynolds[17], M. Rezaei Estabragh[178], O.L. Rezanova[119b,119a],
P. Reznicek[140], E. Ricci[75a,75b], R. Richter[113], S. Richter[45a,45b], E. Richter-Was[83b], M. Ridel[133],
P. Rieck[123], P. Riedler[36], M. Rijssenbeek[152], A. Rimoldi[70a,70b], M. Rimoldi[46], L. Rinaldi[23b,23a],
T.T. Rinn[169], M.P. Rinnagel[112], G. Ripellino[151], I. Riu[13], P. Rivadeneira[46],
J.C. Rivera Vergara[172], F. Rizatdinova[127], E. Rizvi[92], C. Rizzi[54], B.A. Roberts[174],
B.R. Roberts[17], S.H. Robertson[102,v], M. Robin[46], D. Robinson[32], C.M. Robles Gajardo[144f],
M. Robles Manzano[98], A. Robson[57], A. Rocchi[73a,73b], C. Roda[71a,71b], S. Rodriguez Bosca[61a],
Y. Rodriguez Garcia[22a], A. Rodriguez Rodriguez[52], A.M. Rodríguez Vera[164b], S. Roe[36],
J.T. Roemer[167], A.R. Roepe[126], J. Roggel[178], O. Røhne[131], R.A. Rojas[172], B. Roland[52],
C.P.A. Roland[65], J. Roloff[29], A. Romaniouk[110], M. Romano[23b], A.C. Romero Hernandez[169],
N. Rompotis[90], M. Ronzani[123], L. Roos[133], S. Rosati[72a], B.J. Rosser[134], E. Rossi[4],
E. Rossi[69a,69b], L.P. Rossi[55b], L. Rossini[46], R. Rosten[125], M. Rotaru[27b], B. Rottler[52],
D. Rousseau[64], D. Rousso[32], G. Rovelli[70a,70b], A. Roy[169], A. Rozanov[100], Y. Rozen[157],
X. Ruan[33g], A.J. Ruby[90], T.A. Ruggeri[1], F. Rühr[52], A. Ruiz-Martinez[170], A. Rummler[36],
Z. Rurikova[52], N.A. Rusakovich[79], H.L. Russell[172], L. Rustige[38], J.P. Rutherfoord[7],
E.M. Rüttinger[146], K. Rybacki[89], M. Rybar[140], E.B. Rye[131], A. Ryzhov[120],
J.A. Sabater Iglesias[54], P. Sabatini[170], L. Sabetta[72a,72b], H.F-W. Sadrozinski[143], R. Sadykov[79],
F. Safai Tehrani[72a], B. Safarzadeh Samani[153], M. Safdari[150], S. Saha[102], M. Sahinsoy[113],

A. Sahu[178], M. Saimpert[142], M. Saito[160], T. Saito[160], D. Salamani[36], G. Salamanna[74a,74b],
A. Salnikov[150], J. Salt[170], A. Salvador Salas[13], D. Salvatore[41b,41a], F. Salvatore[153],
A. Salzburger[36], D. Sammel[52], D. Sampsonidis[159], D. Sampsonidou[60d,60c], J. Sánchez[170],
A. Sanchez Pineda[4], V. Sanchez Sebastian[170], H. Sandaker[131], C.O. Sander[46],
I.G. Sanderswood[89], J.A. Sandesara[101], M. Sandhoff[178], C. Sandoval[22b], D.P.C. Sankey[141],
A. Sansoni[51], C. Santoni[38], H. Santos[137a,137b], S.N. Santpur[17], A. Santra[176], K.A. Saoucha[146],
A. Sapronov[79], J.G. Saraiva[137a,137d], J. Sardain[100], O. Sasaki[81], K. Sato[165], C. Sauer[61b],
F. Sauerburger[52], E. Sauvan[4], P. Savard[163,ae], R. Sawada[160], C. Sawyer[141], L. Sawyer[95],
I. Sayago Galvan[170], C. Sbarra[23b], A. Sbrizzi[23b,23a], T. Scanlon[94], J. Schaarschmidt[145],
P. Schacht[113], D. Schaefer[37], U. Schäfer[98], A.C. Schaffer[64], D. Schaile[112], R.D. Schamberger[152],
E. Schanet[112], C. Scharf[18], N. Scharmberg[99], V.A. Schegelsky[135], D. Scheirich[140], F. Schenck[18],
M. Schernau[167], C. Scheulen[53], C. Schiavi[55b,55a], Z.M. Schillaci[26], E.J. Schioppa[67a,67b],
M. Schioppa[41b,41a], B. Schlag[98], K.E. Schleicher[52], S. Schlenker[36], K. Schmieden[98], C. Schmitt[98],
S. Schmitt[46], L. Schoeffel[142], A. Schoening[61b], P.G. Scholer[52], E. Schopf[132], M. Schott[98],
J. Schovancova[36], S. Schramm[54], F. Schroeder[178], H-C. Schultz-Coulon[61a], M. Schumacher[52],
B.A. Schumm[143], Ph. Schune[142], A. Schwartzman[150], T.A. Schwarz[104], Ph. Schwemling[142],
R. Schwienhorst[105], A. Sciandra[143], G. Sciolla[26], F. Scuri[71a], F. Scutti[103], C.D. Sebastiani[90],
K. Sedlaczek[47], P. Seema[18], S.C. Seidel[115], A. Seiden[143], B.D. Seidlitz[29], T. Seiss[37], C. Seitz[46],
J.M. Seixas[80b], G. Sekhniaidze[69a], S.J. Sekula[42], L. Selem[4], N. Semprini-Cesari[23b,23a], S. Sen[49],
V. Senthilkumar[170], L. Serin[64], L. Serkin[66a,66b], M. Sessa[74a,74b], H. Severini[126], S. Sevova[150],
F. Sforza[55b,55a], A. Sfyrla[54], E. Shabalina[53], R. Shaheen[151], J.D. Shahinian[134],
N.W. Shaikh[45a,45b], D. Shaked Renous[176], L.Y. Shan[14a], M. Shapiro[17], A. Sharma[36],
A.S. Sharma[1], S. Sharma[46], P.B. Shatalov[121], K. Shaw[153], S.M. Shaw[99], P. Sherwood[94], L. Shi[94],
C.O. Shimmin[179], Y. Shimogama[175], J.D. Shinner[93], I.P.J. Shipsey[132], S. Shirabe[54],
M. Shiyakova[79], J. Shlomi[176], M.J. Shochet[37], J. Shojaii[103], D.R. Shope[151], S. Shrestha[125],
E.M. Shrif[33g], M.J. Shroff[172], P. Sicho[138], A.M. Sickles[169], E. Sideras Haddad[33g],
O. Sidiropoulou[36], A. Sidoti[23b], F. Siegert[48], Dj. Sijacki[15], F. Sili[88], J.M. Silva[20],
M.V. Silva Oliveira[36], S.B. Silverstein[45a], S. Simion[64], R. Simoniello[36], E.L. Simpson[57],
N.D. Simpson[96], S. Simsek[21d], S. Sindhu[53], P. Sinervo[163], V. Sinetckii[111], S. Singh[149],
S. Singh[163], S. Sinha[46], S. Sinha[33g], M. Sioli[23b,23a], I. Siral[129], S.Yu. Sivoklokov[111],
J. Sjölin[45a,45b], A. Skaf[53], E. Skorda[96], P. Skubic[126], M. Slawinska[84], V. Smakhtin[176],
B.H. Smart[141], J. Smiesko[140], S.Yu. Smirnov[110], Y. Smirnov[110], L.N. Smirnova[111,q],
O. Smirnova[96], E.A. Smith[37], H.A. Smith[132], R. Smith[150], M. Smizanska[89], K. Smolek[139],
A. Smykiewicz[84], A.A. Snesarev[109], H.L. Snoek[117], S. Snyder[29], R. Sobie[172,v], A. Soffer[158],
C.A. Solans Sanchez[36], E.Yu. Soldatov[110], U. Soldevila[170], A.A. Solodkov[120], S. Solomon[52],
A. Soloshenko[79], K. Solovieva[52], O.V. Solovyanov[120], V. Solovyev[135], P. Sommer[146], H. Son[166],
A. Sonay[13], W.Y. Song[164b], A. Sopczak[139], A.L. Sopio[94], F. Sopkova[28b], V. Sothilingam[61a],
S. Sottocornola[70a,70b], R. Soualah[122c], A.M. Soukharev[119b,119a], Z. Soumaimi[35e], D. South[46],
S. Spagnolo[67a,67b], M. Spalla[113], M. Spangenberg[174], F. Spanò[93], D. Sperlich[52], G. Spigo[36],
M. Spina[153], S. Spinali[89], D.P. Spiteri[57], M. Spousta[140], E.J. Staats[34], A. Stabile[68a,68b],
R. Stamen[61a], M. Stamenkovic[117], A. Stampekis[20], M. Standke[24], E. Stanecka[84], B. Stanislaus[17],
M.M. Stanitzki[46], M. Stankaityte[132], B. Stapf[46], E.A. Starchenko[120], G.H. Stark[143], J. Stark[100],
D.M. Starko[164b], P. Staroba[138], P. Starovoitov[61a], S. Stärz[102], R. Staszewski[84],
G. Stavropoulos[44], J. Steentoft[168], P. Steinberg[29], A.L. Steinhebel[129], B. Stelzer[149,164a],
H.J. Stelzer[136], O. Stelzer-Chilton[164a], H. Stenzel[56], T.J. Stevenson[153], G.A. Stewart[36],
M.C. Stockton[36], G. Stoicea[27b], M. Stolarski[137a], S. Stonjek[113], A. Straessner[48],
J. Strandberg[151], S. Strandberg[45a,45b], M. Strauss[126], T. Strebler[100], P. Strizenec[28b],
R. Ströhmer[173], D.M. Strom[129], L.R. Strom[46], R. Stroynowski[42], A. Strubig[45a,45b],

S.A. Stucci[29], B. Stugu[16], J. Stupak[126], N.A. Styles[46], D. Su[150], S. Su[60a], W. Su[60d,145,60c],
X. Su[60a,64], K. Sugizaki[160], V.V. Sulin[109], M.J. Sullivan[90], D.M.S. Sultan[75a,75b],
L. Sultanaliyeva[109], S. Sultansoy[3b], T. Sumida[85], S. Sun[104], S. Sun[177],
O. Sunneborn Gudnadottir[168], M.R. Sutton[153], M. Svatos[138], M. Swiatlowski[164a], T. Swirski[173],
I. Sykora[28a], M. Sykora[140], T. Sykora[140], D. Ta[98], K. Tackmann[46,u], A. Taffard[167],
R. Tafirout[164a], R.H.M. Taibah[133], R. Takashima[86], K. Takeda[82], E.P. Takeva[50], Y. Takubo[81],
M. Talby[100], A.A. Talyshev[119b,119a], K.C. Tam[62b], N.M. Tamir[158], A. Tanaka[160], J. Tanaka[160],
R. Tanaka[64], J. Tang[60c], Z. Tao[171], S. Tapia Araya[78], S. Tapprogge[98],
A. Tarek Abouelfadl Mohamed[105], S. Tarem[157], K. Tariq[60b], G. Tarna[27b], G.F. Tartarelli[68a],
P. Tas[140], M. Tasevsky[138], E. Tassi[41b,41a], G. Tateno[160], Y. Tayalati[35e], G.N. Taylor[103],
W. Taylor[164b], H. Teagle[90], A.S. Tee[177], R. Teixeira De Lima[150], P. Teixeira-Dias[93], J.J. Teoh[163],
K. Terashi[160], J. Terron[97], S. Terzo[13], M. Testa[51], R.J. Teuscher[163,v], N. Themistokleous[50],
T. Theveneaux-Pelzer[18], O. Thielmann[178], D.W. Thomas[93], J.P. Thomas[20], E.A. Thompson[46],
P.D. Thompson[20], E. Thomson[134], E.J. Thorpe[92], Y. Tian[53], V. Tikhomirov[109,aa],
Yu.A. Tikhonov[119b,119a], S. Timoshenko[110], E.X.L. Ting[1], P. Tipton[179], S. Tisserant[100],
S.H. Tlou[33g], A. Tnourji[38], K. Todome[23b,23a], S. Todorova-Nova[140], S. Todt[48], M. Togawa[81],
J. Tojo[87], S. Tokár[28a], K. Tokushuku[81], R. Tombs[32], M. Tomoto[81,114], L. Tompkins[150],
P. Tornambe[101], E. Torrence[129], H. Torres[48], E. Torró Pastor[170], M. Toscani[30], C. Tosciri[37],
D.R. Tovey[146], A. Traeet[16], I.S. Trandafir[27b], C.J. Treado[123], T. Trefzger[173], A. Tricoli[29],
I.M. Trigger[164a], S. Trincaz-Duvoid[133], D.A. Trischuk[171], W. Trischuk[163], B. Trocmé[58],
A. Trofymov[64], C. Troncon[68a], F. Trovato[153], L. Truong[33c], M. Trzebinski[84], A. Trzupek[84],
F. Tsai[152], M. Tsai[104], A. Tsiamis[159], P.V. Tsiareshka[106], A. Tsirigotis[159,s], V. Tsiskaridze[152],
E.G. Tskhadadze[156a], M. Tsopoulou[159], Y. Tsujikawa[85], I.I. Tsukerman[121], V. Tsulaia[17],
S. Tsuno[81], O. Tsur[157], D. Tsybychev[152], Y. Tu[62b], A. Tudorache[27b], V. Tudorache[27b],
A.N. Tuna[36], S. Turchikhin[79], I. Turk Cakir[3a], R. Turra[68a], P.M. Tuts[39], S. Tzamarias[159],
P. Tzanis[10], E. Tzovara[98], K. Uchida[160], F. Ukegawa[165], P.A. Ulloa Poblete[144c], G. Unal[36],
M. Unal[11], A. Undrus[29], G. Unel[167], K. Uno[160], J. Urban[28b], P. Urquijo[103], G. Usai[8],
R. Ushioda[161], M. Usman[108], Z. Uysal[21b], V. Vacek[139], B. Vachon[102], K.O.H. Vadla[131],
T. Vafeiadis[36], C. Valderanis[112], E. Valdes Santurio[45a,45b], M. Valente[164a], S. Valentinetti[23b,23a],
A. Valero[170], A. Vallier[100], J.A. Valls Ferrer[170], T.R. Van Daalen[145], P. Van Gemmeren[6],
S. Van Stroud[94], I. Van Vulpen[117], M. Vanadia[73a,73b], W. Vandelli[36], M. Vandenbroucke[142],
E.R. Vandewall[127], D. Vannicola[158], L. Vannoli[55b,55a], R. Vari[72a], E.W. Varnes[7], C. Varni[17],
T. Varol[155], D. Varouchas[64], K.E. Varvell[154], M.E. Vasile[27b], L. Vaslin[38], G.A. Vasquez[172],
F. Vazeille[38], D. Vazquez Furelos[13], T. Vazquez Schroeder[36], J. Veatch[53], V. Vecchio[99],
M.J. Veen[117], I. Veliscek[132], L.M. Veloce[163], F. Veloso[137a,137c], S. Veneziano[72a],
A. Ventura[67a,67b], A. Verbytskyi[113], M. Verducci[71a,71b], C. Vergis[24], M. Verissimo De Araujo[80b],
W. Verkerke[117], J.C. Vermeulen[117], C. Vernieri[150], P.J. Verschuuren[93], M. Vessella[101],
M.L. Vesterbacka[123], M.C. Vetterli[149,ae], A. Vgenopoulos[159], N. Viaux Maira[144f], T. Vickey[146],
O.E. Vickey Boeriu[146], G.H.A. Viehhauser[132], L. Vigani[61b], M. Villa[23b,23a],
M. Villaplana Perez[170], E.M. Villhauer[50], E. Vilucchi[51], M.G. Vincter[34], G.S. Virdee[20],
A. Vishwakarma[50], C. Vittori[23b,23a], I. Vivarelli[153], V. Vladimirov[174], E. Voevodina[113],
M. Vogel[178], P. Vokac[139], J. Von Ahnen[46], E. Von Toerne[24], B. Vormwald[36], V. Vorobel[140],
K. Vorobev[110], M. Vos[170], J.H. Vossebeld[90], M. Vozak[117], L. Vozdecky[92], N. Vranjes[15],
M. Vranjes Milosavljevic[15], V. Vrba[139,*], M. Vreeswijk[117], N.K. Vu[100], R. Vuillermet[36],
O.V. Vujinovic[98], I. Vukotic[37], S. Wada[165], C. Wagner[101], W. Wagner[178], S. Wahdan[178],
H. Wahlberg[88], R. Wakasa[165], M. Wakida[114], V.M. Walbrecht[113], J. Walder[141], R. Walker[112],
W. Walkowiak[148], A.M. Wang[59], A.Z. Wang[177], C. Wang[60a], C. Wang[60c], H. Wang[17],
J. Wang[62a], P. Wang[42], R.-J. Wang[98], R. Wang[59], R. Wang[6], S.M. Wang[155], S. Wang[60b],

T. Wang[60a], W.T. Wang[77], W.X. Wang[60a], X. Wang[14c], X. Wang[169], X. Wang[60c], Y. Wang[60d], Z. Wang[104], Z. Wang[60d,49,60c], Z. Wang[104], A. Warburton[102], R.J. Ward[20], N. Warrack[57], A.T. Watson[20], M.F. Watson[20], G. Watts[145], B.M. Waugh[94], A.F. Webb[11], C. Weber[29], M.S. Weber[19], S.A. Weber[34], S.M. Weber[61a], C. Wei[60a], Y. Wei[132], A.R. Weidberg[132], J. Weingarten[47], M. Weirich[98], C. Weiser[52], T. Wenaus[29], B. Wendland[47], T. Wengler[36], N.S. Wenke[113], N. Wermes[24], M. Wessels[61a], K. Whalen[129], A.M. Wharton[89], A.S. White[59], A. White[8], M.J. White[1], D. Whiteson[167], L. Wickremasinghe[130], W. Wiedenmann[177], C. Wiel[48], M. Wielers[141], N. Wieseotte[98], C. Wiglesworth[40], L.A.M. Wiik-Fuchs[52], D.J. Wilbern[126], H.G. Wilkens[36], D.M. Williams[39], H.H. Williams[134], S. Williams[32], S. Willocq[101], P.J. Windischhofer[132], F. Winklmeier[129], B.T. Winter[52], M. Wittgen[150], M. Wobisch[95], A. Wolf[98], R. Wölker[132], J. Wollrath[167], M.W. Wolter[84], H. Wolters[137a,137c], V.W.S. Wong[171], A.F. Wongel[46], S.D. Worm[46], B.K. Wosiek[84], K.W. Woźniak[84], K. Wraight[57], J. Wu[14a,14d], S.L. Wu[177], X. Wu[54], Y. Wu[60a], Z. Wu[142,60a], J. Wuerzinger[132], T.R. Wyatt[99], B.M. Wynne[50], S. Xella[40], L. Xia[14c], M. Xia[14b], J. Xiang[62c], X. Xiao[104], M. Xie[60a], X. Xie[60a], I. Xiotidis[153], D. Xu[14a], H. Xu[60a], H. Xu[60a], L. Xu[60a], R. Xu[134], T. Xu[60a], W. Xu[104], Y. Xu[14b], Z. Xu[60b], Z. Xu[150], B. Yabsley[154], S. Yacoob[33a], N. Yamaguchi[87], Y. Yamaguchi[161], H. Yamauchi[165], T. Yamazaki[17], Y. Yamazaki[82], J. Yan[60c], S. Yan[132], Z. Yan[25], H.J. Yang[60c,60d], H.T. Yang[17], S. Yang[60a], T. Yang[62c], X. Yang[60a], X. Yang[14a], Y. Yang[42], Z. Yang[104,60a], W-M. Yao[17], Y.C. Yap[46], H. Ye[14c], J. Ye[42], S. Ye[29], X. Ye[60a], I. Yeletskikh[79], M.R. Yexley[89], P. Yin[39], K. Yorita[175], C.J.S. Young[52], C. Young[150], M. Yuan[104], R. Yuan[60b,i], X. Yue[61a], M. Zaazoua[35e], B. Zabinski[84], G. Zacharis[10], E. Zaid[50], A.M. Zaitsev[120,z], T. Zakareishvili[156b], N. Zakharchuk[34], S. Zambito[36], D. Zanzi[52], O. Zaplatilek[139], S.V. Zeißner[47], C. Zeitnitz[178], J.C. Zeng[169], D.T. Zenger Jr[26], O. Zenin[120], T. Ženiš[28a], S. Zenz[92], S. Zerradi[35a], D. Zerwas[64], B. Zhang[14c], D.F. Zhang[146], G. Zhang[14b], J. Zhang[6], K. Zhang[14a], L. Zhang[14c], M. Zhang[169], R. Zhang[177], S. Zhang[104], X. Zhang[60c], X. Zhang[60b], Z. Zhang[64], H. Zhao[145], P. Zhao[49], T. Zhao[60b], Y. Zhao[143], Z. Zhao[60a], A. Zhemchugov[79], Z. Zheng[150], D. Zhong[169], B. Zhou[104], C. Zhou[177], H. Zhou[7], N. Zhou[60c], Y. Zhou[7], C.G. Zhu[60b], C. Zhu[14a,14d], H.L. Zhu[60a], H. Zhu[14a], J. Zhu[104], Y. Zhu[60a], X. Zhuang[14a], K. Zhukov[109], V. Zhulanov[119b,119a], D. Zieminska[65], N.I. Zimine[79], S. Zimmermann[52,*], J. Zinsser[61b], M. Ziolkowski[148], L. Živković[15], A. Zoccoli[23b,23a], K. Zoch[54], T.G. Zorbas[146], O. Zormpa[44], W. Zou[39], L. Zwalinski[36]

1   *Department of Physics, University of Adelaide, Adelaide; Australia*
2   *Department of Physics, University of Alberta, Edmonton AB; Canada*
3   *(a)Department of Physics, Ankara University, Ankara;(b)Division of Physics, TOBB University of Economics and Technology, Ankara; Turkey*
4   *LAPP, Univ. Savoie Mont Blanc, CNRS/IN2P3, Annecy; France*
5   *Université de Paris, CNRS/IN2P3, AstroParticule et Cosmologie, Paris; France*
6   *High Energy Physics Division, Argonne National Laboratory, Argonne IL; United States of America*
7   *Department of Physics, University of Arizona, Tucson AZ; United States of America*
8   *Department of Physics, University of Texas at Arlington, Arlington TX; United States of America*
9   *Physics Department, National and Kapodistrian University of Athens, Athens; Greece*
10 *Physics Department, National Technical University of Athens, Zografou; Greece*
11 *Department of Physics, University of Texas at Austin, Austin TX; United States of America*
12 *Institute of Physics, Azerbaijan Academy of Sciences, Baku; Azerbaijan*
13 *Institut de Física d'Altes Energies (IFAE), Barcelona Institute of Science and Technology, Barcelona; Spain*
14 *(a)Institute of High Energy Physics, Chinese Academy of Sciences, Beijing;(b)Physics Department, Tsinghua University, Beijing;(c)Department of Physics, Nanjing University, Nanjing;(d)University of Chinese Academy of Science (UCAS), Beijing; China*
15 *Institute of Physics, University of Belgrade, Belgrade; Serbia*

16 *Department for Physics and Technology, University of Bergen, Bergen; Norway*

17 *Physics Division, Lawrence Berkeley National Laboratory and University of California, Berkeley CA; United States of America*

18 *Institut für Physik, Humboldt Universität zu Berlin, Berlin; Germany*

19 *Albert Einstein Center for Fundamental Physics and Laboratory for High Energy Physics, University of Bern, Bern; Switzerland*

20 *School of Physics and Astronomy, University of Birmingham, Birmingham; United Kingdom*

21 [a] *Department of Physics, Bogazici University, Istanbul;* [b] *Department of Physics Engineering, Gaziantep University, Gaziantep;* [c] *Department of Physics, Istanbul University, Istanbul;* [d] *Istinye University, Sariyer, Istanbul; Turkey*

22 [a] *Facultad de Ciencias y Centro de Investigaciónes, Universidad Antonio Nariño, Bogotá;* [b] *Departamento de Física, Universidad Nacional de Colombia, Bogotá; Colombia*

23 [a] *Dipartimento di Fisica e Astronomia A. Righi, Università di Bologna, Bologna;* [b] *INFN Sezione di Bologna; Italy*

24 *Physikalisches Institut, Universität Bonn, Bonn; Germany*

25 *Department of Physics, Boston University, Boston MA; United States of America*

26 *Department of Physics, Brandeis University, Waltham MA; United States of America*

27 [a] *Transilvania University of Brasov, Brasov;* [b] *Horia Hulubei National Institute of Physics and Nuclear Engineering, Bucharest;* [c] *Department of Physics, Alexandru Ioan Cuza University of Iasi, Iasi;* [d] *National Institute for Research and Development of Isotopic and Molecular Technologies, Physics Department, Cluj-Napoca;* [e] *University Politehnica Bucharest, Bucharest;* [f] *West University in Timisoara, Timisoara; Romania*

28 [a] *Faculty of Mathematics, Physics and Informatics, Comenius University, Bratislava;* [b] *Department of Subnuclear Physics, Institute of Experimental Physics of the Slovak Academy of Sciences, Kosice; Slovak Republic*

29 *Physics Department, Brookhaven National Laboratory, Upton NY; United States of America*

30 *Departamento de Física (FCEN) and IFIBA, Universidad de Buenos Aires and CONICET, Buenos Aires; Argentina*

31 *California State University, CA; United States of America*

32 *Cavendish Laboratory, University of Cambridge, Cambridge; United Kingdom*

33 [a] *Department of Physics, University of Cape Town, Cape Town;* [b] *iThemba Labs, Western Cape;* [c] *Department of Mechanical Engineering Science, University of Johannesburg, Johannesburg;* [d] *National Institute of Physics, University of the Philippines Diliman (Philippines);* [e] *University of South Africa, Department of Physics, Pretoria;* [f] *University of Zululand, KwaDlangezwa;* [g] *School of Physics, University of the Witwatersrand, Johannesburg; South Africa*

34 *Department of Physics, Carleton University, Ottawa ON; Canada*

35 [a] *Faculté des Sciences Ain Chock, Réseau Universitaire de Physique des Hautes Energies - Université Hassan II, Casablanca;* [b] *Faculté des Sciences, Université Ibn-Tofail, Kénitra;* [c] *Faculté des Sciences Semlalia, Université Cadi Ayyad, LPHEA-Marrakech;* [d] *LPMR, Faculté des Sciences, Université Mohamed Premier, Oujda;* [e] *Faculté des sciences, Université Mohammed V, Rabat;* [f] *Mohammed VI Polytechnic University, Ben Guerir; Morocco*

36 *CERN, Geneva; Switzerland*

37 *Enrico Fermi Institute, University of Chicago, Chicago IL; United States of America*

38 *LPC, Université Clermont Auvergne, CNRS/IN2P3, Clermont-Ferrand; France*

39 *Nevis Laboratory, Columbia University, Irvington NY; United States of America*

40 *Niels Bohr Institute, University of Copenhagen, Copenhagen; Denmark*

41 [a] *Dipartimento di Fisica, Università della Calabria, Rende;* [b] *INFN Gruppo Collegato di Cosenza, Laboratori Nazionali di Frascati; Italy*

42 *Physics Department, Southern Methodist University, Dallas TX; United States of America*

43 *Physics Department, University of Texas at Dallas, Richardson TX; United States of America*

44 *National Centre for Scientific Research "Demokritos", Agia Paraskevi; Greece*

45 [a] *Department of Physics, Stockholm University;* [b] *Oskar Klein Centre, Stockholm; Sweden*

46 *Deutsches Elektronen-Synchrotron DESY, Hamburg and Zeuthen; Germany*

47 *Fakultät Physik , Technische Universität Dortmund, Dortmund; Germany*

48 *Institut für Kern- und Teilchenphysik, Technische Universität Dresden, Dresden; Germany*

49 *Department of Physics, Duke University, Durham NC; United States of America*

50 *SUPA - School of Physics and Astronomy, University of Edinburgh, Edinburgh; United Kingdom*

51 *INFN e Laboratori Nazionali di Frascati, Frascati; Italy*

52 *Physikalisches Institut, Albert-Ludwigs-Universität Freiburg, Freiburg; Germany*

53 *II. Physikalisches Institut, Georg-August-Universität Göttingen, Göttingen; Germany*

54 *Département de Physique Nucléaire et Corpusculaire, Université de Genève, Genève; Switzerland*

55 [a] *Dipartimento di Fisica, Università di Genova, Genova;* [b] *INFN Sezione di Genova; Italy*

56 *II. Physikalisches Institut, Justus-Liebig-Universität Giessen, Giessen; Germany*

57 *SUPA - School of Physics and Astronomy, University of Glasgow, Glasgow; United Kingdom*

58 *LPSC, Université Grenoble Alpes, CNRS/IN2P3, Grenoble INP, Grenoble; France*

59 *Laboratory for Particle Physics and Cosmology, Harvard University, Cambridge MA; United States of America*

60 [a] *Department of Modern Physics and State Key Laboratory of Particle Detection and Electronics, University of Science and Technology of China, Hefei;* [b] *Institute of Frontier and Interdisciplinary Science and Key Laboratory of Particle Physics and Particle Irradiation (MOE), Shandong University, Qingdao;* [c] *School of Physics and Astronomy, Shanghai Jiao Tong University, Key Laboratory for Particle Astrophysics and Cosmology (MOE), SKLPPC, Shanghai;* [d] *Tsung-Dao Lee Institute, Shanghai; China*

61 [a] *Kirchhoff-Institut für Physik, Ruprecht-Karls-Universität Heidelberg, Heidelberg;* [b] *Physikalisches Institut, Ruprecht-Karls-Universität Heidelberg, Heidelberg; Germany*

62 [a] *Department of Physics, Chinese University of Hong Kong, Shatin, N.T., Hong Kong;* [b] *Department of Physics, University of Hong Kong, Hong Kong;* [c] *Department of Physics and Institute for Advanced Study, Hong Kong University of Science and Technology, Clear Water Bay, Kowloon, Hong Kong; China*

63 *Department of Physics, National Tsing Hua University, Hsinchu; Taiwan*

64 *IJCLab, Université Paris-Saclay, CNRS/IN2P3, 91405, Orsay; France*

65 *Department of Physics, Indiana University, Bloomington IN; United States of America*

66 [a] *INFN Gruppo Collegato di Udine, Sezione di Trieste, Udine;* [b] *ICTP, Trieste;* [c] *Dipartimento Politecnico di Ingegneria e Architettura, Università di Udine, Udine; Italy*

67 [a] *INFN Sezione di Lecce;* [b] *Dipartimento di Matematica e Fisica, Università del Salento, Lecce; Italy*

68 [a] *INFN Sezione di Milano;* [b] *Dipartimento di Fisica, Università di Milano, Milano; Italy*

69 [a] *INFN Sezione di Napoli;* [b] *Dipartimento di Fisica, Università di Napoli, Napoli; Italy*

70 [a] *INFN Sezione di Pavia;* [b] *Dipartimento di Fisica, Università di Pavia, Pavia; Italy*

71 [a] *INFN Sezione di Pisa;* [b] *Dipartimento di Fisica E. Fermi, Università di Pisa, Pisa; Italy*

72 [a] *INFN Sezione di Roma;* [b] *Dipartimento di Fisica, Sapienza Università di Roma, Roma; Italy*

73 [a] *INFN Sezione di Roma Tor Vergata;* [b] *Dipartimento di Fisica, Università di Roma Tor Vergata, Roma; Italy*

74 [a] *INFN Sezione di Roma Tre;* [b] *Dipartimento di Matematica e Fisica, Università Roma Tre, Roma; Italy*

75 [a] *INFN-TIFPA;* [b] *Università degli Studi di Trento, Trento; Italy*

76 *Institut für Astro- und Teilchenphysik, Leopold-Franzens-Universität, Innsbruck; Austria*

77 *University of Iowa, Iowa City IA; United States of America*

78 *Department of Physics and Astronomy, Iowa State University, Ames IA; United States of America*

79 *Joint Institute for Nuclear Research, Dubna; Russia*

80 [a] *Departamento de Engenharia Elétrica, Universidade Federal de Juiz de Fora (UFJF), Juiz de Fora;* [b] *Universidade Federal do Rio De Janeiro COPPE/EE/IF, Rio de Janeiro;* [c] *Instituto de Física, Universidade de São Paulo, São Paulo;* [d] *Rio de Janeiro State University, Rio de Janeiro; Brazil*

[81] *KEK, High Energy Accelerator Research Organization, Tsukuba; Japan*

[82] *Graduate School of Science, Kobe University, Kobe; Japan*

[83] [a] *AGH University of Science and Technology, Faculty of Physics and Applied Computer Science, Krakow;* [b] *Marian Smoluchowski Institute of Physics, Jagiellonian University, Krakow; Poland*

[84] *Institute of Nuclear Physics Polish Academy of Sciences, Krakow; Poland*

[85] *Faculty of Science, Kyoto University, Kyoto; Japan*

[86] *Kyoto University of Education, Kyoto; Japan*

[87] *Research Center for Advanced Particle Physics and Department of Physics, Kyushu University, Fukuoka; Japan*

[88] *Instituto de Física La Plata, Universidad Nacional de La Plata and CONICET, La Plata; Argentina*

[89] *Physics Department, Lancaster University, Lancaster; United Kingdom*

[90] *Oliver Lodge Laboratory, University of Liverpool, Liverpool; United Kingdom*

[91] *Department of Experimental Particle Physics, Jožef Stefan Institute and Department of Physics, University of Ljubljana, Ljubljana; Slovenia*

[92] *School of Physics and Astronomy, Queen Mary University of London, London; United Kingdom*

[93] *Department of Physics, Royal Holloway University of London, Egham; United Kingdom*

[94] *Department of Physics and Astronomy, University College London, London; United Kingdom*

[95] *Louisiana Tech University, Ruston LA; United States of America*

[96] *Fysiska institutionen, Lunds universitet, Lund; Sweden*

[97] *Departamento de Física Teorica C-15 and CIAFF, Universidad Autónoma de Madrid, Madrid; Spain*

[98] *Institut für Physik, Universität Mainz, Mainz; Germany*

[99] *School of Physics and Astronomy, University of Manchester, Manchester; United Kingdom*

[100] *CPPM, Aix-Marseille Université, CNRS/IN2P3, Marseille; France*

[101] *Department of Physics, University of Massachusetts, Amherst MA; United States of America*

[102] *Department of Physics, McGill University, Montreal QC; Canada*

[103] *School of Physics, University of Melbourne, Victoria; Australia*

[104] *Department of Physics, University of Michigan, Ann Arbor MI; United States of America*

[105] *Department of Physics and Astronomy, Michigan State University, East Lansing MI; United States of America*

[106] *B.I. Stepanov Institute of Physics, National Academy of Sciences of Belarus, Minsk; Belarus*

[107] *Research Institute for Nuclear Problems of Byelorussian State University, Minsk; Belarus*

[108] *Group of Particle Physics, University of Montreal, Montreal QC; Canada*

[109] *P.N. Lebedev Physical Institute of the Russian Academy of Sciences, Moscow; Russia*

[110] *National Research Nuclear University MEPhI, Moscow; Russia*

[111] *D.V. Skobeltsyn Institute of Nuclear Physics, M.V. Lomonosov Moscow State University, Moscow; Russia*

[112] *Fakultät für Physik, Ludwig-Maximilians-Universität München, München; Germany*

[113] *Max-Planck-Institut für Physik (Werner-Heisenberg-Institut), München; Germany*

[114] *Graduate School of Science and Kobayashi-Maskawa Institute, Nagoya University, Nagoya; Japan*

[115] *Department of Physics and Astronomy, University of New Mexico, Albuquerque NM; United States of America*

[116] *Institute for Mathematics, Astrophysics and Particle Physics, Radboud University/Nikhef, Nijmegen; Netherlands*

[117] *Nikhef National Institute for Subatomic Physics and University of Amsterdam, Amsterdam; Netherlands*

[118] *Department of Physics, Northern Illinois University, DeKalb IL; United States of America*

[119] [a] *Budker Institute of Nuclear Physics and NSU, SB RAS, Novosibirsk;* [b] *Novosibirsk State University Novosibirsk; Russia*

[120] *Institute for High Energy Physics of the National Research Centre Kurchatov Institute, Protvino; Russia*

[121] *Institute for Theoretical and Experimental Physics named by A.I. Alikhanov of National Research Centre "Kurchatov Institute", Moscow; Russia*

122 (a) *New York University Abu Dhabi, Abu Dhabi;* (b) *United Arab Emirates University, Al Ain;* (c) *University of Sharjah, Sharjah; United Arab Emirates*

123 *Department of Physics, New York University, New York NY; United States of America*

124 *Ochanomizu University, Otsuka, Bunkyo-ku, Tokyo; Japan*

125 *Ohio State University, Columbus OH; United States of America*

126 *Homer L. Dodge Department of Physics and Astronomy, University of Oklahoma, Norman OK; United States of America*

127 *Department of Physics, Oklahoma State University, Stillwater OK; United States of America*

128 *Palacký University, Joint Laboratory of Optics, Olomouc; Czech Republic*

129 *Institute for Fundamental Science, University of Oregon, Eugene, OR; United States of America*

130 *Graduate School of Science, Osaka University, Osaka; Japan*

131 *Department of Physics, University of Oslo, Oslo; Norway*

132 *Department of Physics, Oxford University, Oxford; United Kingdom*

133 *LPNHE, Sorbonne Université, Université de Paris, CNRS/IN2P3, Paris; France*

134 *Department of Physics, University of Pennsylvania, Philadelphia PA; United States of America*

135 *Konstantinov Nuclear Physics Institute of National Research Centre "Kurchatov Institute", PNPI, St. Petersburg; Russia*

136 *Department of Physics and Astronomy, University of Pittsburgh, Pittsburgh PA; United States of America*

137 (a) *Laboratório de Instrumentação e Física Experimental de Partículas - LIP, Lisboa;* (b) *Departamento de Física, Faculdade de Ciências, Universidade de Lisboa, Lisboa;* (c) *Departamento de Física, Universidade de Coimbra, Coimbra;* (d) *Centro de Física Nuclear da Universidade de Lisboa, Lisboa;* (e) *Departamento de Física, Universidade do Minho, Braga;* (f) *Departamento de Física Teórica y del Cosmos, Universidad de Granada, Granada (Spain);* (g) *Instituto Superior Técnico, Universidade de Lisboa, Lisboa; Portugal*

138 *Institute of Physics of the Czech Academy of Sciences, Prague; Czech Republic*

139 *Czech Technical University in Prague, Prague; Czech Republic*

140 *Charles University, Faculty of Mathematics and Physics, Prague; Czech Republic*

141 *Particle Physics Department, Rutherford Appleton Laboratory, Didcot; United Kingdom*

142 *IRFU, CEA, Université Paris-Saclay, Gif-sur-Yvette; France*

143 *Santa Cruz Institute for Particle Physics, University of California Santa Cruz, Santa Cruz CA; United States of America*

144 (a) *Departamento de Física, Pontificia Universidad Católica de Chile, Santiago;* (b) *Millennium Institute for Subatomic physics at high energy frontier (SAPHIR), Santiago;* (c) *Instituto de Investigación Multidisciplinario en Ciencia y Tecnología, y Departamento de Física, Universidad de La Serena;* (d) *Universidad Andres Bello, Department of Physics, Santiago;* (e) *Instituto de Alta Investigación, Universidad de Tarapacá, Arica;* (f) *Departamento de Física, Universidad Técnica Federico Santa María, Valparaíso; Chile*

145 *Department of Physics, University of Washington, Seattle WA; United States of America*

146 *Department of Physics and Astronomy, University of Sheffield, Sheffield; United Kingdom*

147 *Department of Physics, Shinshu University, Nagano; Japan*

148 *Department Physik, Universität Siegen, Siegen; Germany*

149 *Department of Physics, Simon Fraser University, Burnaby BC; Canada*

150 *SLAC National Accelerator Laboratory, Stanford CA; United States of America*

151 *Department of Physics, Royal Institute of Technology, Stockholm; Sweden*

152 *Departments of Physics and Astronomy, Stony Brook University, Stony Brook NY; United States of America*

153 *Department of Physics and Astronomy, University of Sussex, Brighton; United Kingdom*

154 *School of Physics, University of Sydney, Sydney; Australia*

155 *Institute of Physics, Academia Sinica, Taipei; Taiwan*

156 (a) *E. Andronikashvili Institute of Physics, Iv. Javakhishvili Tbilisi State University, Tbilisi;* (b) *High Energy Physics Institute, Tbilisi State University, Tbilisi; Georgia*

157 Department of Physics, Technion, Israel Institute of Technology, Haifa; Israel
158 Raymond and Beverly Sackler School of Physics and Astronomy, Tel Aviv University, Tel Aviv; Israel
159 Department of Physics, Aristotle University of Thessaloniki, Thessaloniki; Greece
160 International Center for Elementary Particle Physics and Department of Physics, University of Tokyo, Tokyo; Japan
161 Department of Physics, Tokyo Institute of Technology, Tokyo; Japan
162 Tomsk State University, Tomsk; Russia
163 Department of Physics, University of Toronto, Toronto ON; Canada
164 (a) TRIUMF, Vancouver BC; (b) Department of Physics and Astronomy, York University, Toronto ON; Canada
165 Division of Physics and Tomonaga Center for the History of the Universe, Faculty of Pure and Applied Sciences, University of Tsukuba, Tsukuba; Japan
166 Department of Physics and Astronomy, Tufts University, Medford MA; United States of America
167 Department of Physics and Astronomy, University of California Irvine, Irvine CA; United States of America
168 Department of Physics and Astronomy, University of Uppsala, Uppsala; Sweden
169 Department of Physics, University of Illinois, Urbana IL; United States of America
170 Instituto de Física Corpuscular (IFIC), Centro Mixto Universidad de Valencia - CSIC, Valencia; Spain
171 Department of Physics, University of British Columbia, Vancouver BC; Canada
172 Department of Physics and Astronomy, University of Victoria, Victoria BC; Canada
173 Fakultät für Physik und Astronomie, Julius-Maximilians-Universität Würzburg, Würzburg; Germany
174 Department of Physics, University of Warwick, Coventry; United Kingdom
175 Waseda University, Tokyo; Japan
176 Department of Particle Physics and Astrophysics, Weizmann Institute of Science, Rehovot; Israel
177 Department of Physics, University of Wisconsin, Madison WI; United States of America
178 Fakultät für Mathematik und Naturwissenschaften, Fachgruppe Physik, Bergische Universität Wuppertal, Wuppertal; Germany
179 Department of Physics, Yale University, New Haven CT; United States of America

a Also at Borough of Manhattan Community College, City University of New York, New York NY; United States of America
b Also at Bruno Kessler Foundation, Trento; Italy
c Also at Center for High Energy Physics, Peking University; China
d Also at Centro Studi e Ricerche Enrico Fermi; Italy
e Also at CERN, Geneva; Switzerland
f Also at Département de Physique Nucléaire et Corpusculaire, Université de Genève, Genève; Switzerland
g Also at Departament de Fisica de la Universitat Autonoma de Barcelona, Barcelona; Spain
h Also at Department of Financial and Management Engineering, University of the Aegean, Chios; Greece
i Also at Department of Physics and Astronomy, Michigan State University, East Lansing MI; United States of America
j Also at Department of Physics and Astronomy, University of Louisville, Louisville, KY; United States of America
k Also at Department of Physics, Ben Gurion University of the Negev, Beer Sheva; Israel
l Also at Department of Physics, California State University, East Bay; United States of America
m Also at Department of Physics, California State University, Sacramento; United States of America
n Also at Department of Physics, King's College London, London; United Kingdom
o Also at Department of Physics, St. Petersburg State Polytechnical University, St. Petersburg; Russia

[p] Also at Department of Physics, University of Fribourg, Fribourg; Switzerland

[q] Also at Faculty of Physics, M.V. Lomonosov Moscow State University, Moscow; Russia

[r] Also at Graduate School of Science, Osaka University, Osaka; Japan

[s] Also at Hellenic Open University, Patras; Greece

[t] Also at Institucio Catalana de Recerca i Estudis Avancats, ICREA, Barcelona; Spain

[u] Also at Institut für Experimentalphysik, Universität Hamburg, Hamburg; Germany

[v] Also at Institute of Particle Physics (IPP); Canada

[w] Also at Institute of Theoretical Physics, Ilia State University, Tbilisi; Georgia

[x] Also at Instituto de Fisica Teorica, IFT-UAM/CSIC, Madrid; Spain

[y] Also at Joint Institute for Nuclear Research, Dubna; Russia

[z] Also at Moscow Institute of Physics and Technology State University, Dolgoprudny; Russia

[aa] Also at National Research Nuclear University MEPhI, Moscow; Russia

[ab] Also at Physics Department, An-Najah National University, Nablus; Palestine

[ac] Also at Physikalisches Institut, Albert-Ludwigs-Universität Freiburg, Freiburg; Germany

[ad] Also at The City College of New York, New York NY; United States of America

[ae] Also at TRIUMF, Vancouver BC; Canada

[af] Also at Universita di Napoli Parthenope, Napoli; Italy

[ag] Also at University of Chinese Academy of Sciences (UCAS), Beijing; China

[ah] Also at Yeditepe University, Physics Department, Istanbul; Turkey

[*] Deceased